Department of Mechanical Engineering
Solid Mechanics

ISRN LUTFD2/TFHF–05/5111–SE(1–156)

EVALUATING THE 3DM MODEL - AN EXPERIMENTAL AND FINITE ELEMENT STUDY

Master's Dissertation by

Oscar Elison and Lars Hansson

Supervisors
Johan Tryding, Tetra Pak
Magnus Just, Tetra Pak
Anders Harrysson, Div. of Solid Mechanics
Matti Ristinmaa, Div. of Solid Mechanics

Printed by KFS i LUND AB, Lund ,Sweden

For information, address:
Division of Solid Mechanics, Lund University, Box 118, SE-221 00 Lund, Sweden.
Homepage: http://www.solid.lth.se

Abstract

Tetra Pak strives to further increase the efficiency and lower the risk in the product development process, by increasing the understanding of paper mechanics and package performance. The 3DM model describes the paperboard behaviour and is together with a simulation tool a powerful engineering instrument. The 3DM model consists of a continuum model and an interface model. The continuum model describes the in-plane elastic-plastic deformation of the paperboard plies. The out-of-plane behaviour of the paperboard plies is assumed to be elastic. The interface model is an elastic-plastic cohesive model, which describes the delamination between the paperboard plies.

The objective of this report is to evaluate the 3DM model, using the paperboard converting processes creasing and folding of the paperboard Triplex 360 mN. This evaluation consisted of experimental tests at Stora Enso in Karlstad and simulations in ABAQUS/Standard. The creasing was performed with four different creasing tool geometries and with two different creasing depths. Every creased test specimen was folded twice to a predefined angle. To evaluate the 3DM model, the results from the experimental tests and simulations were compared and analysed. An interface parameter study was also conducted in order to investigate how the different interface parameters affect the results.

This evaluation shows that the 3DM model describes the loading behaviour during creasing and folding well, although with some deviations. During creasing high compressive strains develop in the out-of-plane direction. Since plasticity in the out-of-plane direction is not included in the 3DM model the differences in result could be due to this. In the experimental tests a softening behaviour is visible during folding which is not described by the 3DM model. For unloading during folding the results differs between experimental tests and simulations. This difference could be explained by the absence of paperboard creep in the continuum model. The results from the simulations with the 3DM model are affected by the changes of creasing tool geometries and creasing depths, in the same way as the results from experimental tests. The interface parameter study showed that a small change of a parameter affects the result considerable. Therefore, it is important that the test methods for determining the interface parameters are accurate. A conclusion is that the 3DM model has some difficulties to describe the behaviour of mechanically loaded paperboard. Improvements must be made and with the improvements suggested in this report the 3DM model could be an excellent tool for predicting paperboard behaviour.

Acknowledgments

This master thesis was carried out at Tetra Pak Carton Ambient AB in Lund from October 2004 to March 2005 with supervision from the Division of Solid Mechanics at Lund Institute of Technology.

The initiators of this project were PhD Johan Tryding and MSc Magnus Just at Tetra Pak. As our supervisors they provided most valuable information, helpful technical support and important ideas. To them we owe much gratitude.

We would like to thank our supervisor at the Division of Solid Mechanics, PhD student Anders Harrysson for guidance and feedback throughout this project, both during the research and writing phases. We would also like to show our gratitude to Prof. Matti Ristinmaa for his insightful remarks.

Stora Enso in Karlstad played a key role in this project. Here we would like to thank MSc Göran Niklasson for the important information and his assistance. We thank PhD Jan Lif for letting us use the laboratory and Mr Ivan Strnad for his precise machine operating. We also appreciate the generosity of Mr Dennis Westin at Lorentzen & Wettre who provided us with drawings.

Many thanks to the people at Tetra Pak. Especially to PhD Anders Magnusson for the computer assistance and PhD Georgos Papaspiropoulos for his help in the paper laboratory.

Lund, March 2005

Oscar Elison and Lars Hansson

Contents

Chapter 1

Introduction

1.1 Tetra Pak

As early as 1943 Ruben Rausing started his development work on creating a milk package that requires minimum of material whilst providing maximum hygiene. This endeavour would result in the tetrahedron-shaped package and later on a multinational company. 1951 AB Tetra Pak was established as a subsidiary of Åkerlund & Rausing. Since then the company has expanded its portfolio that today contains a wide variety of products and machines.

In 1993 Tetra Pak and Alfa Laval merged and formed the Tetra Laval Group in which Tetra Pak, Tetra Laval Food and Alfa Laval Agri are included. Today Tetra Pak develops, produces and markets complete processing, packaging and distribution systems for food and beverages. The vision of the company is to commit to making food safe and available, everywhere. For further information, see www.tetrapak.com (20050214)

1.2 Background to assignment

Simulation tools are important instruments in order to have a fast, efficient and low risk product development process. If simulations can describe the behaviour of a product or process and return reliable results, the gain in time and money, when developing new products, are considerable. For Tetra Pak it is of interest to simulate different processes where paper and paperboard materials are converted.

When simulating paperboard, the material model describing its behaviour is essential. To formulate such a model, Tetra Pak together with Stora Enso, AssiDomän, STFI-Packforsk, MIT and ABAQUS Inc started a joint venture research project in 1996. The aim of the

project was to develop design procedures for practical converting and end-use operations. The procedures would be based on finite element implementation of the material model.

After much work the 3DM model consisting of a continuum model and an interface model was formulated. To confirm that the model is reliable and accurate it now has to be thoroughly tested. The outcome from these tests will show if the 3DM model is ready to be implemented in the development processes or if the model has to be improved.

1.3 Problem formulation

Simulating creasing and folding are two processes where the 3DM model can be used to describe the paperboard behaviour. During these two processes difficulties like paperboard delamination and plastic behaviour occurs. The 3DM model should regard and describe this during mechanical loading. However, the model has to be evaluated before implementing it into industrial design and engineering.

1.4 Objectives

This report aims to evaluate the 3DM model during creasing and folding of Triplex 360 mN. The main objective is to compare and analyse the results from experimental tests with simulations made in ABAQUS.

1.5 Delimitations

To obtain a manageable number of test combinations, some restrictions and delimitations were made.

- Four different creasing tool geometries are used
- The creasing is made with two different depths
- Two different folding angles are used
- Simulations and experimental tests are performed on Triplex 360 mN
- The experimental tests are performed at a constant temperature and relative humidity

Chapter 2

A short presentation of paperboard

Paper and paperboard are created using fibers, water and energy. Paper technology is based on achieving an increase in mechanical strength without using adhesives. To do so, hydrophile fibers are mechanically treated in water and from a water suspension shaped to paper. The bindings in paper are primarily hydrogen bridges between the fibers created during the water evaporation, cf. Fellers and Norman (1998)

No clear distinction between paper and paperboard exists. Thick paper is often called paperboard but there is no standard thickness that distinguishes the two qualities.

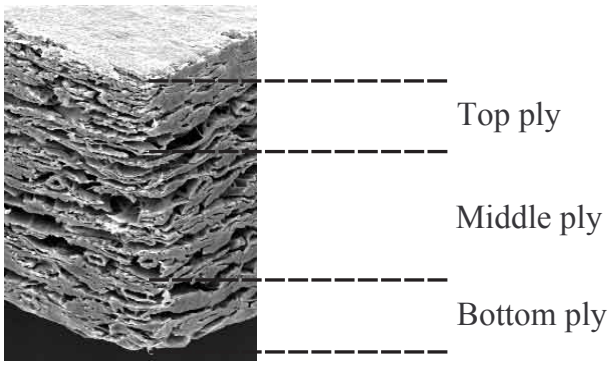

Figure 2.1: Paperboard with different plies

The mechanical properties of paperboard are decided by factors such as the shape of the fibers, their chemical composition and the mechanical treatment in water. Paperboard can be manufactured with a multilayer technique used to increase the bending stiffness. Mechanical and chemical pulps are combined to obtain a higher strength. The mechanical pulp in the middle ply acts as bulk material and the chemical pulp in the top and bottom plies provides strength, see Figure 2.1.

The wood is with a mechanical process dissolved into mechanical pulp. This process damage and weakens the fibers. Mechanical pulp is often used in paperboard. With this method 90 percent of the wood is used.

When creating chemical pulp, the lignin holding the fibers in the wood together is with a chemical method dissolved so that the fibers are separated. The exchange when using the chemical method is between 48 and 60 percent of the wood.

Manufacturing chemical pulp is a more non-destructive process than creating mechanical pulp. This results in a longer average fiber length for the chemical pulp and therefore a higher strength. On the other hand, the chemical process breaks down the cellulose, which reduces the strength of each individual fiber.

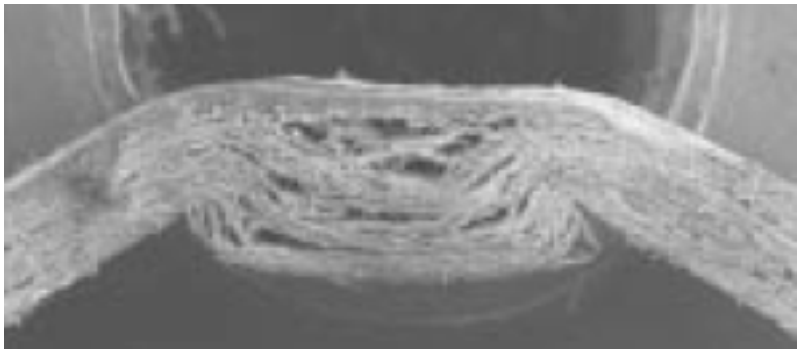

Figure 2.2: Delamination in paperboard, picture taken from Xia (2002)

When paperboard is mechanically loaded, the main deformation comes from the fibers themselves with rather small contribution from fiber reorganisation. In paperboard, damage between the plies and within the plies can occur and cause delamination, see Figure 2.2

Chapter 3

Large deformation theory

In this chapter the foundation of non-linear continuum mechanics used in elasto-plastic theory are briefly examined. The thermodynamic relation will also be discussed. The main purpose is to derive expressions for strains and stresses that develop in materials subjected to large deformation. This is more thoroughly examined in Ottosen and Ristinmaa (2001). These expressions are fundamental for the 3DM model introduced in chapter 4.

3.1 Basic kinematic relations

To start, a point is defined as a certain position in a coordinate system and a particle is defined as an infinitely small part of the material.

$\mathbf{X}$ is the position vector of a particle at the time $t = 0$ in a fixed coordinate system. At the time t the position of this particle is described by the position vector $\mathbf{x}$ according to

$$\mathbf{x} = \mathbf{x}(\mathbf{X}, t) \tag{3.1}$$

This is the *Lagrangian* description where $\mathbf{X}$ are called the material coordinates and refers to the *reference configuration* i.e. the configuration at $t = 0$. The spatial coordinates $\mathbf{x}$ constitutes the *deformed configuration*, see Figure 3.1.

This description can be inverted to provide the *Eulerian* description, where for a given position $\mathbf{x}$ in the deformed configuration it is possible to obtain the corresponding position $\mathbf{X}$ of the same particle in the reference configuration. This is expressed as

$$\mathbf{X} = \mathbf{X}(\mathbf{x}, t) \tag{3.2}$$

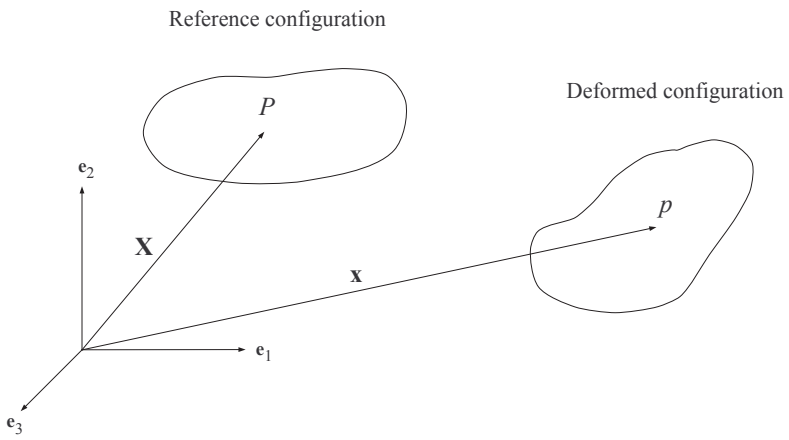

Figure 3.1: Reference and deformed configuration

Consider the vector $d\mathbf{X}$ established by two closely related material points in the reference configuration. The linear map from the reference configuration to the deformed configuration is uniquely defined by

$$d\mathbf{x} = \mathbf{F} d\mathbf{X} \tag{3.3}$$

where

$$\mathbf{F} = \frac{\partial \mathbf{x}}{\partial \mathbf{X}} \tag{3.4}$$

is called the *material deformation gradient* since the derivation is performed with respect to the material coordinates. Note that $\mathbf{F}$ is defined locally since it maps a vector defined by two closely situated material points.

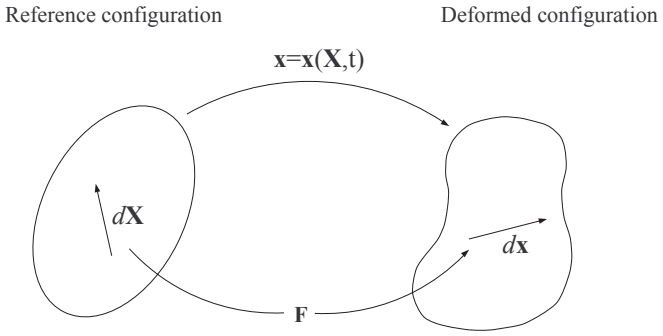

Figure 3.2: Deformation gradient

The Jacobian J is the determinant of the material deformation gradient $\mathbf{F}$

$$J = det\mathbf{F} \tag{3.5}$$

It is shown in Ottosen and Ristinmaa (2001) that a change in volume caused by deformation can be described as

$$\frac{dv}{dV} = \frac{\rho_0}{\rho} = J \tag{3.6}$$

Since dv/dV clearly is a positive quantity we must have that $J > 0$. This provides us with a linear equation system so that in the Eulerian description, $\mathbf{X}$ can be derived according to

$$d\mathbf{X} = \mathbf{F}^{-1} d\mathbf{x} \tag{3.7}$$

Equation (3.7) shows that it exists a unique relation between $d\mathbf{X}$ and $d\mathbf{x}$. This implies that if the deformed position vector $\mathbf{x}$ is known, also the initial position vector can be derived following the Eulerian description.

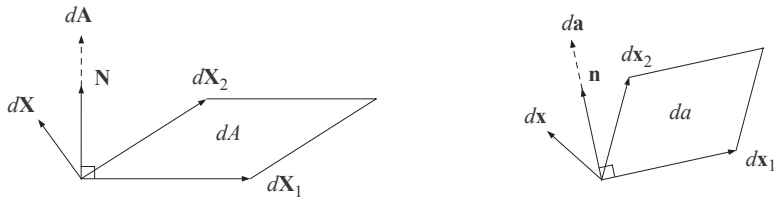

Figure 3.3: The area dA in the reference configuration and the area da in the deformed configuration

To obtain a relation between the areas before and after deformation, the following approach is adopted. Introduce dA which is an infinitely small area spanned up by two vectors $d\boldsymbol{X}_1$ and $d\boldsymbol{X}_2$. To create a vector, $d\mathbf{A}$, the area dA is multiplied with $\mathbf{N}$, a vector normal to the plane. This procedure is also made with the deformed configuration as a starting point and it results in

$$d\mathbf{A} = \mathbf{N}dA \qquad \text{and} \qquad d\mathbf{a} = \mathbf{n}da \tag{3.8}$$

Using $d\mathbf{x} = \mathbf{F}d\mathbf{X}$ and $dv = JdV$, the *Nanson's formula* can be established as

$$d\mathbf{a} = J\mathbf{F}^T d\mathbf{A} \tag{3.9}$$

A decomposition of the material deformation gradient can be made with the polar decomposition theorem of Cauchy, since $\mathbf{F}$ is non-singular. The theorem states that it exists two unique symmetric positive definite tensors $\mathbf{U}$ and $\mathbf{V}$ and an orthogonal tensor $\mathbf{R}$, such that

$$\mathbf{F} = \mathbf{RU} = \mathbf{VR} \tag{3.10}$$

where $\mathbf{U}$ and $\mathbf{V}$ are called the *right and left stretch tensor*, respectively.

It can be shown that the decomposition can be written as

$$d\mathbf{x} = \mathbf{RU}d\mathbf{X} \tag{3.11}$$

indicating that the body first is stretched and then rotated. Note that for uniaxial deformation for isotropic materials and for anisotropic materials with aligned material directions, the following in matrix notation is valid

$$\mathbb{R} = \mathbb{I} \qquad \text{and} \qquad \mathbb{U} = \begin{bmatrix} \frac{l}{l_0} & & \\ & \frac{a}{a_0} & \\ & & \frac{b}{b_0} \end{bmatrix}$$

where l_0, a_0 and b_0 are the lenght, height and width of the initial test sample.

3.2 Strain tensor

The strain tensor is a quantity to measure only the deformation of the body and not the rigid body motion. There are many different strain tensors that can be used, but here the Lagrangian strain tensor will be explained.

To start with, it is stated that a change of distance between two particles is related to the deformation of a body. The length of the two vectors $d\mathbf{X}$ and $d\mathbf{x}$ in Figure 3.2 can be written as

$$dS^2 = d\mathbf{X}^T d\mathbf{X} \qquad \text{and} \qquad ds^2 = d\mathbf{x}^T d\mathbf{x} \tag{3.12}$$

A relation between the lengths in the reference and the deformed configuration is given by

$$ds^2 = d\mathbf{X}^T \mathbf{C} d\mathbf{X} \tag{3.13}$$

where

$$\mathbf{C} = \mathbf{F}^T\mathbf{F} \tag{3.14}$$

The tensor is symmetric, i.e. $\mathbf{C} = \mathbf{C}^T$, and is called the *Right Cauchy-Green deformation tensor*. As noted in (3.15) it is clear that this quantity only contains information of the deformation and not the rotation of the body since

$$\mathbf{C} = \mathbf{F}^T\mathbf{F} = \mathbf{U}^T\mathbf{R}^T\mathbf{R}\mathbf{U} = \mathbf{U}^T\mathbf{U} \tag{3.15}$$

To measure the change of distance before and after the deformation, ds and dS are compared. A rigid body motion makes no contribution to the change in distance between the particles and is therefore not considered.

$$ds^2 - dS^2 = 2d\mathbf{X}^T\mathbf{E}d\mathbf{X} \tag{3.16}$$

where

$$\mathbf{E} = \frac{1}{2}(\mathbf{C} - \mathbf{I}) = \frac{1}{2}(\mathbf{F}^T\mathbf{F} - \mathbf{I}) \tag{3.17}$$

is called the *Lagrangian strain tensor* and is symmetric i.e. $\mathbf{E} = \mathbf{E}^T$

With the Lagrangian description, the position of a particle in the deformed configuration can be described using a displacement vector $\mathbf{u}$ according to

$$\mathbf{x} = \mathbf{u}(\mathbf{X}, t) + \mathbf{X} \tag{3.18}$$

Combining (3.3) and (3.18) results in

$$\mathbf{F} = \frac{\partial \mathbf{x}}{\partial \mathbf{X}} = \frac{\partial \mathbf{u}}{\partial \mathbf{X}} + \mathbf{I} \tag{3.19}$$

Inserting (3.19) into (3.17) it is possible to derive a new expression for the Lagrangian strain tensor

$$\mathbf{E} = \frac{1}{2}(\frac{\partial \mathbf{u}}{\partial \mathbf{X}} + \frac{\partial \mathbf{u}}{\partial \mathbf{X}} + \frac{\partial \mathbf{u}}{\partial \mathbf{X}}\frac{\partial \mathbf{u}}{\partial \mathbf{X}}) \tag{3.20}$$

With small displacements gradients no distinction needs to be taken between the material coordinates $\mathbf{X}$ and the spatial coordinates $\mathbf{x}$. Therefore the strain tensor reduces to the small strain tensor.

$$\mathbf{E} \approx \boldsymbol{\epsilon} = \frac{1}{2}(\frac{\partial \mathbf{u}}{\partial \mathbf{x}} + \frac{\partial \mathbf{u}}{\partial \mathbf{x}}) \tag{3.21}$$

3.3 Multiplicative split of the deformation gradient

For large strain plasticity, the deformation gradient needs to be further investigated in order to be useful in constitutive theory. To separate the elastic and plastic deformation, the concept of multiplicative split is introduced.

The deformation gradient can be written as

$$\mathbf{F} = \frac{\partial \mathbf{x}}{\partial \mathbf{X}} = \frac{\partial \mathbf{x}}{\partial \bar{\mathbf{x}}} \frac{\partial \bar{\mathbf{x}}}{\partial \mathbf{X}} = \mathbf{F}^e \mathbf{F}^p \tag{3.22}$$

where

$$\mathbf{F}^e = \frac{\partial \mathbf{x}}{\partial \bar{\mathbf{x}}} \qquad\qquad \mathbf{F}^p = \frac{\partial \bar{\mathbf{x}}}{\partial \mathbf{X}} \tag{3.23}$$

The concept is based on introducing a third configuration, complementing the reference and the deformed configuration. It is called the *intermediate configuration* and is denoted $\bar{\mathbf{x}}$, see Figure 3.4 . The state in this new configuration is obtained by an imagined purely elastic unloading from the deformed configuration. This means that in the intermediate configuration only the plastic deformations remain, i.e. it is stress-free.

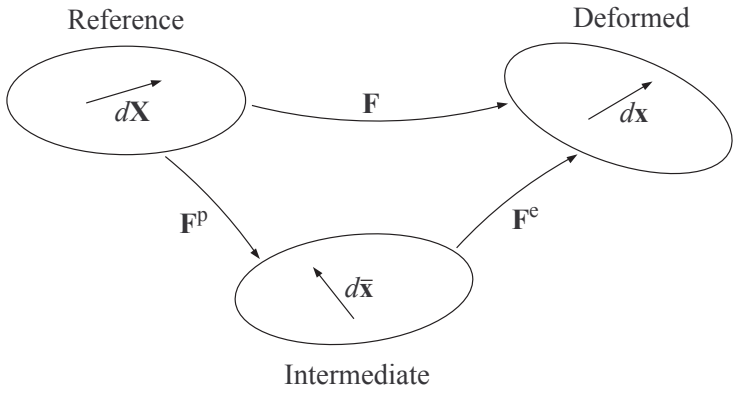

Figure 3.4: The mapping between the different configurations

Inserting (3.22) in the Lagrangian strain tensor results in

$$\mathbf{E} = \mathbf{F}^{pT} \mathbf{E}^e \mathbf{F}^p + \mathbf{E}^p \tag{3.24}$$

where

$$\mathbf{E}^e = \frac{1}{2}(\mathbf{C}^e - \mathbf{I}) \qquad \mathbf{C}^e = \mathbf{F}^{eT}\mathbf{F}^e \tag{3.25}$$

$$\mathbf{E}^p = \frac{1}{2}(\mathbf{C}^p - \mathbf{I}) \qquad \mathbf{C}^p = \mathbf{F}^{pT}\mathbf{F}^p \tag{3.26}$$

Since every rigid body motion results in a specific intermediate configuration, infinitely many choices for this configuration can be made. Therefore, the intermediate configuration is not uniquely defined. This is not problematic because any choice of the intermediate configuration will result in the same formulations. The choice made here for the intermediate configuration is the *isoclinic configuration*, in which the vectors defining the orientation of the substructure are chosen to have the same orientation as the direction vectors in the reference configuration. The isoclinic configuration is in detail described in Dafalias (1986).

3.4 Rate of deformation tensor

It is of most interest to determine the evolution of the deformation gradient, i.e. $\dot{\mathbf{F}}$. To do so, the *spatial velocity gradient* is defined as

$$\mathbf{L} = \frac{\partial \mathbf{v}}{\partial \mathbf{x}} \tag{3.27}$$

The velocity gradient can also be decomposed into an symmetric and anti symmetric part according to

$$\mathbf{D} = \frac{1}{2}(\mathbf{L} + \mathbf{L}^T) \qquad \mathbf{W} = \frac{1}{2}(\mathbf{L} - \mathbf{L}^T) \tag{3.28}$$

where $\mathbf{D}$ is the *rate of deformation tensor* and $\mathbf{W}$ is the *spin tensor*

From (3.27) it follows that

$$\mathbf{L} = \frac{\partial \mathbf{v}}{\partial \mathbf{X}}\frac{\partial \mathbf{X}}{\partial \mathbf{x}} = \frac{\partial \mathbf{v}}{\partial \mathbf{X}}\mathbf{F}^{-1} \tag{3.29}$$

Taking the material time derivative of the deformation gradient results in

$$\dot{\mathbf{F}} = \frac{\partial}{\partial t}\left(\frac{\partial \mathbf{x}}{\partial \mathbf{X}}\right) = \frac{\partial}{\partial \mathbf{X}}\left(\frac{\partial \mathbf{x}}{\partial t}\right) = \frac{\partial \mathbf{v}}{\partial \mathbf{X}} \tag{3.30}$$

Inserting (3.30) into (3.29) the evolution of the deformation gradient then follows as

$$\dot{\mathbf{F}} = \mathbf{L}\mathbf{F} \tag{3.31}$$

3.5 Stress tensors

As mentioned earlier the use of large strain theory results in many choices of strain tensors. Not surprisingly, it is possible to derive a number of stress tensors as well. Here, quantities in the reference configuration will be examined and after investigating the thermodynamics, stress tensors in the intermediate configuration will be established.

Establishing the equations of motion in the Lagrangian description leads, after some calculations, to the *First Piola-Kirchhoff stress tensor*

$$\mathbf{P} = J\boldsymbol{\sigma}\mathbf{F}^{-T} \tag{3.32}$$

where $\mathbf{P}$ is unsymmetric, i.e. $\mathbf{P} \neq \mathbf{P}^T$ and the *Second Piola-Kirchhoff stress tensor*

$$\mathbf{S} = J\mathbf{F}^{-1}\boldsymbol{\sigma}\mathbf{F}^{-T} \tag{3.33}$$

where $\mathbf{S}$ is symmetric, i.e. $\mathbf{S} = \mathbf{S}^T$. The first and the second Piola-Kirchhoff stress tensors are related as

$$\mathbf{S} = \mathbf{F}^{-1}\mathbf{P} \tag{3.34}$$

From the important principle of virtual power the concept of energy conjugated stress and strain tensors are introduced. If the scalar between the stress and strain tensor is the power per unit volume, they are conjugated quantities.

- $\boldsymbol{\sigma}$ and $\mathbf{D}$ are conjugated quantities in the deformed configuration
- $\mathbf{P}$ and $\frac{D\mathbf{F}}{Dt}$ are conjugated quantities in the reference configuration
- $\mathbf{S}$ and $\frac{D\mathbf{E}}{Dt}$ are conjugated quantities in the reference configuration

3.6 Thermodynamics

In the first law of thermodynamics the conservation of energy principle is stated. Energy can not be created nor be destroyed, it can only change form. The first law has no restriction on the direction of a process.

The second law of thermodynamics states that mechanical work can be converted completely into heat but an amount of heat can not be converted entirely into mechanical work. A process will not occur unless it satisfies both the first and the second law of thermodynamics. These laws of thermodynamics are postulates, i.e. they are no laws of nature but are accepted as axioms, cf. Cengel and Boles (1998)

To proceed further, the following definitions are stated

- *State variables are quantities that characterise the state of the system*
- *A state function is a function that only depends on the state of the system and not on the manner in which this state is achieved.*
- *A process is reversible if both the system and all its surroundings can be brought back to their initial conditions. A process that is not reversible is irreversible.*

The second law together with Helmholtz free energy function $\psi(E^e, \kappa)$ as a state function, can be written in the form of a dissipation inequality.

Dissipation inequality in terms of free energy

$$\gamma_0 \geq 0$$

where

$$\gamma_0 = -\varrho_0(\dot{\psi} + s\dot{\theta}) + \mathbf{S} : \dot{\mathbf{E}} - \frac{1}{\theta} J \mathbf{q} \frac{\partial \theta}{\partial \mathbf{x}}$$

where ϱ_0 is the mass density in the reference configuration, s the specific entropy, θ the temperature and $\mathbf{q}$ the heat flux vector.

For isothermal processes the dissipation inequality is expressed as

Dissipation inequality for isothermal processes in terms of free energy ψ

$$\gamma_0 \geq 0$$

where

$$\gamma_0 = -\varrho\dot{\psi} + \mathbf{S} : \dot{\mathbf{E}}$$

When $\gamma_0 = 0$ the process is reversible and when $\gamma_0 > 0$ the process is irreversible.

3.7 Elasto-plasticity

In this part two different formulations of dissipation inequalities for isothermal conditions are derived. From these inequalities two yield functions are obtained. A yield function utilizes the elastic strain and the history of plastic loading to characterise the state of the material that have undergone plastic deformation.

From the dissipation inequality for isothermal processes, the following expression is derived in Ristinmaa (2003)

$$\gamma_0 = \bar{\mathbf{S}} : \dot{\bar{\mathbf{E}}}^p - K\dot{\kappa} \geq 0 \tag{3.35}$$

where $\bar{\mathbf{S}}$ is the second Piola-Kirchhoff stress tensor in the intermediate configuration and related to the first Piola-Kirchhoff stress tensor as

$$\bar{\mathbf{S}} = \mathbf{F}^p \mathbf{P} \mathbf{F}^{pT} \tag{3.36}$$

Also the following definitions are introduced

$$\dot{\bar{\mathbf{E}}}^p = \frac{1}{2}(\mathbf{l}^{pT}\mathbf{C}^e + \mathbf{C}^e\mathbf{l}^p) \tag{3.37}$$

and

$$K = \varrho_0 \frac{\partial \psi}{\partial \kappa} \tag{3.38}$$

where κ is a variable that describes the history of plastic loading and K is the thermodynamic force conjugated to $\dot{\kappa}$.

Since $\bar{\mathbf{S}}$ is conjugated to $\dot{\bar{\mathbf{E}}}^p$ and K is conjugated to κ the yield function is stated as

$$f(\bar{\mathbf{S}}, K; \mathbf{e}_\beta) \tag{3.39}$$

where

$$f \leq 0 \tag{3.40}$$

for all allowable processes. $\mathbf{e}_\beta$ defines the three material directions, $\beta = 1, 2, 3$. One way to fulfill the dissipation inequality (3.35), is the *postulate of maximum dissipation*, i.e. to maximize γ_0 in (3.35) with respect to the constraint (3.40). This results in that the evolution equations can be stated as

$$\dot{\bar{\mathbf{E}}}^p = \dot{\lambda}\frac{\partial f}{\partial \bar{\mathbf{S}}} \qquad\qquad \dot{\kappa} = -\dot{\lambda}\frac{\partial f}{\partial K} \tag{3.41}$$

The so-called Kuhn-Tucker conditions given by

$$\dot{\lambda} \geq 0 \qquad \text{and} \qquad \dot{\lambda} f = 0 \tag{3.42}$$

conclude that if $f < 0$ then $\dot{\lambda} = 0$ (elastic loading) and $\dot{\lambda} > 0$ only occur when $f = 0$ (plastic loading). In the multiplicative split approach, $\mathbf{l}^p$ defines the rate of plastic straining. Since $\bar{\mathbf{E}}^p$ contains both elastic and plastic parameters, the evolution law given by (3.41) must be treated with care.

To reformulate the dissipation inequality into another form, the *Mandel stress* $\boldsymbol{\Sigma}$ is introduced as

$$\boldsymbol{\Sigma} = \mathbf{C}^e \bar{\mathbf{S}} \tag{3.43}$$

With the Mandel stress, (3.35) is reformulated to obtain

$$\gamma_0 = \boldsymbol{\Sigma} : \mathbf{l}^p - K\dot{\kappa} \geq 0 \tag{3.44}$$

The Mandel stress $\boldsymbol{\Sigma}$ is conjugated to $\mathbf{l}^p$ and K is the thermodynamic force conjugated to κ. Thus, the yield function is expressed as

$$f(\boldsymbol{\Sigma}, K; \mathbf{e}_\beta) \tag{3.45}$$

where

$$f \leq 0 \tag{3.46}$$

for all allowable processes. With employment of the postulate of maximum dissipation, the evolution law can be derived with the following result

$$\mathbf{l}^p = \dot{\lambda}\frac{\partial f}{\partial \boldsymbol{\Sigma}} \qquad\qquad \dot{\kappa} = -\dot{\lambda}\frac{\partial f}{\partial K} \tag{3.47}$$

where $\dot{\lambda}$ and f are subjected to the Kuhn-Tucker conditions.

Chapter 4

Continuum model

The 3DM model is divided into a continuum model and an interface model. The continuum model describes the behaviour within a paperboard ply and the interface describes the interaction between two opposing plies, see Ristinmaa (2003). The interface model is introduced in chapter 6.

Paper and paperboard are orthotropic materials as a result of the manufacturing method. The three directions are denoted machine direction (MD), out of plane direction (ZD) and cross direction (CD). These directions are defined by three base vectors $\mathbf{e}_i (i \in \{1, 2, 3\})$ according to Figure 4.1. It is in Xia (2002) assumed that plasticity only occurs within the plane MD-CD.

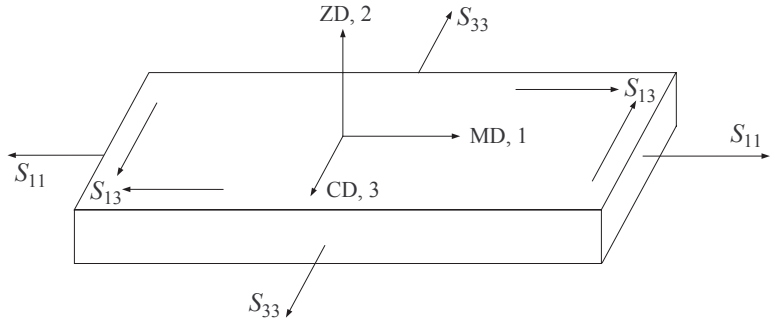

Figure 4.1: A single ply of a paperboard

4.1 Elastic behaviour

The elastic response is modeled as

$$\bar{\mathbf{S}} = \mathbf{A} : \mathbf{E}^e \tag{4.1}$$

which is a linear relationship between the second Piola-Kirchhoff stress tensor $\bar{\mathbf{S}}$ and the elastic strain tensor $\mathbf{E}^e$, both defined in the intermediate configuration. $\mathbf{A}$ describes the elastic orthotropy of the paper. With matrix representation, the elastic response is expressed as

$$\begin{bmatrix} \bar{S}_{11} \\ \bar{S}_{22} \\ \bar{S}_{33} \\ \bar{S}_{12} \\ \bar{S}_{13} \\ \bar{S}_{23} \end{bmatrix} = \begin{bmatrix} \frac{E_1}{1-\nu_{31}\nu_{13}} & 0 & \frac{E_1\nu_{31}}{1-\nu_{31}\nu_{13}} & 0 & 0 & 0 \\ 0 & E_2 & 0 & 0 & 0 & 0 \\ \frac{E_1\nu_{31}}{1-\nu_{31}\nu_{13}} & 0 & \frac{E_3}{1-\nu_{31}\nu_{13}} & 0 & 0 & 0 \\ 0 & 0 & 0 & G_{12} & 0 & 0 \\ 0 & 0 & 0 & 0 & G_{13} & 0 \\ 0 & 0 & 0 & 0 & 0 & G_{23} \end{bmatrix} \begin{bmatrix} E_{11} \\ E_{22} \\ E_{33} \\ 2E_{12} \\ 2E_{13} \\ 2E_{23} \end{bmatrix} \tag{4.2}$$

where $\mathbf{A}$ is symmetric and the out-of-plane Poisson ratios are zero. The elastic modulus in the ZD direction is assumed to be given by

$$E_2 = \begin{cases} E_2^0, & E_{22}^e > 0 \\ E_2^0 exp(-aE_{22}^e), & E_{22}^e < 0 \end{cases} \tag{4.3}$$

4.2 Thermodynamic consistency - elastic part

The hypo-elastic stress-strain law derived from Helmholtzs free energy function is

$$\bar{\mathbf{S}} = \varrho_0 \frac{\partial \psi}{\partial \mathbf{E}^e} \tag{4.4}$$

Assuming the plastic part decouples from the elastic part and use of (4.1) it is derived that

$$\varrho_0 \psi = \frac{1}{2} \mathbf{E}^e : \mathbf{A} : \mathbf{E}^e + \psi^p(\kappa) \tag{4.5}$$

where the non-linear part for compression in the out of plane direction is neglected. Use of (3.36) and (3.34) provides the St. Venant-Kirchoff material model, which is valid for small strains and large rotations

$$\bar{\mathbf{S}} = \varrho_0 \frac{\partial \psi}{\partial \mathbf{E}^e} = \mathbf{A} : \mathbf{E}^e \tag{4.6}$$

This model can not in general predict a correct stress response for compressive strains in the out-of-plane direction. This implies that two different forms of Helmholtz's free energy have to be used.

With

$$\nu_{12} = \nu_{21} = \nu_{23} = \nu_{32} = 0 \tag{4.7}$$

it can be shown that the out-of -plane behaviour is fully decoupled from the in-plane behaviour. This makes it possible to treat the out-of-plane behaviour separately. With compression in the out-of-plane direction, the free energy function is

$$\varrho\psi = (\mathbb{E}^e)^T \mathbb{A}_2 \mathbb{E}^e - \frac{E_2^0}{a^2}(1 + aE_{22}^e)exp(-aE_{22}^e) + \psi^p(\kappa) \tag{4.8}$$

where E_2 is decoupled from $\mathbb{A}$. $\mathbb{A}_2$ is expressed as

$$\begin{bmatrix} \frac{E_1}{1-\nu_{31}\nu_{13}} & 0 & -\frac{E_1\nu_{31}}{1-\nu_{31}\nu_{13}} & 0 & 0 & 0 \\ 0 & 0 & 0 & 0 & 0 & 0 \\ -\frac{E_1\nu_{31}}{1-\nu_{31}\nu_{13}} & 0 & \frac{E_3}{1-\nu_{31}\nu_{13}} & 0 & 0 & 0 \\ 0 & 0 & 0 & G_{12} & 0 & 0 \\ 0 & 0 & 0 & 0 & G_{13} & 0 \\ 0 & 0 & 0 & 0 & 0 & G_{23} \end{bmatrix} \tag{4.9}$$

This model is thermodynamically consistent when the Poisson ratios are chosen according to (4.7).

4.3 Plastic behaviour

The yield function proposed in Xia (2002) is build up as a sum of yield planes, i.e.

$$f(\bar{\mathbf{S}}, \gamma; \mathbf{N}_\alpha) = \sum_{\alpha=1}^{n} \left(\chi_\alpha \frac{\bar{\mathbf{S}} : \mathbf{N}_\alpha}{S_\alpha(\bar{\gamma})} \right)^{2k} - 1 \tag{4.10}$$

where $\bar{\mathbf{S}}$ is the symmetric second Piola-Kirchhoff stress tensor defined in the intermediate configuration. The value k is taken to be a positive integer and is treated more thoroughly later on.

χ_α controls the number of active yield planes in each load case and is given as

$$\chi_\alpha = \begin{cases} 1 & \text{if } \bar{\mathbf{S}} : \mathbf{N}_\alpha > 0 \\ 0 & \text{otherwise} \end{cases} \tag{4.11}$$

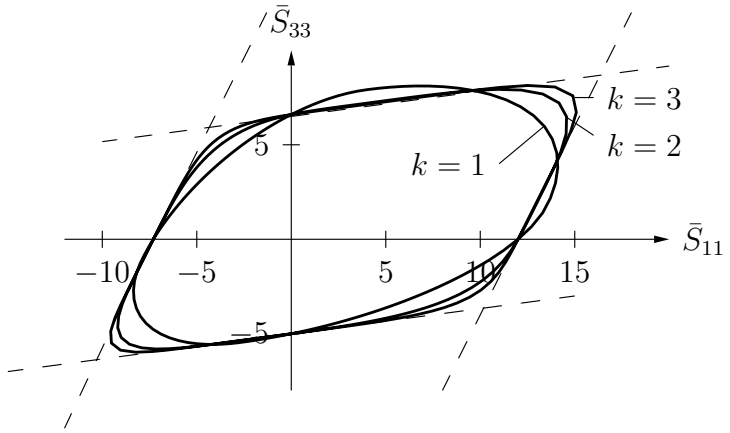

Figure 4.2: The shape of the yield surface for different values of k.

Paperboard's orthotropic behaviour is described by $\mathbf{N}_\alpha$ which consists of constant symmetric second order tensors. The tensors are defined by the gradients of the six yield planes. It is assumed that $\mathbf{N}_\alpha$ is a unit gradient.

The function $S_\alpha(\bar{\gamma})$ describes the isotropic hardening and $\bar{\gamma}$ is the internal variable describing the history of plastic loading, i.e. $\bar{\gamma}$ represents the accumulated plastic strain.

The plastic velocity gradient is given by the following evolution law

$$\mathbf{l}^p = \lambda \frac{\partial f}{\partial \bar{\mathbf{S}}} \tag{4.12}$$

Note that $\mathbf{l}^p$ and $\bar{\mathbf{S}}$ are not energy conjugated. With the proposed yield function (4.10), the yield surface gradient becomes

$$\frac{\partial f}{\partial \bar{\mathbf{S}}} = \sum_{\alpha=1}^{n} a_\alpha \chi_\alpha \mathbf{N}_\alpha \tag{4.13}$$

where

$$a_\alpha = 2k \frac{\Lambda_\alpha^{2k-1}}{S_\alpha} \qquad \text{and} \qquad \Lambda_\alpha = \frac{\bar{\mathbf{S}} : \mathbf{N}_\alpha}{S_\alpha} \tag{4.14}$$

The tensor scalar product $\bar{\mathbf{S}} : \mathbf{N}_\alpha$ is symmetric, therefore $\mathbf{l}^p$ becomes symmetric. The antisymmetric part of $\mathbf{l}^p$ is for the isoclinic configuration related to the changes in micro structure and is assumed to be zero. The magnitude of plastic stretching rate is defined as

$$\dot{\bar{\gamma}} = (\mathbf{l}^p : \mathbf{l}^p)^{1/2} = \lambda \left(\frac{\partial f}{\partial \bar{\mathbf{S}}} : \frac{\partial f}{\partial \bar{\mathbf{S}}} \right)^{1/2} \tag{4.15}$$

4.4 Thermodynamic consistency-plastic part

For elasto-plasticity two different evolution laws for plastic strains were derived

$$\dot{\bar{\mathbf{E}}}^p = \dot{\lambda} \frac{\partial f}{\partial \bar{\mathbf{S}}} \qquad \text{and} \qquad \mathbf{l}^p = \dot{\lambda} \frac{\partial f}{\partial \boldsymbol{\Sigma}} \tag{4.16}$$

Both of the evolution laws fulfill the dissipation inequality, i.e. they fulfill the second law of thermodynamics. The model for plastic evolution in Xia (2002), is a combination of these two and the model is not associative because $\mathbf{l}^p$ and $\bar{\mathbf{S}}$ are not energy conjugated. It is concluded that it is not possible to *a priori* state that the second law of thermodynamics is fulfilled. However, as noted in (3.43) the Mandel stress and the second Piola-Kirchhoff stress in the intermediate configuration becomes identical if it is assumed that the elastic part of the deformation is small, i.e. $\mathbf{C}^e = \mathbf{I}$.

Table 4.1: A summary of the in-plane plasticity model.

Elastic part

-Kinematic relations

$$\mathbf{F}^e = \mathbf{F}\mathbf{F}^{p-1}$$

$$\mathbf{E}^e = \frac{1}{2}(\mathbf{F}^{eT}\mathbf{F}^e - \mathbf{I})$$

-Stress-strain relation

$$\bar{\mathbf{S}} = \mathbf{A} : \mathbf{E}^e$$

Plastic part

-Yield function

$$f = \sum_{\alpha=1}^{n} \left(\chi_\alpha \frac{\bar{\mathbf{S}} : \mathbf{N}_\alpha}{S_\alpha(\bar{\gamma})} \right)^{2k} - 1$$

$$\chi_\alpha = \begin{cases} 1 & \text{if } \bar{\mathbf{S}} : \mathbf{N}_\alpha > 0 \\ 0 & \text{otherwise} \end{cases}$$

-Evolution laws

$$\mathbf{l}^p = \lambda \frac{\partial f}{\partial \bar{\mathbf{S}}}$$

$$\dot{\mathbf{F}}^p = \mathbf{l}^p \mathbf{F}^p$$

$$\dot{\bar{\gamma}} = \lambda (\frac{\partial f}{\partial \bar{\mathbf{S}}} : \frac{\partial f}{\partial \bar{\mathbf{S}}})^{1/2}$$

4.5 Implementation of the continuum model

A more detailed description of the implementation can be found in Nygårds (2004). To start with, the flow direction for each deformation system, i.e. a unit normal to the yield surface, is expressed as

$$\mathbf{K} = \frac{\hat{\mathbf{K}}}{||\hat{\mathbf{K}}||} \tag{4.17}$$

where

$$\hat{\mathbf{K}} = \frac{\partial f}{\partial \bar{\mathbf{S}}} \tag{4.18}$$

With (4.17), the plastic flow rule becomes

$$\mathbf{l}^p = \mathbf{K}\dot{\bar{\gamma}} \tag{4.19}$$

Furthermore, the time τ is introduced as

$$\tau = t + \Delta t$$

The radial return method is used to compute the stresses. The first step is to calculate an elastic trial stress according to

$$\bar{\mathbf{S}}^{tr} = \mathbf{A}\mathbf{E}^e(\tau) \tag{4.20}$$

The yield function determines if plastic deformation occurs in this step. If $f\left(\bar{\mathbf{S}}^{tr}, \bar{\gamma}_{(t)}\right) \leq 0$ the trial step results in a purely elastic response and it follows that

$$\bar{\mathbf{S}}(\tau) = \bar{\mathbf{S}}^{tr} \tag{4.21}$$

If $f\left(\bar{\mathbf{S}}^{tr}, \bar{\gamma}_{(t)}\right) \geq 0$ plastic deformation occurs in this increment and the radial return method goes back to the yield surface stress point in radial direction from the trial stress point, see Figure 4.3. This is formulated as

$$\bar{\mathbf{S}}(\tau) = \bar{\mathbf{S}}^{tr} - \mathbf{A}\Delta\bar{\gamma}\mathbf{K} \tag{4.22}$$

where

$$\Delta\bar{\gamma} = \dot{\bar{\gamma}}\Delta t \tag{4.23}$$

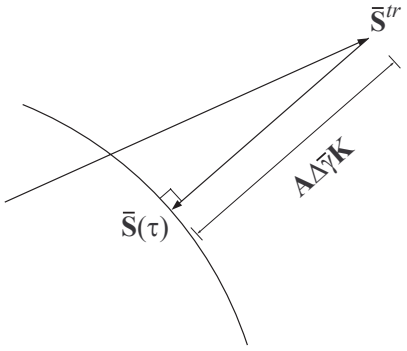

Figure 4.3: The radial return to the yield surface

The radial return method relies on the evaluation of the stresses and hardening parameters at a state that is not known *a priori* and is therefore an implicit method called a backward scheme.

Since $f = 0$ must be fulfilled when determining the stresses $\bar{\mathbf{S}}(\tau)$, there are four non-linear equations to be minimized in order to obtain the four unknowns ($\bar{S}_{11}, \bar{S}_{33}, \bar{S}_{13}$ and $\Delta\bar{\gamma}$). The equations formulating the problem are:

$$\Omega = \begin{bmatrix} \sum_{\alpha=1}^{n} \left(\chi_\alpha \frac{\bar{\mathbf{S}}:\mathbf{N}_\alpha}{S_\alpha(\bar{\gamma})} \right)^{2k} - 1 = 0 \\ \bar{S}_{11}(\tau) - \bar{S}_{11}^{tr} + \Delta\bar{\gamma} A_{11ij} K_{ij} = 0 \\ \bar{S}_{33}(\tau) - \bar{S}_{33}^{tr} + \Delta\bar{\gamma} A_{33ij} K_{ij} = 0 \\ \bar{S}_{13}(\tau) - \bar{S}_{13}^{tr} + \Delta\bar{\gamma} A_{13ij} K_{ij} = 0 \end{bmatrix} \tag{4.24}$$

The set of equations in (4.24) are solved with a Newton-Raphson scheme.

Chapter 5

Calibration of the continuum model

The 3DM model has to be calibrated for the paperboard used. Since this report only considers Triplex 360 mN, this calibration is here performed for this paperboard. In this chapter the initial yield surface and the hardening behaviour is calibrated, see Ristinmaa (2003). The experimental data in Table 5.1 for the multilayer paperboard Triplex 360 mN are provided by Stenberg (2002).

Table 5.1: Experimental data for Material A

	Tensile yield strength (MPa)	Compressive yield strength (MPa)	Plastic strain ratio $d\epsilon_{\perp}^{p}/d\epsilon_{\parallel}^{p}$
MD	12.0	7.3	-0.5
CD	6.5	5.0	-0.133
45°	8.0		

5.1 Yield plane gradients

When calculating $\mathbf{N}_{\alpha}$ for the initial yield surface, it is assumed according to Xia (2002) that only one yield plane is active during the tests. The six planes are labeled according to

α	Plane related to
1	tension MD direction
2	tension CD direction
3	pure shear
4	compression MD direction
5	compression CD direction
6	pure shear

With $\mathbf{N}_\alpha$ describing the gradient of the active plane together with (4.12) and (4.13), it gives that

$$\mathbf{l}^p \propto \mathbf{N}_\alpha \tag{5.1}$$

For MD tensile tests it is assumed that $l^p_{13} = 0$ and (5.1) becomes

$$(l^p_{11}, l^p_{33}) \propto ((N_{11})_{(1)}, (N_{33})_{(1)}) \tag{5.2}$$

With the plastic strain ratio from Table 5.1 it follows that

$$\frac{l^p_{33}}{l^p_{11}} = \frac{(N_{33})_{(1)}}{(N_{11})_{(1)}} = -0.5 \tag{5.3}$$

$\mathbf{N}_\alpha$ is a unit gradient, i.e. $[(N_{11})_{(1)}]^2 + [(N_{33})_{(1)}]^2 = 1$ and it is derived that

$$(N_{11})_{(1)} = 2/\sqrt{5} \qquad (N_{33})_{(1)} = -1/\sqrt{5}$$

For MD compression tests it is assumed that $N_{(4)} = -N_{(1)}$, although the model allows for $N_{(4)}$ to differ from $-N_{(1)}$. For tension and compression in the CD direction, the gradients are calculated following the same procedure as above.

For pure shear loading it is assumed that $l^p_{11} = l^p_{33} = 0$. Using that $\mathbf{N}_\alpha$ is a symmetric unit tensor, it follows that

$$(N_{13})_{(3)} = (N_{31})_{(3)} = \sqrt{2}/2$$

In Table 5.2 the six gradients are shown and it is used that $\alpha = 3$ and $\alpha = 6$ are identical since it is expected that the pure shear loadings S_{13} and $-S_{13}$ can not be distinguished. Figure 5.1 shows the yield planes and the gradients when $\bar{S}_{13} = 0$.

Table 5.2: $\mathbf{N}_\alpha$ components

α	$(N_{11})_\alpha$	$(N_{33})_\alpha$	$(N_{13})_\alpha$
1	$2/\sqrt{5}$	$-1/\sqrt{5}$	0
2	$-2/\sqrt{229}$	$15/\sqrt{229}$	0
3	0	0	$\sqrt{2}/2$
4	$-2/\sqrt{5}$	$1/\sqrt{5}$	0
5	$2/\sqrt{229}$	$-15/\sqrt{229}$	0
6	0	0	$-\sqrt{2}/2$

It can easily be shown that the assumption that only one yield plane is active is incorrect. Using (4.11) and Table 5.2 during tension in the MD-direction it follows that yield planes 1 and 5 are active. Yet, with large values of k it will show that it is an acceptable assumption.

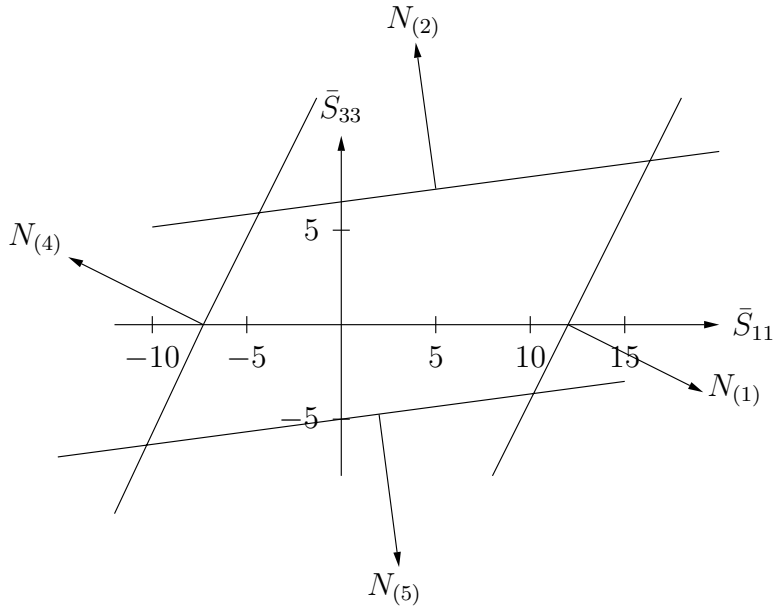

Figure 5.1: The yield planes and gradients when $\bar{S}_{13} = 0$

5.2 Initial yielding

Contrary to determining the gradients, several yield planes can be active when calibrating the initial yielding.

$\mathbf{F} = \mathbf{F}^e\mathbf{F}^p$ becomes $\mathbf{F}^e\mathbf{I} = \mathbf{F}$ since initial yielding is considered where the yield surface is reached when loading in the elastic region. Considering tension in MD direction and using

Table 5.3: Initial values of S_α

$S^0_{(1)} = S_{(1)}$ (MPa)	$S^0_{(2)} = S_{(2)}$ (MPa)	$S^0_{(3)} = S_{(3)}$ (MPa)	$S^0_{(4)} = S_{(4)}$ (MPa)	$S^0_{(5)} = S_{(5)}$ (MPa)
10.7	6.6	5.9	6.5	5.0

$\bar{\mathbf{S}} = \mathbf{F}^{-1}\mathbf{P}$ together with (3.19) and assuming that the stresses in Table 5.1 are nominal stresses we get

$$\bar{S}^t_{11} = \frac{(P^t_{y0})_{11}}{1+\epsilon_{11}} \qquad \epsilon_{11} = \frac{l - l_0}{l_0} \tag{5.4}$$

In (5.4) $(P^t_{y0})_{11}$ is the tensile strength in the MD direction and ϵ_{11} is the nominal strain calculated from the length of the specimen in current and reference configuration. Expression (5.4) also holds for compression if $\bar{S}^c_{11}$ and $(P^c_{y0})_{11}$ are used instead. Expression (5.4) is also valid for tension/compression in the CD direction if the notations are changed. Since the elastic strain before yielding is very small, (5.4) can be approximated as $\bar{S}^t_{11} = (P^c_{y0})_{11}$. This approximation holds for every considered direction.

Using the yield function (4.10) and (4.11) with the yield plane gradients from Table 5.2 the following equation is derived

$$\left(\frac{\bar{S}^t_{11}(N_{11})_{(1)}}{S_{(1)}}\right)^{2k} + \left(\frac{\bar{S}^t_{11}(N_{11})_{(5)}}{S_{(5)}}\right)^{2k} - 1 = 0$$

In the same fashion the equations for compression in the MD direction and tension/compression in the CD direction are derived. These four equations contains four unknowns: $S_{(1)}, S_{(2)}, S_{(4)}$ and $S_{(5)}$. Consequently, these four hardening parameters can be calculated independent of the choice of k.

With tensile tests performed 45 ° to the MD axis, the remaining quantities $S_{(3)} = S_{(6)}$ can be derived. Since orthotropy exists, the coordinate system is changed according to Mohrs circle of stress. The stress tensor $\bar{\mathbf{S}}$ in bases $\mathbf{e}_i$ becomes

$$\bar{\mathbf{S}} = \frac{\bar{S}^{45}}{2}\begin{bmatrix} 1 & 0 & 1 \\ 0 & 0 & 0 \\ 1 & 0 & 1 \end{bmatrix} \tag{5.5}$$

where $\bar{S}^{45}$ is the initial yield stress in the direction 45 ° to the MD axis. Proceeding in the same manner as before $S_{(3)}$ can be calculated.

The data in Table 5.3 are obtained with k=3. Figure 4.2 shows the shape of the yield surface for different values of k and it is evident that $k \geq 2$ is required. With $k < 2$ it is

in the figure obvious that the gradients for the yield planes and the initial yield surface do not match at the calibration points. Therefore, the plastic velocity gradient $\mathbf{l}^p$ will not develop correctly.

5.3 The hardening behaviour

Since the material parameters are different in the three material directions it follows that the hardening behaviour is anisotropic. The model proposed in Xia (2002) is expressed as

$$S_\alpha = S_\alpha^0 + A_\alpha \tanh(B_\alpha \bar{\gamma}) + C_\alpha \bar{\gamma} \tag{5.6}$$

and describes the isotropic hardening behaviour. Equation (5.6) must be calibrated for each considered material direction, i.e. calibration of the development of each yield plane. The quantity $\bar{\gamma}$ describes the hardening and must be identified for each direction. First $\bar{\gamma}$ is calibrated vs. the uniaxial stresses. Considering tension in the MD direction, with (4.11), (4.13), (4.15) and the data in Table 5.2 it follows that

$$\dot{\bar{\gamma}} = \lambda(a_1^2(\bar{\gamma}) + a_1(\bar{\gamma})a_5(\bar{\gamma})\frac{38}{\sqrt{1145}}) \tag{5.7}$$

The plastic strain rate (4.12) together with (4.13) gives

$$l_{11}^p = \lambda(a_1(\bar{\gamma})\frac{2}{\sqrt{5}} + a_5(\bar{\gamma})\frac{2}{\sqrt{229}}) \tag{5.8}$$

Combining (5.7) and (5.8), the plastic multiplier λ is eliminated to obtain the expression

$$\dot{\bar{\gamma}} = \frac{(a_1^2(\bar{\gamma}) + a_5^2(\bar{\gamma}) + a_1(\bar{\gamma})a_5(\bar{\gamma})\frac{38}{\sqrt{1145}})}{a_1(\bar{\gamma})\frac{2}{\sqrt{5}} + a_5(\bar{\gamma})\frac{2}{\sqrt{229}}} l_{11}^p \tag{5.9}$$

To derive the quantity $\bar{\gamma}$, (5.9) needs to be integrated but an explicit expression is not possible to obtain. In order to achieve a correct calibration, an analogous equation must be derived and integrated numerically. Here a simplified approach is adopted, starting with the assumption that the ratio between the strain components remain fixed during the entire loading. With (4.12), (4.13), (4.15) and the data in Table 5.2 it follows that the plastic strain rate magnitude can be expressed as

$$\dot{\bar{\gamma}} = ((l_{11}^p)^2 + (l_{33}^p)^2)^{1/2} \tag{5.10}$$

The assumption allows the use of (5.3) which for both tension and compression gives

$$\dot{\bar{\gamma}} = \frac{\sqrt{5}}{2} l^p_{11} \qquad \Rightarrow \qquad \bar{\gamma} = \frac{\sqrt{5}}{2} \int l^p_{11} dt \tag{5.11}$$

With $\dot{\mathbf{F}}^p = \mathbf{l}^p \mathbf{F}^p$ and the decomposition $\mathbf{F}$=$\mathbf{RU}$ it follows that

$$\dot{F}^p_{11} = l^p_{11} F^p_{11} \qquad \Rightarrow \qquad \ln U^p_{11} = \int l^p_{11} dt = \frac{2}{\sqrt{5}} \bar{\gamma} \tag{5.12}$$

since there is no rotation. The use of $\ln U_{11} = \ln U^e_{11} + \ln U^p_{11}$ with (5.12) results in

$$\bar{\gamma} = \frac{\sqrt{5}}{2} (\ln U_{11} - \ln U^e_{11}) \tag{5.13}$$

In order to obtain $\bar{\gamma}$ it is necessary to derive expressions for U_{11} and U^e_{11}. $\ln U_{11}$ is recognized as the logarithmic strain

$$\ln U_{11} = \ln \left(\frac{l}{l_0} \right) \tag{5.14}$$

From the elastic strain tensor (3.25) used with the elastic response (4.1) it follows that

$$(U^e_{11})^2 = 2 \frac{\bar{S}_{11}}{E_1} + 1 \tag{5.15}$$

Using (3.36) and $\mathbf{S} = \mathbf{F}^{-1} \mathbf{P}$ the stress S_{11} can be related to the nominal stress P_{11} from the experimental measurements as

$$\bar{S}_{11} = \frac{U^p_{11}}{U^e_{11}} P_{11} \tag{5.16}$$

With (5.15) and (5.16) and using the multiplicative decomposition $U_{11} = U^e_{11} U^p_{11}$ it follows that

$$((U^e_{11})^2 - 1)(U^e_{11})^2 = 2 \frac{P_{11}}{E_1} U_{11} \tag{5.17}$$

In (5.17) P_{11} and $U_{11} = l/l_0$ are obtained from stress vs. strain plots from experimental tests. Following the same procedure as above, $\bar{\gamma}$ can be obtained for compression in the MD direction and tension/compression in the CD direction. To calibrate the shear stress vs. $\bar{\gamma}$, additional approximations have to be made. From (4.11), (4.12) and (4.13) plus

assuming that the ratio between the plastic strain components remain fixed during loading in 45 ° to the MD direction it is obtained that

$$\begin{bmatrix} l^p_{11} \\ l^p_{33} \\ l^p_{13} \end{bmatrix} \propto \frac{\Lambda^{2k-1}_{(1)}}{S_{(1)}} \begin{bmatrix} (N_{11})_{(1)} \\ (N_{33})_{(1)} \\ 0 \end{bmatrix} + \frac{\Lambda^{2k-1}_{(2)}}{S_{(2)}} \begin{bmatrix} (N_{11})_{(2)} \\ (N_{33})_{(2)} \\ 0 \end{bmatrix} + \frac{\Lambda^{2k-1}_{(3)}}{S_{(3)}} \begin{bmatrix} 0 \\ 0 \\ (N_{13})_{(3)} \end{bmatrix} \tag{5.18}$$

With the data from Table 5.2 and (5.3) the ratios between the plastic strain rate components are obtained.

$$\frac{l^p_{11}}{l^p_{13}} = -0.0078 \qquad \frac{l^p_{33}}{l^p_{13}} = 0.0591 \tag{5.19}$$

With (4.15) and (5.19) it follows that

$$\dot{\bar{\gamma}} = \left((l^p_{11})^2 + (l^p_{33})^2 + 2(l^p_{13})^2\right)^{1/2} \approx \sqrt{2} l^p_{13} \tag{5.20}$$

Two bases, $\boldsymbol{e}_n$ along the 45 ° direction and $\boldsymbol{e}_m$ in the perpendicular direction, are introduced. Mohrt's circle of stress gives that $l^p_{nn} = l^p_{13}$. Thus (5.20) can be written as

$$\int l^p_{nn} dt = \frac{1}{\sqrt{2}} \bar{\gamma} \tag{5.21}$$

Adopting the same approach as for the MD direction it gives that

$$\bar{\gamma} = \sqrt{2}(\ln U_{nn} - \ln U^e_{nn}) \tag{5.22}$$

Note that this is a rough approximation since it can be shown that the elastic and plastic strains are not coaxial. Assuming that E_n being Young's modulus in the 45 ° direction it follows that

$$((U^e_{nn})^2 - 1)(U^e_{nn})^2 = 2\frac{P_{nn}}{E_n} U_{nn} \tag{5.23}$$

Equations (5.22) and (5.23) are used to obtain $\bar{\gamma}$ for shear stress.

Determining the constants A_α, B_α and C_α.

The hardening behaviour for each direction is described as

$$\begin{aligned} S_1 &= S_1^0 + A_1 \tanh(B_1\bar{\gamma}) + C_1\bar{\gamma} \\ S_2 &= S_2^0 + A_2 \tanh(B_2\bar{\gamma}) + C_2\bar{\gamma} \\ S_3 &= S_3^0 + A_3 \tanh(B_3\bar{\gamma}) + C_3\bar{\gamma} \\ S_4 &= S_4^0 + A_4 \tanh(B_4\bar{\gamma}) + C_4\bar{\gamma} \\ S_5 &= S_5^0 + A_5 \tanh(B_5\bar{\gamma}) + C_5\bar{\gamma} \\ S_6 &= S_3 \end{aligned} \tag{5.24}$$

The experimental data plots the nominal stress $P = F/A_0$ vs. the strain $\epsilon = (l - l_0)/l_0$. This data is recalculated to obtain the second Piola-Kirchhoff stress $\bar{\mathbf{S}}$ vs. $\bar{\gamma}$ as the strain measure. It is then a minimisation problem to determine the constants so that the hardening behaviour functions fit the recalculated data. This problem is solved by implementation of the numerical *least squares method*.

Considering tension in the MD direction, a given sampling of recalculated data $(S_1^i,\bar{\gamma}^i)$ where $i = 1, 2, 3...n$ makes it possible to construct the following function

$$\begin{aligned} \omega_1 &= S_1^1 - S_1^0 - A_1 \tanh(B_1\bar{\gamma}^1) - C_1\bar{\gamma}^1 \\ \omega_2 &= S_1^2 - S_1^0 - A_1 \tanh(B_1\bar{\gamma}^2) - C_1\bar{\gamma}^2 \\ &\vdots \\ \omega_n &= S_1^n - S_1^0 - A_1 \tanh(B_1\bar{\gamma}^n) - C_1\bar{\gamma}^n \end{aligned} \tag{5.25}$$

The constants has to be chosen so that $\boldsymbol{\omega}$ is minimised. Let vector $\mathbf{a}$ contain the constants A_1, B_1 and C_1 in such a way that the increment of $\mathbf{a}$ can solve the following square system

$$\left(\frac{\partial \boldsymbol{\omega}}{\partial \mathbf{a}}\right)_i^T \left(\frac{\partial \boldsymbol{\omega}}{\partial \mathbf{a}}\right)_i d\mathbf{a} = -\left(\frac{\partial \boldsymbol{\omega}}{\partial \mathbf{a}}\right)_i^T \boldsymbol{\omega}_i \tag{5.26}$$

$$\mathbf{a}_{i+1} = \mathbf{a}_i + d\mathbf{a} \tag{5.27}$$

The iteration procedure continues until the size of $(d\mathbf{a})$ is sufficiently small and as a result the constants are determined.

Chapter 6

Interface model

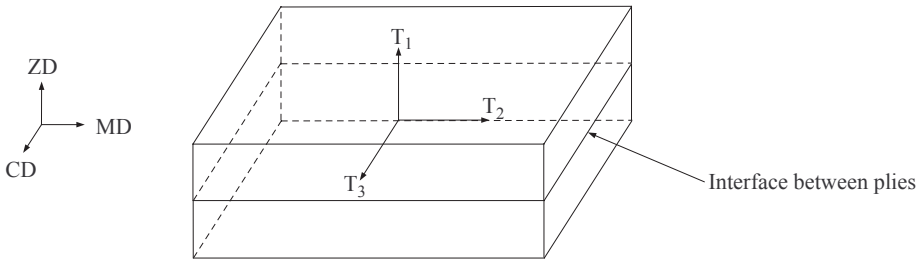

Figure 6.1: An interface between two paperboard plies

Delamination in paperboard can occur between two plies or within a ply. The interface model is developed by Xia (2002) and describes the behaviour between two surfaces and should be used where risk for delamination appears. A detailed discussion of the interface model has been given by Nygårds (2004). Similarly to the continuum model, the directions in the paperboard are the machine direction (MD), the cross direction (CD) and the out of plane direction (ZD). For each point in the interface a local coordinate system defined as n, t_1 and t_2 is used. These directions are equivalent to ZD, MD and CD, respectively and are in equations denoted as 1, 2 and 3. For the calculations the following conventions are adopted

$$a_i b_i = \sum_{i=1}^{n} a_i b_i \tag{6.1}$$

α	Direction	Description
1	n	ZD tension
2	t_1	MD shear
3	t_2	CD shear

(6.2)

6.1 Kinematics

When describing the relative displacement between two opposing plies, it can be divided into an elastic and a plastic part.

$$\delta_i = \delta_i^e + \delta_i^p \tag{6.3}$$

Likewise, for a time increment Δt the total displacement increment is

$$\Delta\delta_i = \Delta\delta_i^e + \Delta\delta_i^p \tag{6.4}$$

6.2 Constitutive equations

Using the incremental relative displacement, the change in the traction vector across the interface is

$$\Delta T_\alpha = K_\alpha(\bar{\delta}^p)(\Delta\delta_\alpha - \Delta\delta_\alpha^p) \tag{6.5}$$

In (6.5), $K_\alpha(\bar{\delta}^p)$ is the components for the interface stiffness in the α-direction. The decrease in interface stiffness due to that the interface deforms, is a function of the equivalent plastic displacement $\bar{\delta}^p = \sqrt{\Delta\delta_i^p \Delta\delta_i^p}$. The interface stiffness can then be written as

$$K_\alpha(\bar{\delta}^p) = K_\alpha^0\big(1 - R_\alpha^k D(\bar{\delta}^p)\big) \tag{6.6}$$

where K_α^0 is the initial interface stiffness, R_α^k is a material constant and $D(\bar{\delta}^p)$ is the interface damage. The damage is a positive scalar

$$D(\bar{\delta}^p) = \tanh\left(\frac{\bar{\delta}^p}{C}\right) \tag{6.7}$$

where C is a material constant.

If the paperboard is under high compression, the normal stiffness is increased in order to prevent penetration of the different plies. The increase in stiffness is described as

$$K_1^0 = K_1^0 exp\big(n_c A_1 \tanh(-B_1\delta_1)\big) \qquad if \qquad \delta_1 < 0 \tag{6.8}$$

where A_1, B_1 and n_c are material constants.

6.3 Yield criterion

For the interface model, the start for yielding is defined as

$$f(T, \bar{\delta}^p) = \sum_{\alpha=2}^{n} \frac{S_1 T_\alpha^2}{S_\alpha(\bar{\delta}^p)^2} + T_1 - S_1 = 0 \tag{6.9}$$

$S_\alpha(\bar{\delta}^p)$ is the instantaneous interface strength, which like the instantaneous interface stiffness, also depends on the equivalent plastic displacement.

$$S_\alpha(\bar{\delta}^p) = S_\alpha^0\big(1 - R_\alpha^s D(\bar{\delta}^p)\big) \tag{6.10}$$

where S_α^0 are the initial interface strengths determined from experiments. Figure 6.3 shows the shape of the interface yield surface.

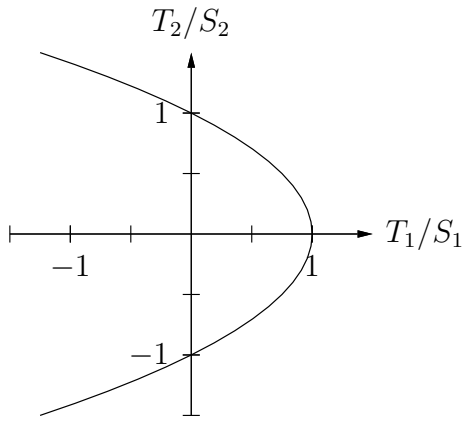

Figure 6.2: The shape of the interface yield surface when $T_3 = 0$

6.4 Flow rule

The plastic flow rule can be expressed as

$$\Delta\delta_i^p = \chi M_i \Delta\bar{\delta}^p \tag{6.11}$$

In (6.11), M_i are the components of the unit flow. It can be written as

$$M_i = \frac{\hat{M}_i}{\sqrt{\hat{M}_i \hat{M}_i}} \tag{6.12}$$

The value of χ depends on which value the yield criterion takes.

$$\chi = \begin{cases} 1 & \text{if } f = 0 \text{ and } T_i \Delta\delta_i^p > 0 \\ 0 & \text{if } f < 0 \text{ or } f = 0 \text{ and } T_i \Delta\delta_i^p < 0 \end{cases} \tag{6.13}$$

The plastic flow directions for non-associated flow are expressed as

$$\hat{M}_1 = \mu(\bar{\delta}^p)\frac{\partial f}{\partial T_1} = \mu(\bar{\delta}^p) \tag{6.14}$$

$$\hat{M}_\alpha = \frac{\partial f}{\partial T_\alpha} = 2\frac{S_1(\bar{\delta}^p)}{S_\alpha(\bar{\delta}^p)^2}T_\alpha \quad \alpha = 2, 3 \tag{6.15}$$

where μ is a frictional function which depend on the equivalent plastic displacement. ($\mu = 1$ corresponds to associated flow). Using the material constants A and B it is expressed as

$$\mu = A\big(1 - BD(\bar{\delta}^p)\big) \tag{6.16}$$

6.5 Implementation

The elastic trial step at time τ is computed as

$$T_\alpha^{tr}(\tau) = T_\alpha(t) + K_\alpha(t)\Delta\delta_\alpha \tag{6.17}$$

If plastic deformation occurs in this increment, the radial return method will return the traction state to the yield surface in a direction perpendicular to the yield surface using the flow rule (6.11):

$$T_\alpha(\tau) = T_\alpha^{tr} - \Delta\bar{\delta}^p K_\alpha M_\alpha \tag{6.18}$$

The traction state (T_1, T_2, T_3) at time τ and the equivalent plastic displacement increment $(\Delta\bar{\delta}^p)$ during time Δt, constitute the four unknowns which must be computed. Thus, the following system of equations has to be solved with a Newton-Raphson scheme.

$$\Gamma = \begin{bmatrix} \sum_{\alpha=2}^{n} \frac{S_1(\tau)}{S_\alpha(\tau)^2}T_\alpha(\tau)^2 + T_1(\tau) - S_1(\tau) = 0 \\ T_1(\tau) - T_1^{tr}(\tau) + \Delta\bar{\delta}^p K_1(\tau)M_1(\tau) = 0 \\ T_2(\tau) - T_2^{tr}(\tau) + \Delta\bar{\delta}^p K_2(\tau)M_2(\tau) = 0 \\ T_3(\tau) - T_3^{tr}(\tau) + \Delta\bar{\delta}^p K_3(\tau)M_3(\tau) = 0 \end{bmatrix} \tag{6.19}$$

6.6 Calibration

The model parameters are determined using the results from out-of-plane uniaxial ZD tension tests and shear testing in the MD and CD directions. To determine the interface properties between plies, a paperboard consisting of two plies is used. There will be deformations in the plies and the interface during the experimental test. To compensate for this when determining the initial stiffness (K_i^0), the two plies and the interface are considered as three springs in series. For ZD tension the total elongation is expressed as

$$\delta = \left(\frac{t_1}{E_{ZD}^1} + \frac{t_2}{E_{ZD}^2} + \frac{1}{K_n^0} \right) \sigma \qquad or \qquad \delta = C_n \sigma \tag{6.20}$$

where E_{ZD}^1 and E_{ZD}^2 are the Young's moduli in the ZD-direction for the two plies. The plies thickness are denoted t_1 and t_2. From these expression K_n^0 is obtained. The stiffness in the two shear directions are obtained in the same manner. The parameter C_n are determined by curve fitting of (6.10) to the experimental measured softening of the stress-displacement curve, where the peak stress is assumed to be equal to the initial yield stress, S_i^0. To determine the interface properties in the case when delamination occurs within a plie, a single layer paperboard is tested. The slope of a straight line from the start up to the peak stress gives the initial stiffness K_i^0, thus a linear response. See Figure 6.3. The residual strengths R_i^s in (6.10) are determined from tests. Although R_n^s is zero, it is for numerical reasons set to a small positive value.

As the number of interfaces in the paperboard model are increased, the total paperboard stiffness is decreased. Therefore, each interface stiffness must be increased to prevent this weakening effect. The initial interface stiffness in equation (6.20) should approach "infinity" to obtain the continuum stiffness but due to numerical difficulties this is not possible.

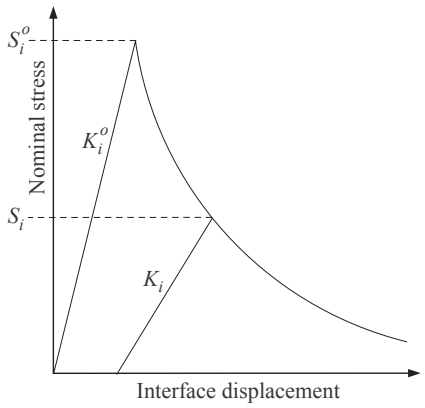

Figure 6.3: The interface stiffness change as the interface deforms

Chapter 7

Finite Element Method

This chapter begins with deriving the expression of virtual power from which most of the engineering relations can be obtained. The principle of virtual power is the foundation for the finite element formulation, which is briefly examined here. Large deformations are considered and the expressions are defined in the reference configuration.

7.1 Principle of virtual power

From the balance law for linear momentum the equation of motion in the Lagrangian description is, in Ristinmaa and Ljung (2002), derived as

$$\frac{\partial \mathbf{P}}{\partial \mathbf{X}} + \rho_o \mathbf{b} = \rho_o \ddot{\mathbf{u}} \tag{7.1}$$

where $\mathbf{b}$ is the body force per unit mass, ρ_o is the density and $\mathbf{u}$ is the nodal displacement. In order to find an expression for the virtual power, (7.1) is multiplied with a virtual, arbitrary velocity $\mathbf{w}(\mathbf{x}, t)$.

$$\int_V \mathbf{w}^T \frac{\partial \mathbf{P}}{\partial \mathbf{X}} dV + \int_V \rho_o \mathbf{w}^T \mathbf{b} dV = \int_V \rho_o \mathbf{w}^T \ddot{\mathbf{u}} dV \tag{7.2}$$

The first part of (7.2) are rewritten using the Green-Gauss theorem together with the divergence theorem.

$$\int_V \mathbf{w}^T \frac{\partial \mathbf{P}}{\partial \mathbf{X}} dV = \int_{s^o} \mathbf{w}^T \mathbf{t}^o ds^o - \int_V \nabla_o \mathbf{w} : \mathbf{P} dV \tag{7.3}$$

where the surface traction is defined as $\mathbf{t}^o = \mathbf{P}\mathbf{n}^o$.

Inserting (7.3) into (7.2) gives

$$\int_V \rho_o \mathbf{w}^T \ddot{\mathbf{u}} dV + \int_V \nabla_o \mathbf{w} : \mathbf{P} dV - \int_{s^o} \mathbf{w}^T \mathbf{t}^o ds^o - \int_V \rho_o \mathbf{w}^T \mathbf{b} dV = 0 \tag{7.4}$$

The formulation is so far made with the first Piola-Kirchhoff stress tensor which is non-symmetric. A symmetric stress tensor is more preferable in the expression and therefore the relation between the first and the second Piola-Kirchhoff stress tensors, (3.34), is inserted in (7.4). Also defining that

$$\hat{\mathbf{F}} = \nabla_o \mathbf{w} \quad \text{and} \quad \hat{\mathbf{E}} = \hat{\mathbf{F}}\mathbf{F} \tag{7.5}$$

the expression for the virtual work are written as

$$\int_V \rho_o \mathbf{w}^T \ddot{\mathbf{u}} dV + \int_V \hat{\mathbf{E}} : \mathbf{S} dV - \int_{s^o} \mathbf{w}^T \mathbf{t}^o ds^o - \int_V \rho_o \mathbf{w}^T \mathbf{b} dV = 0 \tag{7.6}$$

7.2 FE formulation

The strain can be expressed as

$$\hat{\mathbf{E}} = \mathbf{B}\mathbf{a} \tag{7.7}$$

where $\mathbf{B}$ is a function of $\mathbf{a}$ and is non-linear. An approximation for the displacement field $\mathbf{a}$, is made with the global shape function $\mathbf{N}$ and the nodal displacements $\mathbf{u}$.

$$\mathbf{a}(\mathbf{X}, t) = \begin{bmatrix} \mathbf{N}_1(\mathbf{X}) \\ \mathbf{N}_2(\mathbf{X}) \end{bmatrix} \mathbf{u}(t) = \mathbf{N}(\mathbf{X})\mathbf{u}(t) \tag{7.8}$$

The arbitrary virtual velocities are, according to Galerkin's method, approximated with the same global shape functions as in (7.8).

$$\mathbf{w}(\mathbf{X}, t) = \mathbf{N}(\mathbf{X})\mathbf{c}(t) \tag{7.9}$$

Using the established approximations, (7.6) is rewritten as

$$\mathbf{c}^T \left(\int_V \rho_o \mathbf{N}^T \mathbf{N} \ddot{\mathbf{a}} dV + \int_V \mathbf{B}^T \mathbf{S} dV - \int_{s^o} \mathbf{N}^T \mathbf{t}^o ds^o - \int_V \rho_o \mathbf{N}^T \mathbf{b} dV \right) = 0 \tag{7.10}$$

The fact that **c** can be chosen arbitrary, results in that (7.10) can be written in a compact fashion

$$\mathbf{M\ddot{a}} + \mathbf{F}_{int} - \mathbf{F}_{ext} = 0 \tag{7.11}$$

where

$$\mathbf{M} = \int_V \rho_o \mathbf{N}^T \mathbf{N} dV \tag{7.12}$$

$$\mathbf{F}_{int} = \int_V \mathbf{B}^T \mathbf{S} dV \tag{7.13}$$

$$\mathbf{F}_{ext} = \int_{s^o} \mathbf{N}^T \mathbf{t}^o ds^o + \int_V \rho_o \mathbf{N}^T \mathbf{b} dV \tag{7.14}$$

In the 3DM model the mass is not incorporated thus equation (7.11) is reduced to a static description. When the 3DM model is implemented in ABAQUS/Standard the equilibrium is expressed as

$$\mathbf{F}_{int} - \mathbf{F}_{ext} = \mathbf{R} \tag{7.15}$$

where **R** is the residual which can be changed with the option *Controls in order to modify the convergence criteria in ABAQUS/Standard, see ABAQUS Inc. (2003). Note that ABAQUS/Standard uses the Cauchy stress, σ, and not the second Piola-Kirchhoff stress tensor used in this chapter.

Chapter 8

Experimental test setup

The experimental tests at the Stora Enso Research Center in Karlstad consisted of creasing and folding test specimens of the multi-layer paperboard Triplex 360 mN. The objectives were to gather data from experimental tests to compare with the results obtained from the simulations.

8.1 Test specimens

The paperboard used in the tests was Triplex 360 mN. All specimens were cut in the MD-direction with the length 80±1 mm and the width 38±1 mm in the CD-direction. The thickness was measured to 0.460±0.25 mm. The specimens were pre-conditioned at a relative humidity of 50% and at a temperature of 23°C, cf. TAPPI T 402 sp98 (1998). Since the mechanical behaviour of paperboard is moisture dependent, the test specimens were pre-conditioned for at least 24 hours before the tests. All test procedures were performed in the controlled climate.

8.2 Creasing

Before folding the paperboard into a finished package, the paperboard is creased in order to obtain a more controlled folding process. The purpose of creasing is to introduce high shear stresses in the areas around the crease, see Figure 8.1. In the creased zone the paperboard is delaminated and plastically deformed, thus the folding resistance is decreased. This enables folding without development of cracks in the paperboard surface and a package with well defined edges is obtained.

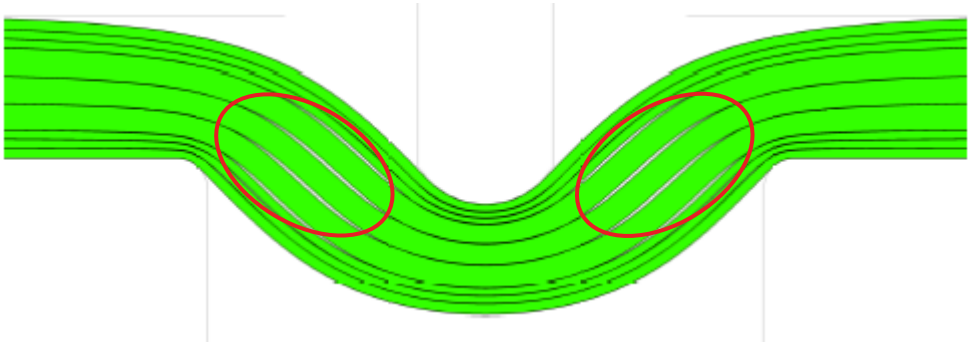

Figure 8.1: The areas (outlined) where high shear stresses develop during creasing

During the creasing process the male die is pressed vertically into the female die with the test specimen in between, see Figure 8.2. Note that there is no rotation of the male die. The test specimen was subjected to a constant web tension of 1000 N/m during the creasing. All the specimens were creased in the CD-direction with a male die displacement velocity of 1 mm/s.

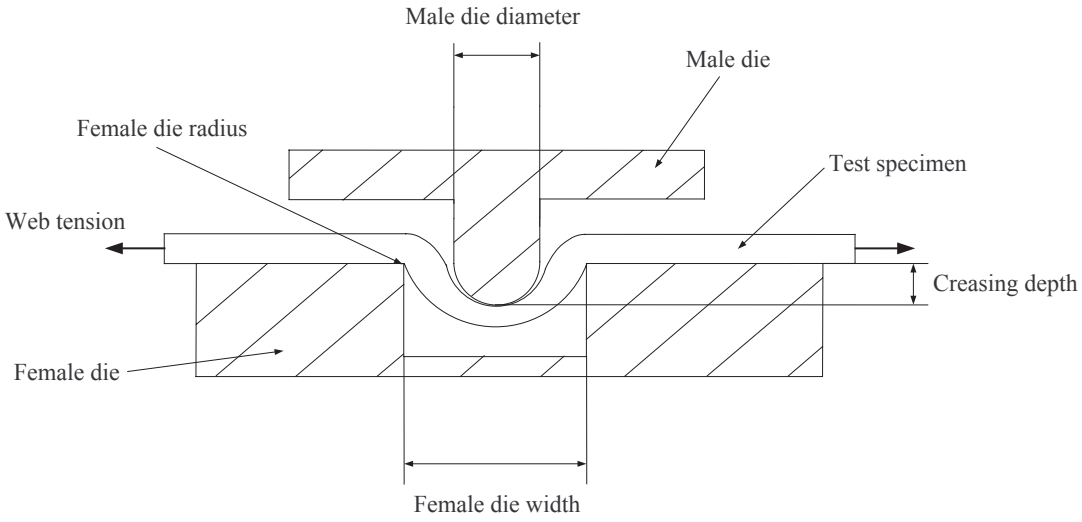

Figure 8.2: Schematic drawing of the MTS Creasing tool

The creasing test setup measured the reaction force magnitude (N) on the male die versus the male die position (mm), see Figure 8.3. The reaction force was measured with the time increment 0.001 s.

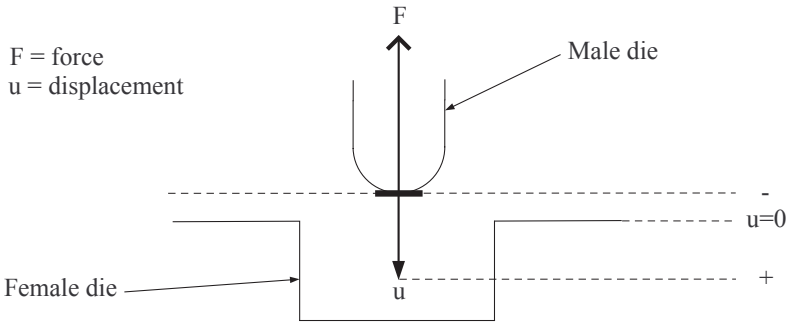

Figure 8.3: The measured reaction force and displacement

With the Stora Enso designed MTS creasing tool used in the experimental tests, see Figure 8.4, the crease geometry is controlled by varying the male die diameter, the female die width and the creasing depth.

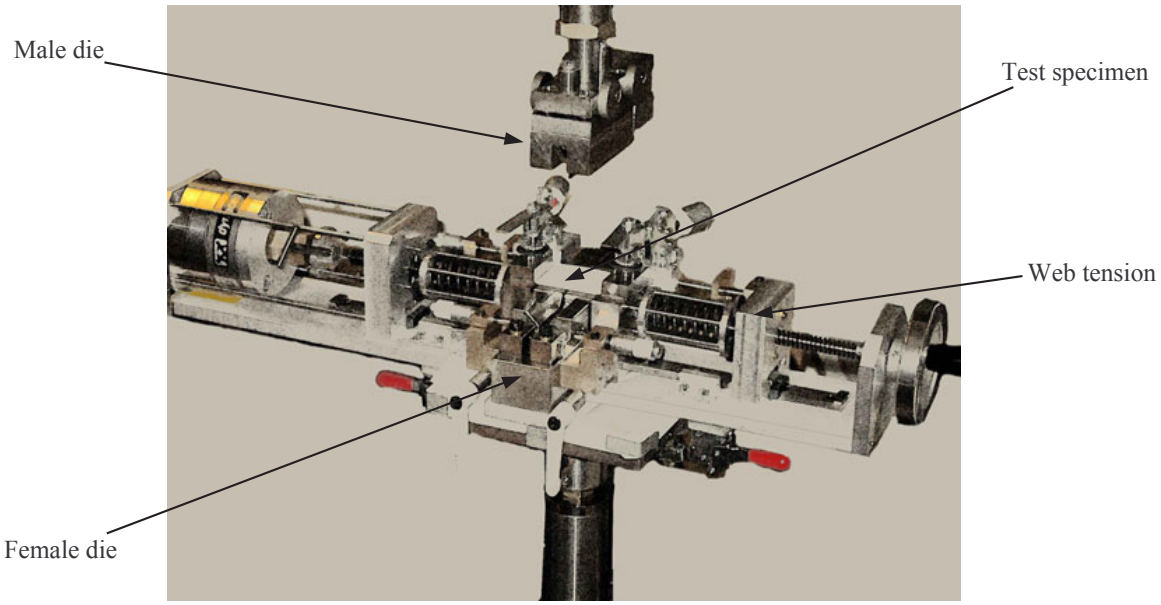

Figure 8.4: MTS creasing tool

The tests were performed with eight different configurations of the MTS creasing tool, see Table 8.1. The configurations were chosen so that the effect of different geometries could be studied. In all configurations the female die radius is 0.1 mm. When creasing to -50 μm the male die stops at a distance of 50 μm above the female die's top surface. During creasing to the depth 150 μm the male die stops at a distance of 150 μm below the top surface of the female die. Immediately after the creasing depth is reached, the male die starts to move upwards vertically.

Table 8.1: The different creasing tool configurations

Configuration	Male (mm)	Female (mm)	Depth (μm)
1	0.5	1.4	-50
2	0.5	1.4	150
3	0.5	1.8	-50
4	0.5	1.8	150
5	0.7	1.6	-50
6	0.7	1.6	150
7	0.7	1.8	-50
8	0.7	1.8	150

The two different male dies used in the MTS creasing tool are in detail described by the drawings (not scaled) in Figure 8.5. The male die measurements were obtained with a microscope.

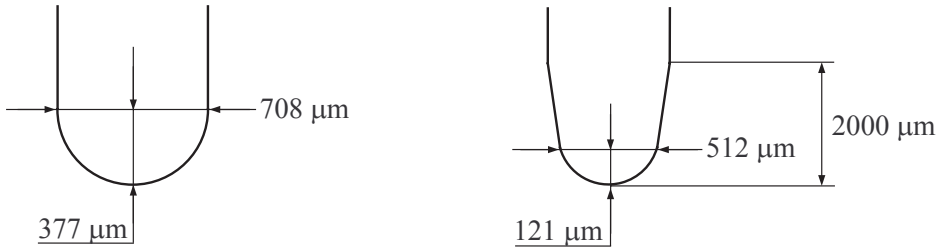

Figure 8.5: The 0.7 mm and 0.5 mm male dies used in the MTS creasing tool

The characteristic creasing behaviour of the paperboard can be seen in Figure 8.6. The loading starts at -460 μm which is where the contact between the male die and the test specimen is initiated. The loading continues until the creasing depth is reached and then the unloading starts. 16 specimens were creased in every configuration.

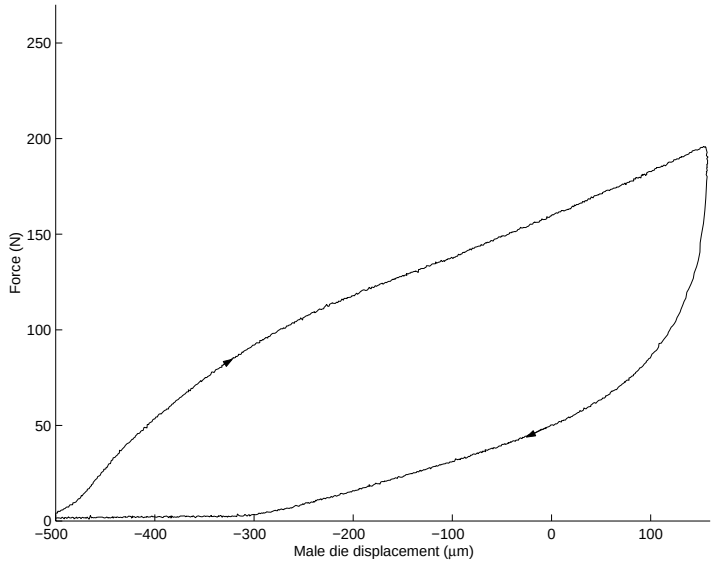

Figure 8.6: Plot showing the creasing of a test specimen

8.3 Folding

A Lorentzen & Wettre PTS bending force tester was used for folding the test specimens, see Figure 8.7.

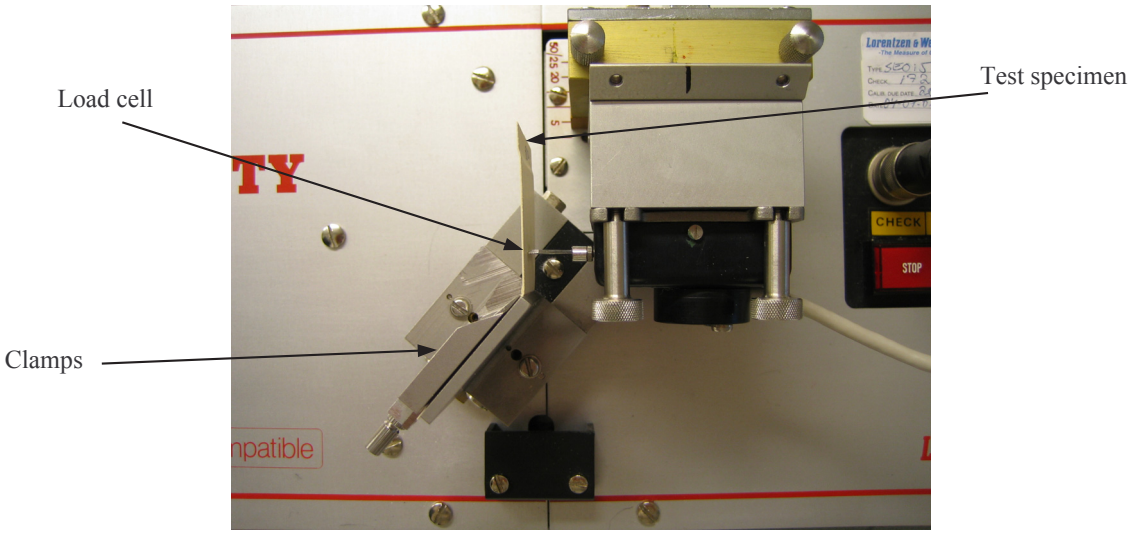

Figure 8.7: PTS bending force tester

The specimen is placed in the fixture, which rotates to a predefined angle. To determine the position of the center of rotation, video clips of the folding process recorded by Stora Enso were studied. The center of rotation is marked in Figure 8.8. The fixture has an upper and a lower clamp. The distance from the upper clamp to the center of the crease is 0.7 mm. At a distance of 10 mm from the upper clamp, a load cell measures the reaction force during the folding. The load cell is a SG3-5N with a stiffness of 131.6 N/mm, cf. www.swema.com (20050330).

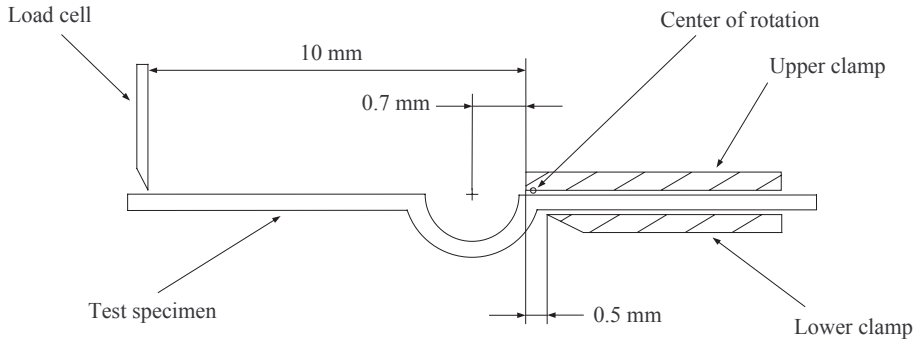

Figure 8.8: Schematic drawing of the bending force tester

At Stora Enso two different rotation angles were used. Half of the specimens in every configuration were folded to 45° and then folded back after zero seconds relaxation time.

After 10 s relaxation time the specimen was re-folded to 45° and folded back after zero seconds relaxation time. The folding of the other half of the specimens followed the same procedure except that the rotation angle was set to 90°. The folding test setup measured the reaction force magnitude (mN) versus the rotation angle (°), which was recorded with the increment of 0.18°, see Figure 8.9.

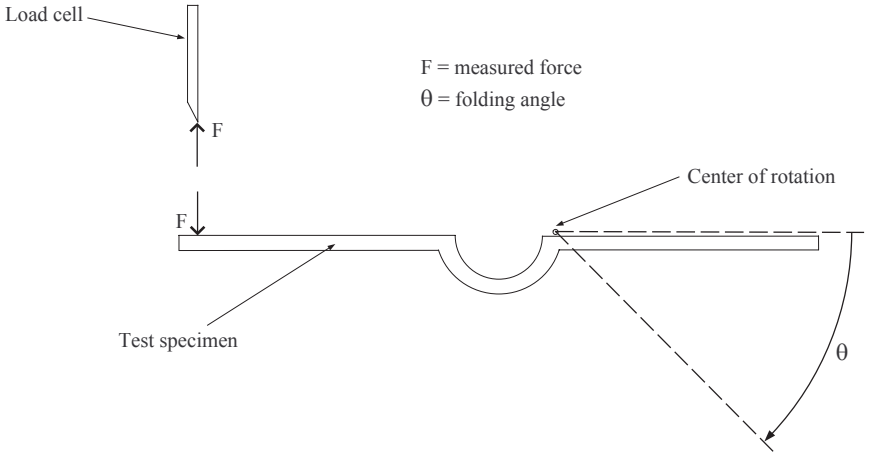

Figure 8.9: The measured reaction force and the recorded rotation angle

The characteristic folding behaviour of the paperboard is shown in Figure 8.10. The loading starts at the angle 0° and continues until 45° is reached. Immediately after the maximum angle is reached, the unloading starts. When the fixture with the test specimen has rotated back to 0° it stops for 10 s before the second folding is initiated.

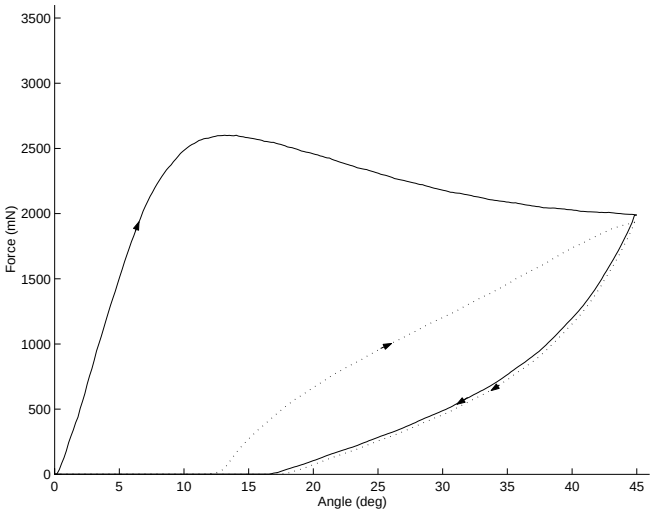

Figure 8.10: Plot showing the folding of a test specimen

Chapter 9

Simulation setup

In this chapter a brief introduction to ABAQUS version 6.4 are made. A description of the model used in the simulations is also introduced. Finally, a description of how the analyses were performed and which problems that occurred are discussed. All results from the simulations are presented in chapter 10.

9.1 ABAQUS

ABAQUS is an engineering simulation program based on the finite element method. It can solve many types of problems, from linear to nonlinear analysis. In the program an extensive library of elements and material models are included. In ABAQUS there are two main solvers, ABAQUS/Standard and ABAQUS/Explicit.

ABAQUS/Standard is a general-purpose finite element module and uses implicit time integration. For each step equilibrium has to be obtained. It analyses many types of problems, for example static, dynamic and thermal. The 3DM model is for the time being only written for an implicit solver and therefore ABAQUS/Standard is used in this report.

ABAQUS/Explicit is an explicit dynamics finite element module. In order to avoid that equilibrium needs to be achieved for each integration step, small steps are taken with this solver.

In ABAQUS/Standard an interactive, graphical environment called the Complete Abaqus Environment (CAE) is used for modelling, managing and monitoring analysis and visualizing results. In the CAE the different parts used in an analysis are created. Parts can also be imported from other CAD programs. The parts are assigned material properties and assembled into a model. After configuring the analysis procedure and applying loads and boundary conditions, the model is ready to be meshed.

From the CAE an input file containing all the model information are generated. In this file, user-defined material properties (UMAT) and surface interaction properties (UINTER), see Appendix H, need to be introduced when the 3DM model is used. Also the number of solution dependent variables (SDV) is defined, see Table 9.1. After the model is completely defined, it is submitted for calculations.

Table 9.1: Solution dependent variables, SDV, all set by the user

SDV	Notation	Description
SDV(1-9)	$\mathbf{F}^e$	Elastic deformation gradient
SDV(10-18)	$\mathbf{F}^p$	Plastic deformation gradient
SDV(19-27)	$\bar{\mathbf{S}}$	Second Piola-Kirchhoff stress
SDV(28-33)	S^I	Instantaneous hardening on each deformation system
SDV(34-42)	$\mathbf{K}$	Flow directions for each deformation system
SDV(43)	E_{22}	Green strain in 22-direction
SDV(44)	γ_t	Effective strain at time t
SDV(45)	γ_τ	Effective strain at time τ

Output from ABAQUS/Standard to the user are the total deformation gradient at time t, $\mathbf{F}(t)$, the Cauchy stress at time t, $\boldsymbol{\sigma}(t)$, an estimate of the total deformation gradient at time $\tau = t + \Delta t$, $\mathbf{F}(\tau)$ and a set of solution dependent variables, SDV, at time t defined by the user. Given the output from ABAQUS/Standard the UMAT is then used to calculate and return the Cauchy stress at time τ, $\boldsymbol{\sigma}(\tau)$, the solution dependent variables and the material jacobian, $\mathbf{W}$, which is the derivative of the Cauchy stress with respect to the relative strain tensor. In Figure 9.1 a schematic overview of the interaction between ABAQUS and UMAT is shown.

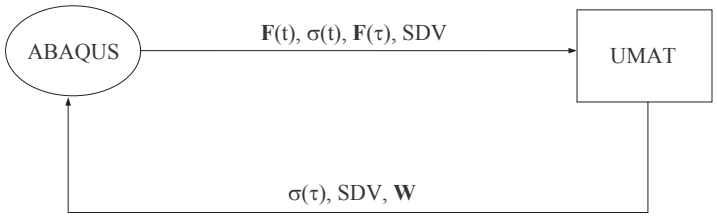

Figure 9.1: The interaction between ABAQUS and UMAT

9.2 Creasing and folding model

The paperboard in ABAQUS/Standard is a two-dimensional model assembled by three plies and has the total thickness 460 μm. To describe the delamination that occurs within the paperboard the interface model is used between the plies and within the plies. The model proposed by Xia (2002) suggested four interfaces, between the plies and two within

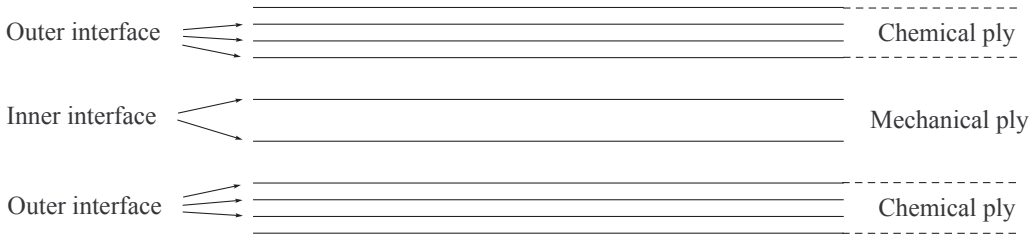

Figure 9.2: Material and interface properties

the middle ply. In order to better describe the paperboard behaviour, interfaces are here also included in the top and bottom plies, according to private discussions with Just (2005). Each ply is divided into three layers with interface properties between them. The increased number of interfaces is introduced so that the paperboard can delaminate in the chemical pulp. The ability to delaminate in the top and bottom plies is important due to the high shear stresses that develop in the paperboard around the male die and the female die radius. The increased number of interfaces in the model has a weakening effect to the paperboard and therefore the stiffness of the interfaces needs to be increased. In Figure 9.2 it is shown where the outer and inner interface properties act in the paperboard. The inner interface describes the delamination properties of the mechanical ply and the outer interface describes the delamination properties between the chemical and the mechanical plies. Note that the outer interface properties are also used to characterise the delamination within the chemical plies since no experimental data is available for this.

The plies in the paperboard have different material properties, see Figure 9.2. The middle ply is set to the mechanical material properties and the top and bottom plies are set to the chemical material properties. The parameters for mechanical and chemical material properties as well as for the outer and inner interface properties can be seen in Appendix H. An obvious difference between them is that the chemical plies are stiffer than the mechanical.

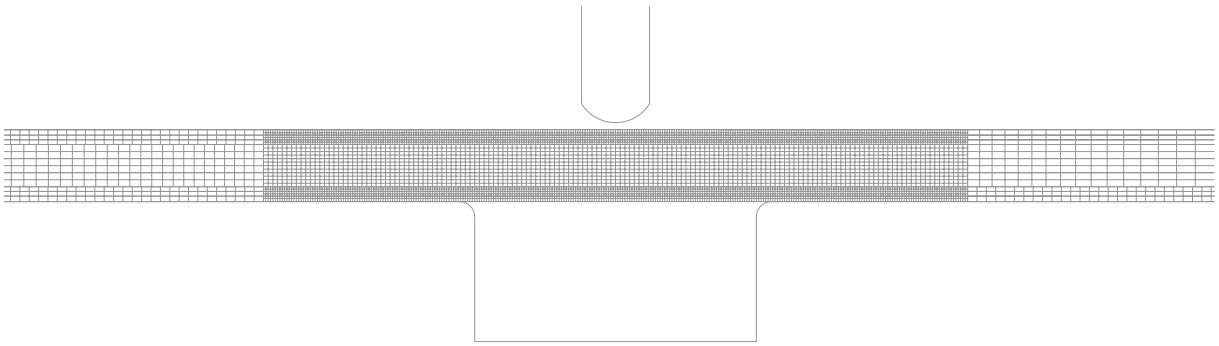

Figure 9.3: The paperboard mesh and the rigid bodies male and female die

When meshing the paperboard a two-dimensional, 4-node, plane strain, quadrilateral solid element is used. In ABAQUS/Standard the element is labelled CPE4. In the creasing area where the male and female die interact with the paperboard, there is a finer mesh, see Figure 9.3. In the top and bottom plies the element length is 15 μm and in the middle ply it is 30 μm. This can be compared to the size of a fiber, which is approximately 20 μm thick and a few millimeters long, cf. Figure 2.1. The mesh is also refined where the load cell is applied and the element length is set to 20 μm. In the remaining parts of the paperboard the element length varies from 60 to 150 μm.

The non-deformable parts in the model are created as rigid bodies. The motions of the rigid bodies are described using reference points and in a two-dimensional model they have three degrees of freedom. In the model the male and female die, the stoppers, the clamps and the load cell are rigid bodies. Note that stoppers are not included in the test equipment but used in the model to keep the paperboard in place during creasing, cf. Figure 8.2 and Figure 9.4. The clamps and the load cell are assumed to have a friction coefficient of 0.3. The male die, the female die and the stoppers are assumed frictionless.

9.3 Simulation procedure

The simulation is divided into 12 different steps, step 1 to 7 regard the creasing and step 8 to 12 regard the folding, see Table 9.2 and Appendix I.

Table 9.2: The different steps performed in the simulations.

Step	Action
1	Apply web tension
2	Male die punch
3	Male die remove
4	Add clamps
5	Remove male and female die, stoppers and web tension
6	Contact change
7	Remove the fixation of mesh nodes
8	Add load cell
9	Folding
10	Relax
11	Re-folding
12	Relax

Creasing

When creasing, a web tension of 1000 N/m in the MD-direction is applied to the paperboard, step 1. To prevent paperboard movement when applying the web tension, the nodes in a vertical symmetry plane are fixed in the MD direction. The vertical symmetry plane is along the center of the male die and through the middle of the paperboard. In Figure 9.4 the stoppers can be seen on each side of the paperboard. During creasing the male die displacement and its vertical reaction force are measured, step 2 and 3. Due to that the paperboard is modelled two dimensionally, the reaction force has to be multiplied with the width of a test specimen from the experimental tests before comparing results.

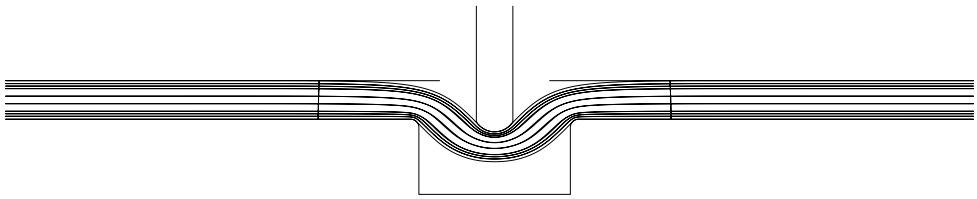

Figure 9.4: Creasing overview showing male and female die and stoppers

Folding

The web tension, the stoppers, the male and female die and the fixed nodes are all removed before folding, step 5 and 7. Instead the clamps and the load cell are put in place, step 4 and 8, to obtain the folding setup, cf. Figure 9.5. The clamps rotate around the reference point, i.e. the center of rotation, and control the folding. The first folding is complete when the clamps are back in the initial position. For every specimen two consecutive foldings are performed. During folding, the rotate angle of the clamps and the vertical reaction force on the load cell are recorded. The reaction force on the load cell also needs to be multiplied with the width of the test specimen before comparing results. As mentioned in chapter 8 the load cell in the experimental tests has a stiffness of 131.6 N/mm. The load cell in the simulations is a fixed rigid body but this difference has, according to calculations, a negligible affect on the results.

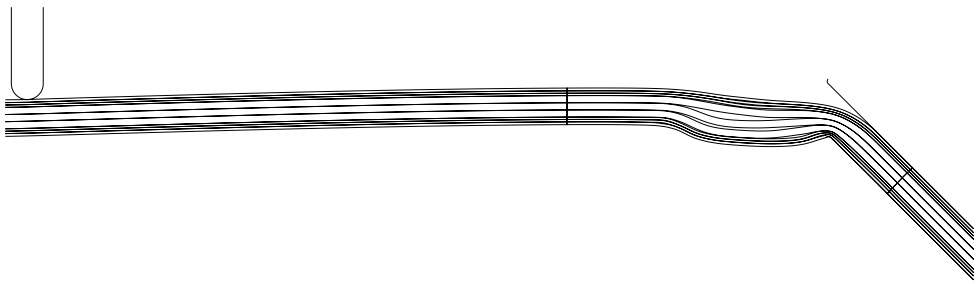

Figure 9.5: Folding overview showing load cell and clamps

Chapter 10

Results

In this chapter the results from the experimental tests at Stora Enso and the simulations are presented. An interface parameter study was also performed and the simulation results from this study are also presented. For every configuration, a number of property variables are calculated. The property variables describe the characteristic Triplex 360 mN behaviour during creasing and folding with the different configurations. These property variables are then used in chapter 11 for comparing the results from the experimental tests with the simulation results.

10.1 Experimental tests

For each of the eight creasing tool configurations 16 creasing tests were performed. Because of limited access time to the creasing tool, results from only five specimens in every configuration were recorded. For every configuration eight of the creased test specimens were folded to 45°, the other half to 90°. The folding results from all 128 specimens were recorded. See Appendix F. The results from the 90° foldings are excluded. This is further discussed in section 10.2 below.

The creasing result for each configuration is the mean value of the results from five specimens. The folding result for each configuration is the mean value of the results from 8 specimens.

10.1.1 Creasing

For every configuration the initial elastic stiffness, K^{ini}, the unloading stiffness, K^{unl}, and the yield force, F_y, are approximate values calculated from the mean curve with the help of Matlab. The stored energy, E^{st}, the male die displacement, d_0, when the first contact

with the paperboard is initiated and the residual deformation, ΔD, are mean values. The maximum force, F^{max}, is calculated with a 95% confidence interval, see Table F.1. The defined property variables for creasing are shown in Figure 10.1.

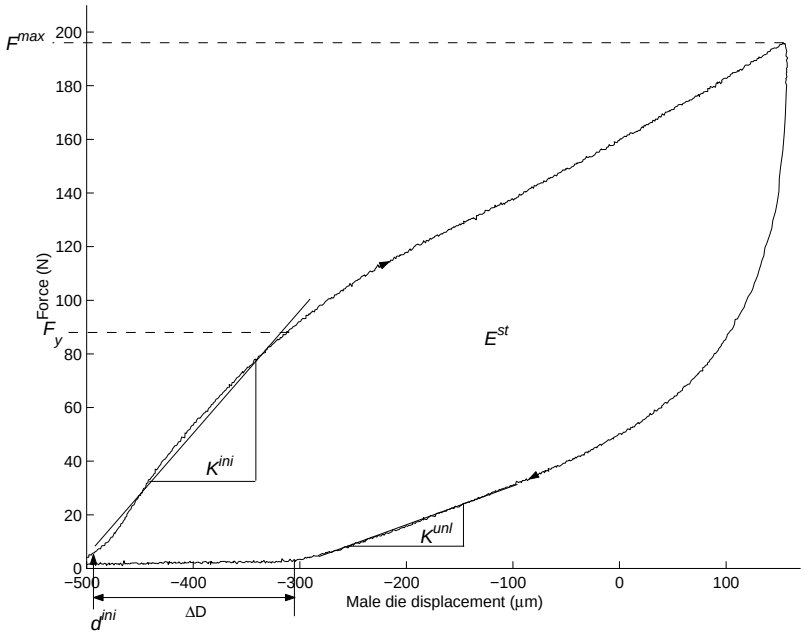

Figure 10.1: Creasing property variables

Figure 10.1 shows the characteristic creasing behaviour of Triplex 360mN. The stored energy, or the amount of energy used to plastically deform and delaminate the paperboard, is the area under the loading curve up to the maximum force minus the area under the unloading curve. The experimental test results from creasing for all configurations are presented in Appendix A.

The male die displacement when the first contact with the paperboard is initiated, d_0, should be -460 μm, since this is the paperboard thickness. This is not the case for some of the configurations in the experimental tests, see Table 10.1. This is due to that the test specimen rises to a convex shape because of the pressure applied in the MTS creasing tool at the specimen ends. The deviation in paperboard thickness also affects the initial conditions.

In Table 10.1 the values of the property variables describing the creasing, are for every configuration shown.

Table 10.1: The creasing results from experimental tests. M/F/D refer to the different creasing tool configurations of the male and female die and the creasing depth.

Conf	d_0 (μm)	K^{ini} (N/mm)	F_y (N)	F^{max} (N)
1	-482	552	103	184.6 ± 5.1
2	-476	528	110	265.3 ± 5.2
3	-483	563	63	145.2 ± 3.4
4	-475	516	75	197.1 ± 5.9
5	-464	588	71	160.4 ± 1.7
6	-463	560	79	229.2 ± 2.2
7	-460	538	65	140.6 ± 3.4
8	-466	541	65	194.5 ± 7.7
	K^{unl} (N/mm)	Δd (μm)	E^{st} (Nmm)	M/F/D
1	218	165	34	0.5/1.4/-50
2	149	207	69	0.5/1.4/150
3	195	159	28	0.5/1.8/-50
4	135	185	55	0.5/1.8/150
5	210	152	28	0.7/1.6/-50
6	155	209	60	0.7/1.6/150
7	200	151	25	0.7/1.8/-50
8	138	213	52	0.7/1.8/150

10.1.2 Folding

As previously stated, each test specimen was folded twice in a sequence. In Figure 10.2 the characteristic folding behaviour for Triplex 360 mN is shown. The experimental test results from folding for all configurations are presented in Appendix A.

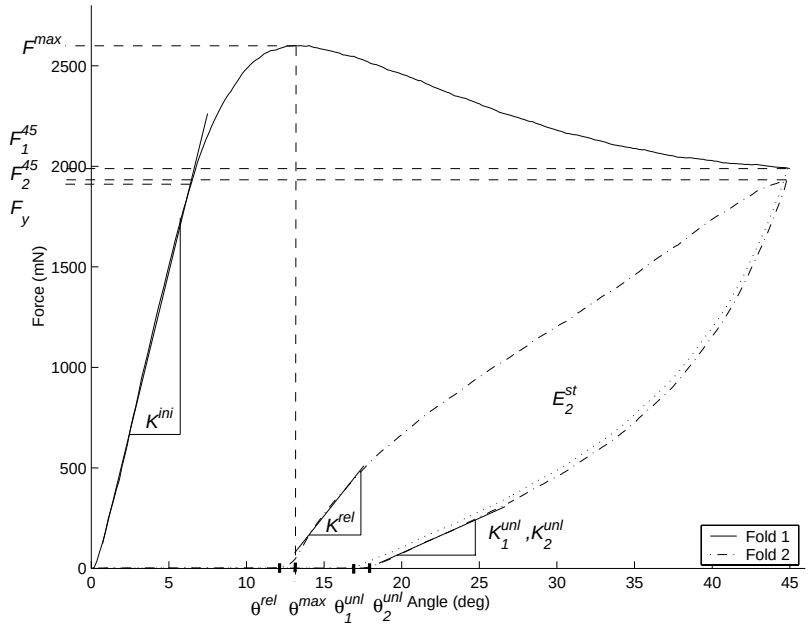

Figure 10.2: Folding property variables

In Figure 10.2 thirteen property variables are defined. The property variables for the first folding, the initial stiffness, K^{ini}, the yield force, F_y, the unloading stiffness for the first folding, K_1^{unl}, are approximate values calculated from the mean value curve with the help of Matlab. The maximum force angle, θ^{max}, the force at 45°, F_1^{45}, and the angle at which the unloading stops, θ_1^{unl}, are mean values. The maximum force, F^{max}, is calculated with a 95% confidence interval, see Table F.2.

The property variables for the second folding, the reload stiffness, K^{rel}, and the unload stiffness, K_2^{unl}, are approximate values calculated from the mean value curve with the help of Matlab. The angle at which reloading start, θ^{rel}, the force at 45°, F_2^{45}, the angle at which the unloading stops, θ_2^{unl}, and the stored energy during the second folding, E_2^{st}, are mean values.

In Table 10.2 and Table 10.3 the property variables from the folding are shown.

Table 10.2: Experimental results from the first folding.

Conf	K^{ini}(mN/θ)	F_y (mN)	F^{max} (mN)	θ^{max}	F_1^{45} (mN)	K_1^{unl}(mN/θ)	θ_1^{unl}
1	360	2484	3047.3 ± 50.1	12.6	2383	36	18.0
2	270	1498	2180.9 ± 24.2	14.0	1892	32	17.3
3	389	2948	3575.9 ± 66.2	12.8	2560	39	18.0
4	318	1924	2602.8 ± 35.5	13.1	1989	34	16.7
5	384	2834	3290.9 ± 36.4	11.5	2502	35	18.2
6	302	1726	2390.3 ± 29.9	14.0	2009	32	17.5
7	383	2904	3451.6 ± 67.5	12.6	2440	37	18.2
8	313	1787	2504.5 ± 47.2	14.0	1965	33	17.5

Table 10.3: Experimental results from the second folding.

Conf	θ^{rel}	K^{rel} (mN/θ)	F_2^{45} (mN)	K_2^{unl} (mN/θ)	θ_2^{unl}	E_2^{st} (F*θ)
1	13.9	105	2337.0 ± 42.8	37	19.3	18604
2	12.8	91	1850.3 ± 34.8	34	18.2	16770
3	13.9	116	2498.0 ± 64.8	41	19.1	20653
4	12.1	95	1936.1 ± 27.8	35	17.8	18330
5	13.7	106	2445.4 ± 48.8	36	19.1	19761
6	11.9	88	1973.4 ± 31.8	34	18.4	17646
7	13.9	109	2383.0 ± 50.5	38	19.3	19776
8	13.3	95	1911.9 ± 46.9	34	18.5	16873

10.2 Simulations

During the simulations the default convergence criterions set in ABAQUS/Standard have been difficult to obtain. Both during creasing and folding the criterion for convergence has been eased. In ABAQUS/Standard, the option *Controls has been used to modify the criterions for convergence, see equation (7.15). The *Controls settings for every simulation are presented in Appendix G

Despite much effort to fold the paperboard to 90°, it have not been possible to do so. There were convergence problems and the simulations were aborted before the folding was complete.

10.2.1 Creasing

The characteristic creasing behaviour in simulations for Triplex 360 mN is shown in Figure 10.3. The same property variables used for describing the creasing in the experimental tests are used, see Figure 10.1. The yield force and the stiffnesses are approximate values calculated from the simulation result plots and the values for the remaining property variables are directly obtained from the simulation results.

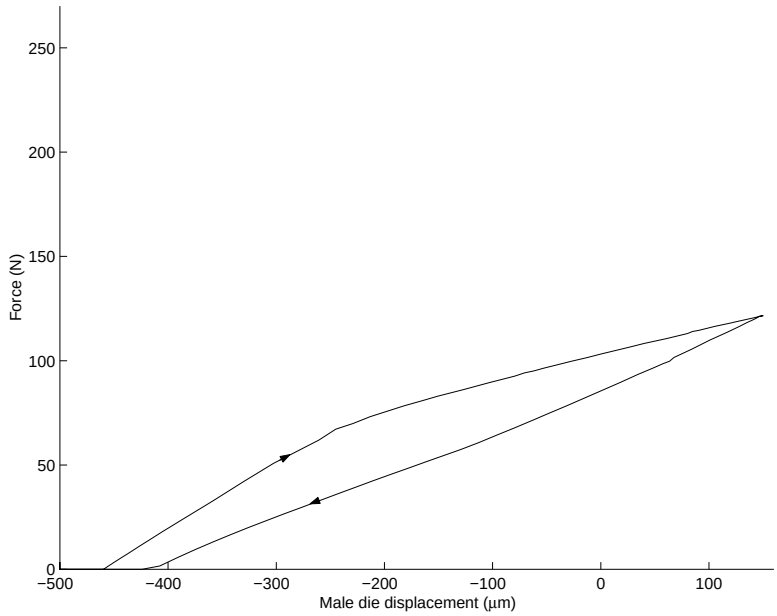

Figure 10.3: The characteristic simulation creasing behaviour of Triplex 360mN

The creasing results from the simulations for all configurations are presented in Appendix A and the values of the property variables are shown in Table 10.4.

Table 10.4: Simulation creasing results.

Conf	d_0 (μm)	K^{ini} (N/mm)	F_y (N)	F^{max} (N)
1	-460	388	95	128
2	-460	385	93	170
3	-460	331	70	97
4	-460	325	70	122
5	-460	362	84	115
6	-460	360	81	155
7	-460	335	76	101
8	-460	336	69	129
	K^{unl} (N/mm)	Δd (μm)	E^{st} (Nmm)	M/F/D
1	324	19	5	0.5/1.4/-50
2	271	33	13	0.5/1.4/150
3	251	35	6	0.5/1.8/-50
4	211	36	12	0.5/1.8/150
5	284	33	6	0.7/1.6/-50
6	248	36	13	0.7/1.6/150
7	262	42	6	0.7/1.8/-50
8	220	45	13	0.7/1.8/150

10.2.2 Folding

Figure 10.4 shows the characteristic folding behaviour in simulations for Triplex 360 mN. The folding results from the simulations for all configurations are presented in Appendix A.

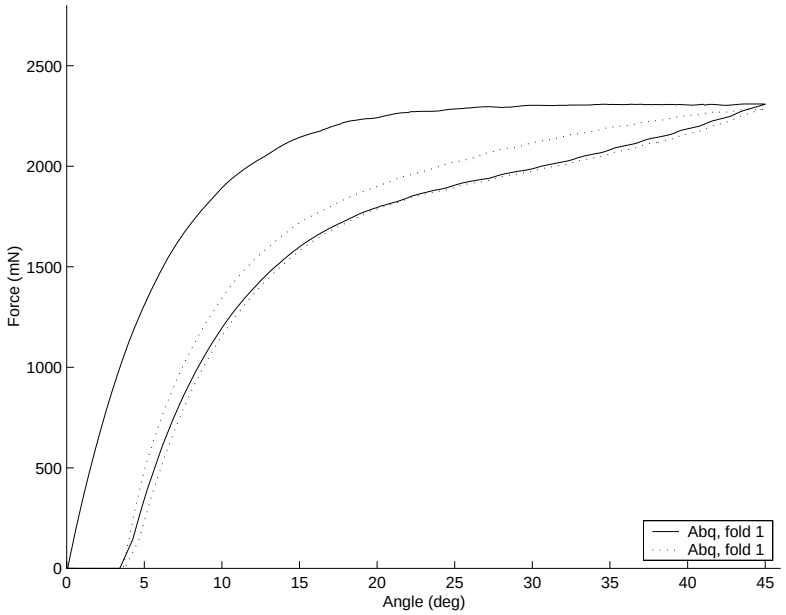

Figure 10.4: The characteristic simulation folding behaviour of Triplex 360mN

The values of the property variables from the folding simulations are shown in Table 10.5 and Table 10.6. The stiffnesses and the yield forces are approximate values. The values for the other property variables are directly obtained from the simulation results.

Table 10.5: Simulation results from the first folding.

Conf	K^{ini} (mN/θ)	F_y (mN)	F^{max} (mN)	θ^{max}	F_1^{45} (mN)	K_1^{unl} (mN/θ)	θ_1^{unl}
1	366	971	2575	42.1	2571	242	2.9
2	309	999	2307	45.0	2307	253	3.2
3	389	923	2556	31.7	2550	244	2.9
4	341	786	2310	43.6	2309	213	3.4
5	387	920	2525	45.0	2525	252	3.2
6	318	1022	2328	45.0	2328	238	3.5
7	384	1097	2540	42.4	2537	243	3.0
8	310	973	2281	43.6	2280	232	3.8

Table 10.6: Simulation results from the second folding.

Conf	θ^{rel}	K^{rel} (mN/θ)	F_2^{45} (mN)	K_2^{unl} (mN/θ)	θ_2^{unl}	E_2^{st} (F*θ)
1	3.2	353	2558	247	3.2	10131
2	3.6	300	2289	240	3.7	4739
3	3.3	366	2527	221	3.7	10322
4	3.6	289	2287	211	3.7	5479
5	3.3	368	2512	241	3.6	9529
6	3.6	349	2302	231	4.0	5296
7	3.3	383	2510	233	3.9	9862
8	3.8	318	2255	236	4.3	4616

10.3 Parameter study

This parameter study will identify how the different material parameters affect the simulation results. In Stenberg (2002) it is shown that it is difficult to experimentally determine the interface parameters. The continuum parameters however, are easier to determine and are therefore considered more accurate. Consequently, this parameter study is focused on the interface model and not the continuum model. In the parameter study configuration 4 is used. All modified interface parameters are described in Appendix H.

In Table 10.7 there is a description of the eight different studies that were conducted. Note that due to converging problems, the simulation for Study (a) was aborted during the second folding and the simulation for Study (h) was aborted when the first folding was initiated.

Table 10.7: The modified parameters for simulations with configuration 4

Study	Modified parameters
a	Increased normal and shear stiffness: $10 * (K_n^0, K_{t_1}^0, K_{t_2}^0)$
b	Increased stiffness in shear: $10 * (K_{t_1}^0, K_{t_2}^0)$
c	Decrease of interface damage: 2∗C
d	Increase of interface damage: 0.5∗C
e	Increase of initial yield stress in tension: $2 * S_n^0$
f	Decrease of initial yield stress in tension: $0.5 * S_n^0$
g	Increase of initial yield stress in shear: $1.8 * (S_{t_1}^0, S_{t_2}^0)$
h	Increased stiffness with modified initial yield stress: $10 * (K_{t_1}^0, K_{t_2}^0)$, $1.2 * (S_{t_1}^0, S_{t_2}^0)$ and $0.6 * S_n^0$

10.3.1 Creasing

The creasing result plots from the simulations with modified parameters for configuration 4 are shown in Appendix B and the values of the property variables are presented in Table 10.8.

Table 10.8: Simulation creasing results for configuration 4 with modified parameters.

Conf	d_0 (μm)	K^{ini} (N/mm)	F_y (N)	F^{max} (N)
a	-460	450	56	131
b	-460	396	66	126
c	-460	324	71	125
d	-460	324	71	114
e	-460	324	70	112
f	-460	324	80	133
g	-460	324	98	147
h	-460	425	77	154
	K^{unl} (N/mm)	Δd (μm)	E^{st} (Nmm)	M/F/D
a	168	103	21	0.5/1.8/150
b	210	73	17	0.5/1.8/150
c	228	40	12	0.5/1.8/150
d	228	24	11	0.5/1.8/150
e	208	40	14	0.5/1.8/150
f	246	23	9	0.5/1.8/150
g	288	7	6	0.5/1.8/150
h	205	74	18	0.5/1.8/150

10.3.2 Folding

The folding results from the simulations with modified parameters for configuration 4 are presented in Appendix B and the values of the property variables from the first folding are shown in Table 10.9 and from the second folding in Table 10.10.

Table 10.9: Simulation results from the first folding with modified parameters and configuration 4

Study	K^{ini} (mN/θ)	F_y (mN)	F^{max} (mN)	θ^{max}	F_1^{45} (mN)	K_1^{unl} (mN/θ)	θ_1^{unl}
a	260	579	2097	45.0	2097	174	7.4
b	281	688	2312	43.8	2311	176	5.3
c	292	1055	2412	45.0	2412	248	3.5
d	279	937	2060	45.0	2060	174	3.6
e	319	1098	2446	23.8	2385	217	2.3
f	359	827	2360	45.0	2360	250	3.0
g	403	1145	2674	44.4	2671	335	2.3
h	-	-	-	-	-	-	-

Table 10.10: Simulation results from the second folding with modified parameters and configuration 4

Study	θ^{rel}	K^{rel} (mN/θ)	F_2^{45} (mN)	K_2^{unl} (mN/θ)	θ_2^{unl}	E_2^{st} (F*θ)
a	7.4	272	-	-	-	-
b	5.4	321	2262	217	6.2	10808
c	3.5	376	2410	236	3.7	7122
d	4.2	304	1972	187	3.7	4875
e	2.5	374	2323	218	2.1	12061
f	3.6	394	2319	247	3.9	4550
g	2.4	458	2667	342	2.3	5484
h	-	-	-	-	-	-

Chapter 11

Comparing simulation results with experimental test results

The results from a comparison between the experimental tests and the simulations are presented in this chapter. Also a comparison between the results from the parameter study and the experimental tests are performed. All comparisons are based on the results presented in the previous chapter.

11.1 Standard parameters

For each of the eight different configurations, the simulation results are compared with the results from experimental tests. The difference in percent between the two results will be calculated using the following expression:

$$\frac{X^{exp} - X^{sim}}{X^{exp}} * 100 = \textit{Difference (\%)} \tag{11.1}$$

where X^{exp} is a property variable for the experimental test and X^{sim} is the corresponding property variable for the simulation. When the difference approaches zero there is an equality between the experimental tests and simulations. A negative difference indicates that the experimental value is smaller than the value from the simulation. Accordingly, a positive difference indicates that the simulation value is smaller than the experimental test value.

11.1.1 Creasing

The results from comparing the creasing property variables from the experimental test in Table 10.1 with the property variables from the simulation in Table 10.4 are shown in Table 11.1.

Table 11.1: Creasing differences between experimental tests and simulations

Conf.	Initial stiff.	Yield force	Max force	Unload stiff.	Res. def.	Stored energy
1	30%	8%	30%	-49%	88%	85%
2	27%	16%	36%	-82%	84%	81%
3	41%	-11%	33%	-29%	78%	80%
4	37%	7%	38%	-56%	80%	78%
5	39%	-18%	28%	-35%	78%	78%
6	36%	-3%	32%	-60%	83%	79%
7	38%	-17%	29%	-31%	72%	76%
8	38%	-7%	33%	-59%	79%	76%

11.1.2 Folding

The results from comparing the folding property variables from the experimental test in Table 10.2 and Table 10.3 with the property variables from the simulation in Table 10.5 and Table 10.6 are shown in Table 11.2. The damage is defined as the difference in force at 45° between the first and second folding, i.e. F_1^{45} - F_2^{45}. Note that some property variables are excluded in the comparison in order to obtain a better overview.

Table 11.2: Folding differences between experimental tests and simulations

Conf	Initial stiffness	Force at 45°, 1st fold	Residual deformation, reload
1	-2%	-8%	77%
2	-15%	-22%	72%
3	0%	0%	76%
4	-7%	-16%	70%
5	-1%	-1%	76%
6	-5%	-16%	70%
7	0%	-4%	76%
8	1%	-16%	72%
	Reload stiffness	Damage at 45°	Stored energy, 2nd fold
1	-235%	72%	46%
2	-229%	57%	72%
3	-216%	62%	50%
4	-203%	58%	70%
5	-247%	75%	52%
6	-298%	29%	70%
7	-250%	53%	50%
8	-235%	53%	73%

11.2 Parameter study

As for the standard parameters, the difference between the experimental results and the results from the parameter study are calculated as a percentage. The differences are determined by using the formula (11.1). The parameter study is performed using configuration 4 and therefore only this configuration is considered in the results.

11.2.1 Creasing

The results from comparing the creasing property variables from the experimental tests in Table 10.1 with the property variables from the simulations with modified parameters in Table 10.8, are shown in Table 11.3.

Table 11.3: Creasing differences for configuration 4 between experimental tests and simulations with modified parameters. The results from Table 11.1 for configuration 4 with original parameters are shown at the bottom of every column.

Study	Init. stiff.	Yield force	Max force	Unload stiff.	Res. def.	Stored energy
a	2%	40%	34%	-26%	51%	62%
b	13%	30%	36%	-58%	66%	70%
c	29%	24%	37%	-71%	81%	78%
d	29%	24%	42%	-71%	89%	79%
e	29%	25%	43%	-56%	81%	76%
f	29%	14%	32%	-84%	89%	83%
g	29%	-5%	25%	-116%	97%	88%
h	7%	17%	22%	-54%	95%	67%
Conf4	37%	7%	38%	-56%	80%	78%

11.2.2 Folding

The results from comparing the folding property variables from the experimental tests in the Tables 10.2 and 10.3 with the property variables from the simulations with modified parameters in the Tables 10.9 and 10.10, are shown in Table 11.4. Note that due to the converging problems mentioned earlier, the results for Study (h) and the results from the second folding for Study (a) are not included.

Table 11.4: Folding differences for configuration 4 between experimental tests and simulations with altered parameters. The results from Table 11.2 for configuration 4 with original parameters are shown at the bottom of every column.

Study	Initial stiffness	Force at 45°, 1st fold	Residual deformation, reload
a	18%	-5%	39%
b	12%	-16%	55%
c	8%	-21%	71%
d	12%	-4%	65%
e	0%	-20%	80%
f	-13%	-19%	70%
g	-24%	-34%	80%
h	-	-	-
Conf4	-7%	-16%	70%
	Reload stiffness	Damage at 45°	Stored energy, 2nd fold
a	-185%	-	-
b	-237%	8%	41%
c	-295%	96%	61%
d	-219%	-67%	73%
e	-292%	-17%	34%
f	-313%	21%	75%
g	-380%	91%	70%
h	-	-	-
Conf4	-203%	58%	70%

Chapter 12

Discussion

In this chapter remarks based on the results presented in the two previous chapters are made. Thereafter the conclusions from the evaluation of the 3DM model are stated. Also some suggestions for future work are made.

12.1 Remarks

During the creasing the loading behaviour is similar between experimental tests and simulations. In the simulations the initial stiffness has dependency of the creasing tool geometry. With a small clearance space, i.e. the intervening space between the male and female die, the initial stiffness is higher. This tendency is not visible in the experimental tests. The magnitude of the initial stiffness in the simulations is not as big as for the experimental tests. The difference in magnitude is between 30% and 40%. The results for the yield force show, for both experimental tests and simulations, a clear geometry dependency. The small clearance space between the male and female die, increases the yield force and this is visible in both experimental tests and simulations. The difference in yield forces is approximately 15%. The force measurements when the creasing depth is reached show the same tendencies for experimental tests and simulations. The force is geometry and creasing depth dependent. A deep crease with a small clearance gives a higher force in both experimental tests and simulations. A noticeable trend is that shallow creasings give a more accurate result than deep creasings. The difference in maximum force is circa 35%.

The magnitude for the unloading stiffness during the creasing is dependent on the creasing depth. This trend is visible for both experimental tests and simulations. The difference in magnitude is about 30% and 60% for shallow and deep creasings, respectively. In the experimental tests the residual deformation is highly dependent of the creasing depth. This inclination is also visible in the simulations, although the relative difference in residual deformation between shallow and deep creasings is not as big. The difference in residual

deformation magnitude is approximately 80%. The stored energy during the creasing for experimental tests and simulations is very similar. The stored energy for the deep creasings is twice as big as for the shallow creasings. This trend is visible for both experimental tests and simulations. The differences in energy magnitude between experimental tests and simulations are circa 80%.

The initial stiffness for the first foldings has good agreements between the experimental tests and simulations. The magnitudes are similar and the creasing depth dependency is visible in both experimental tests and simulations. The yield force however, has a clear creasing depth dependency in the experimental tests. This tendency is not visible in the simulations. The maximum forces in the experimental tests develop at the folding angle 13°. This should be compared to the simulations where the maximum forces develop at the maximum folding angle of 45°. Both experimental tests and simulations show a creasing depth dependency during the folding although it is more obvious in the experimental tests. The forces at 45° are lower for the shallow creasings than for the deep creasings. This tendency is visible for the experimental tests as well as for the simulations. The simulations with shallow creasings correspond better to the experimental tests than the simulations with deep creasings. The differences in the unloading stiffness are substantial but the creasing depth dependency is visible in both experimental tests and simulations. The unloading angle, θ_1^{unl}, has in the experimental test, a noticeable creasing depth dependency. This dependency is harder to distinguish in the simulation results. Also, the unloading angle magnitude differs between experimental tests and simulations.

During the second foldings, the reload angle for the experimental tests has no creasing tool geometry dependency and this is also valid for the simulations. The creasing depth however, affects the results for both the experimental tests and simulations but the deep creasings for the experimental tests give lower reload angles in contrary to simulations, where the shallow creasings result in lower reload angles. The reload stiffness in experimental tests and simulations are creasing depth dependent but the differences in magnitude are approximately 240%. The forces at 45° during the second foldings are still creasing depth dependent for both experimental tests and simulations. The difference in the damage at 45° is approximately 60%. For both the experimental tests and the simulations the magnitudes of the unload stiffness are similar to the unloading stiffness during the first foldings, but the creasing depth dependency for the simulations is no longer present. After the second folding the unloading angles for both experimental tests and simulations have increased but the creasing depth dependency is only obvious in the experimental tests. The difference in stored energy during the second foldings are circa 50% for the shallow creasings and circa 70% for the deep creasings. The creasing depth dependency is consequently visible in the experimental tests as well as for the simulations.

The results from the parameter study during creasing, showed that an increase in interface stiffness improved the initial stiffness during creasing and the difference between experimental tests and simulation is 2%. With the modification of interface parameters no significant improvement in yield forces are obtained. Although, by increasing the initial

yield stress in shear, the yield force is 5% larger than for the experimental test. Study (h) resulted in that the maximum force during creasing approaches the maximum force in the experimental test and the difference is 22%. By increasing the initial normal and initial shear stiffness, the difference in unloading stiffness is approximately halved and is 26%. The same study also increased the residual deformation and the stored energy in the simulation and the difference between the experimental test and the simulation is 51% and 62%, respectively.

When folding, the parameter study showed that an increase of the initial yield stress in ZD tension, made the initial stiffness during folding in the experimental test and in the simulation compatible, i.e. there is no difference in the result. The difference in force at 45° between the experimental test and simulation during the first folding is 5%, when the normal and shear stiffness are increased. The same study increased the residual deformation and the difference is 39%. None of the conducted studies managed to significantly improve the reload stiffness in the simulations. With an increase of the initial stiffness in shear the damage at 45° is compatible with the damage in the experimental test and the difference is 8%. Note in Table 11.4 that a modification of the damage parameter C, i.e. study (c) and (d), has a huge impact on the damage at 45°. The difference in stored energy between the experimental test and the simulation is reduced to 41% from 70% when increasing the initial stiffness in shear.

12.2 Conclusions

The comparison between the experimental tests and the simulations has shown that the 3DM model describes the loading behaviour during creasing and folding well, although with some deviations. During loading when folding in the experimental tests, a defined bend is clearly visible when the folding angle is circa 14%. After the bend the measured force rapidly decreases. This bend is not present in the simulations, except for the case when the initial yield strength in tension was increased, where the result showed a (very) small bend. The bend with the following softening behaviour could be explained by extensive delamination in the experimental test specimens and since the fiber structure in the paperboard are approximated with interfaces, the 3DM model has difficulties describing the bend.

There is an obvious difference in unloading behaviour during creasing and folding between the experimental tests and simulations. Since the unloading behaviour was not affected by modifying the interface parameters, the differences are likely due to factors not included in the 3DM model. The difference in unloading during folding could be explained by that the creep in paperboard is not included in the 3DM model. Also the fact that the paperboard fiber structure is approximated with interfaces could explain the differences in result between experimental tests and simulations. During the unloading in the experimental tests the force magnitude decreases rapidly. This is not visible during the unloading in

the simulations. Instead, the test specimen springs back and the initial decrease in force magnitude is much slower.

The difference between the experimental tests and the simulations when comparing the maximum forces and the unloading stiffness increases with an increase of creasing depth. This difference in maximum force could be due to the reason that the compression behaviour in the ZD direction is not described accurate enough in the continuum model. In the continuum model, the out-of-plane behaviour for compression is entirely non-linear elastic, cf. equation (4.3). The difference in unloading stiffness and residual deformation after creasing between experimental tests and simulations could be explained by the fact that there is a difference in the unloading behaviour during uniaxial compression in the ZD direction, between the continuum model and the experimental tests. The continuum model has the same stress-strain response for compression and unloading, whereas in the experimental tests, the stress-strain behaviour yield different paths for compression and unloading, cf. Figure 12.1.

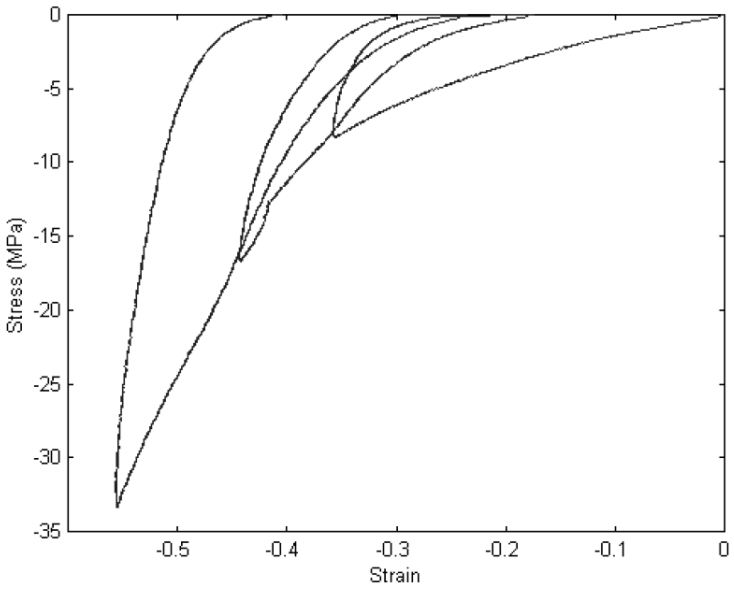

Figure 12.1: Stress-strain data for alternate loading in uniaxial ZD compression (Courtesy of N. Stenberg).

The parameter study showed that the interface parameters are very important. Even small changes of the interface parameters affect the results. Especially the increased interface stiffness contributes to a substantial improvement of the simulation results. Therefore, it is important that the test methods for determining the interface parameters are precise and accurate.

When changing configurations in the experimental tests, the results change accordingly. During the simulations with the different configurations, the same relative differences in

results are obtained. This means that the 3DM model describes the change of initial conditions good, excluding the magnitudes, which deviate.

In the simulation, the initial stiffness during the first and second fold has not changed. A conclusion is that the folding has not affected the stiffness. In the experimental test the folding has an obvious weakening effect, i.e. the initial stiffness for the second folding has decreased.

Note that since the creasing results from the simulations are not similar to the results from experimental tests, the initial conditions during folding are not the same. This should be regarded when comparing the folding results from the simulations and the experimental tests. Appendix E shows the differences in residual deformation after creasing between the conducted studies. In Just and Pålsson (2003) it is shown that there is a clear relationship between the residual deformation after creasing and the folding behaviour.

12.3 Further work

Before implementing the 3DM model as an engineering tool, the following proposals for future work and improvements are made.

- Include out-of-plane plastic strain for compression in the 3DM continuum model, since high compressive strains develop during creasing.
- Include paperboard creep in the 3DM continuum model for a better description of the unloading behaviour.
- Incorporate the Mandel stress into the theoretical framework so that the stress and the plastic velocity gradient are energy conjugated.
- Additional testing of Triplex 360 mN for a more precise characterisation with a low standard deviation of the interface parameters.
- Benchmark study; evaluate future improvements of the 3DM model using the results presented in this report.

Bibliography

Y.A. Cengel and M.A. Boles. *Thermodynamics, an engineering approach*. McGraw-Hill Education, 1998.

Y.F. Dafalias. Issues on the constitutive formulation at large elastic deformations, part 1:kinematics. *ACTA Mechanica*, (69):119–138, 1986.

C. Fellers and B. Norman. *Pappersteknik*. Department of Solid Mechanics, Royal Institute of Technology, 1998.

ABAQUS Inc. *ABAQUS Version 6.4 Documentation*. 2003.

M. Just. *Unpublished work*. 2005.

M. Just and M. Pålsson. *Roller-nip Influence on Crease Geometry and Bending Stiffness*. Division of Solid Mechanics, University of Lund, 2003.

M. Nygårds. *The 3DM model 3.2*. STFI-Packforsk, 2004.

N.S. Ottosen and M. Ristinmaa. *Introduction to Large Strain Inelasticity*. Division of Solid Mechanics, University of Lund, 2001.

M. Ristinmaa. *Review of Plasticity Model for Paper and Paperboard*. Division of Solid Mechanics, University of Lund, 2003.

M. Ristinmaa and C. Ljung. *An Introduction to Stability Analysis*. Division of Solid Mechanics, University of Lund, 2002.

TAPPI T 402 sp98. *Standard conditioning and testing atmospheres for paper, board, pulp handsheets and related products*. TAPPI, 1998.

N. Stenberg. *On the out-of-plane mechanical behaviour of paper materials*. Department of Solid Mechanics, Royal Institute of Technology, 2002.

www.swema.com. 20050330.

www.tetrapak.com. 20050214.

Q.S. Xia. *Mechanics of inelastic deformation and delamination in paperboard*. Department of Mechanical Engineering, Massachusetts Institute of Technology, Cambridge, MA, USA, 2002.

Appendix A

Configuration 1-8 with initial parameters

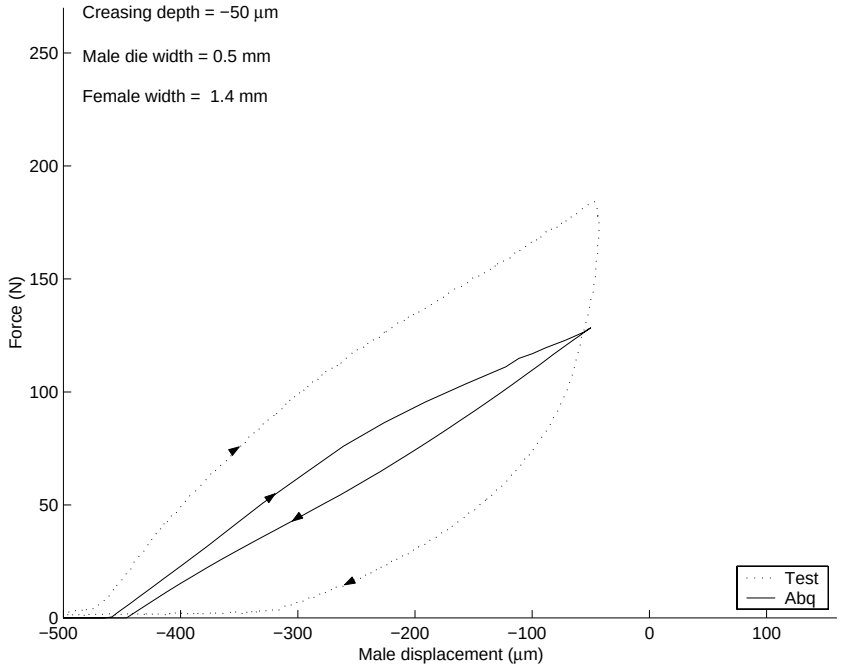

Figure A.1: Creasing, configuration 1

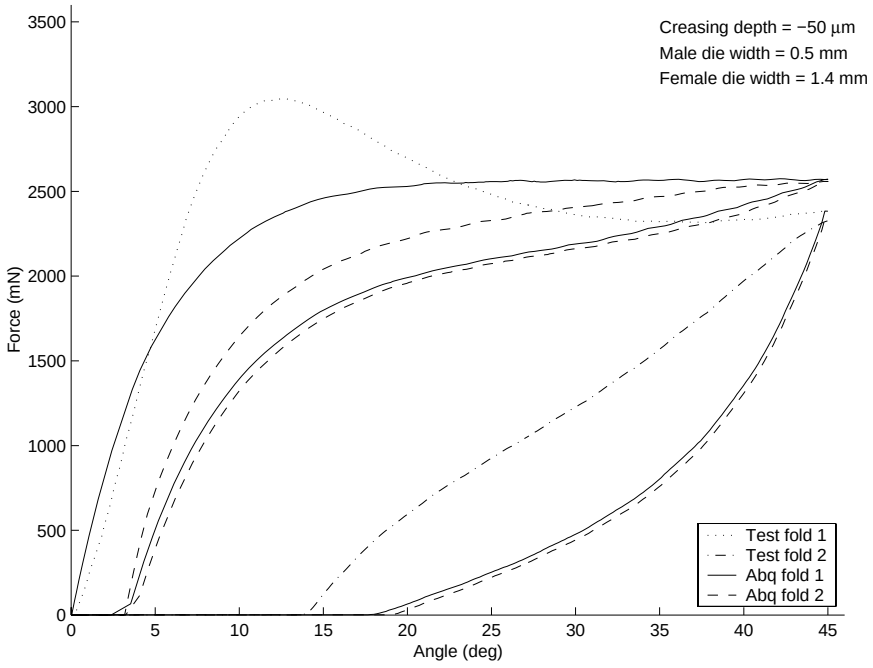

Figure A.2: Folding, configuration 1

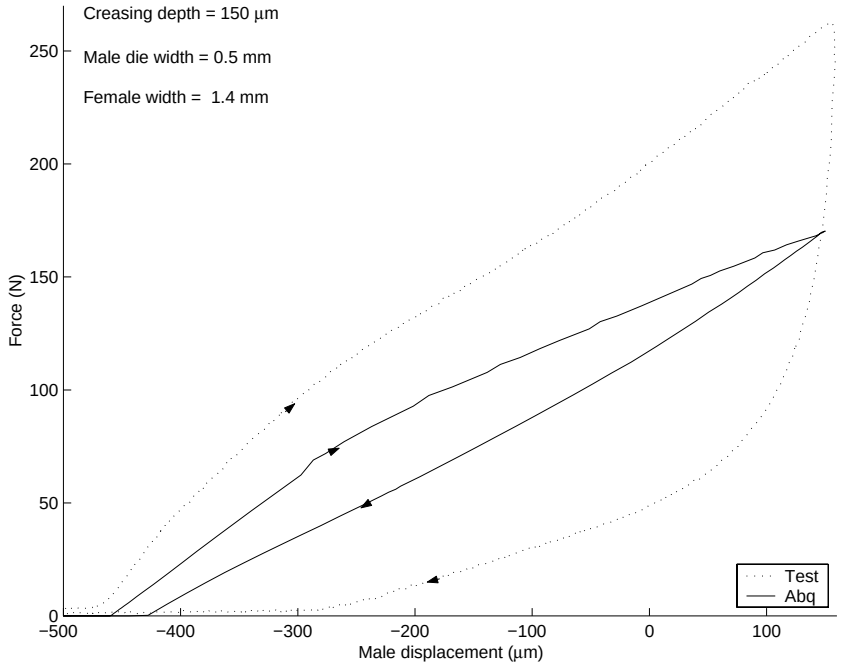

Figure A.3: Creasing, configuration 2

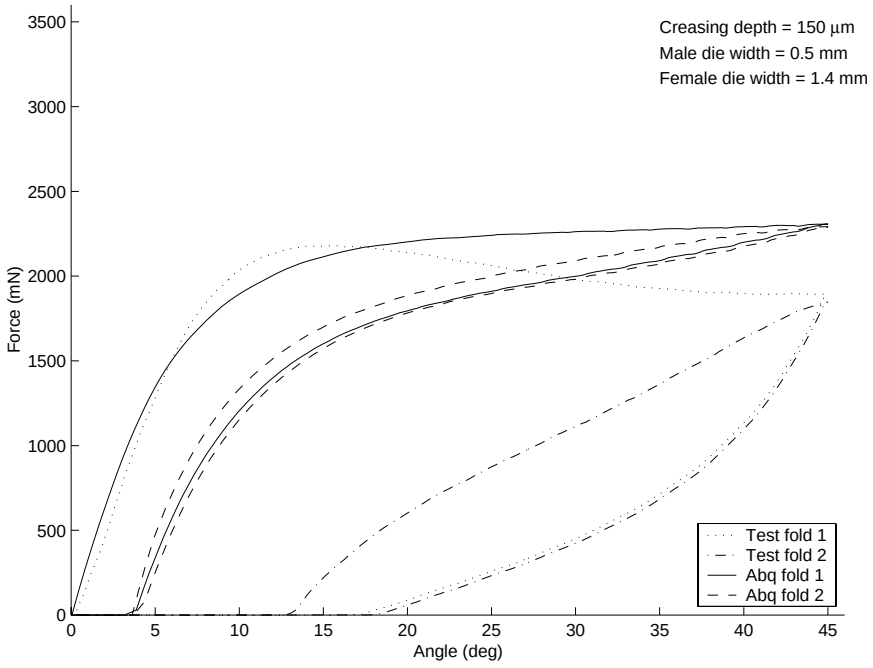

Figure A.4: Folding, configuration 2

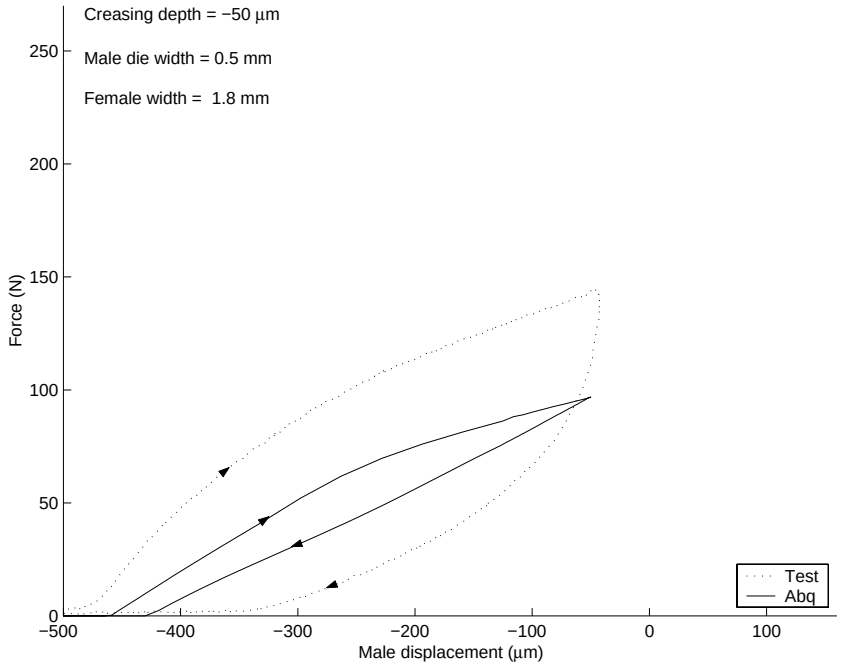

Figure A.5: Creasing, configuration 3

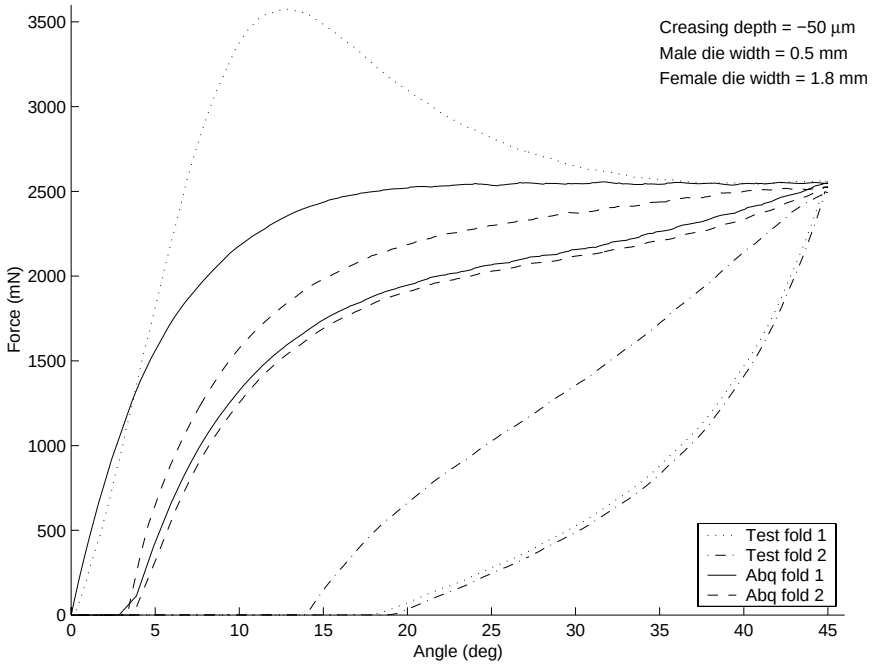

Figure A.6: Folding, configuration 3

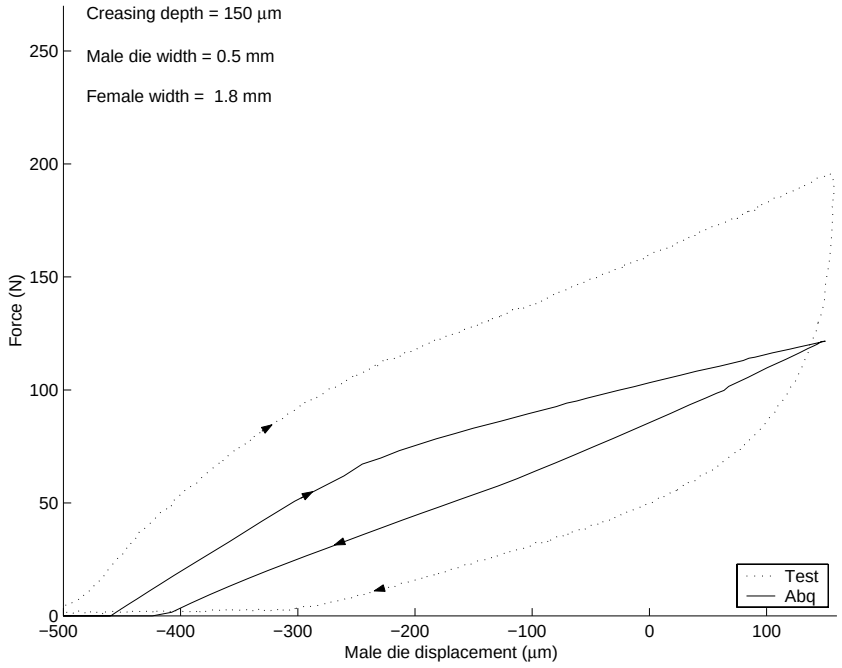

Figure A.7: Creasing, configuration 4

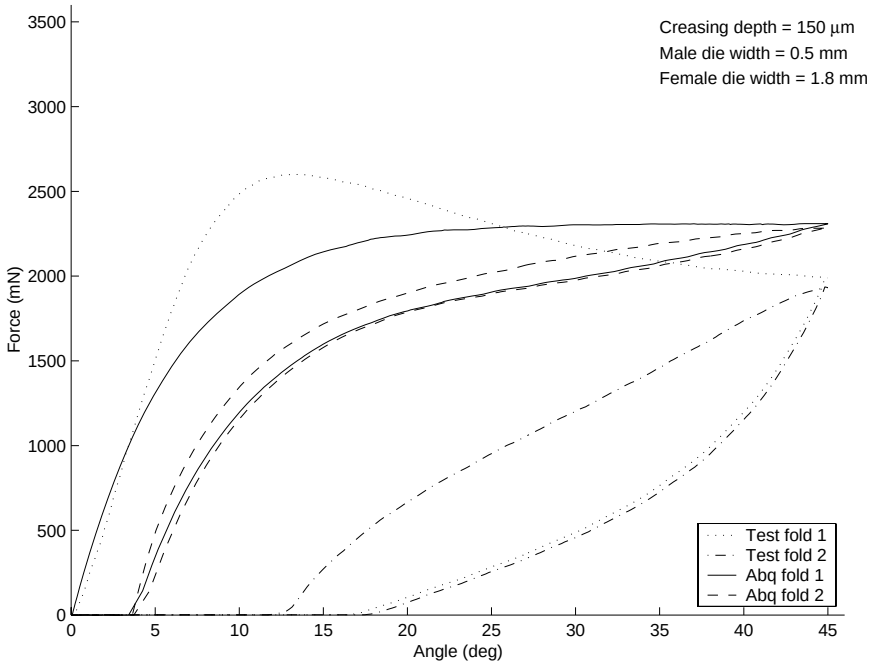

Figure A.8: Folding, configuration 4

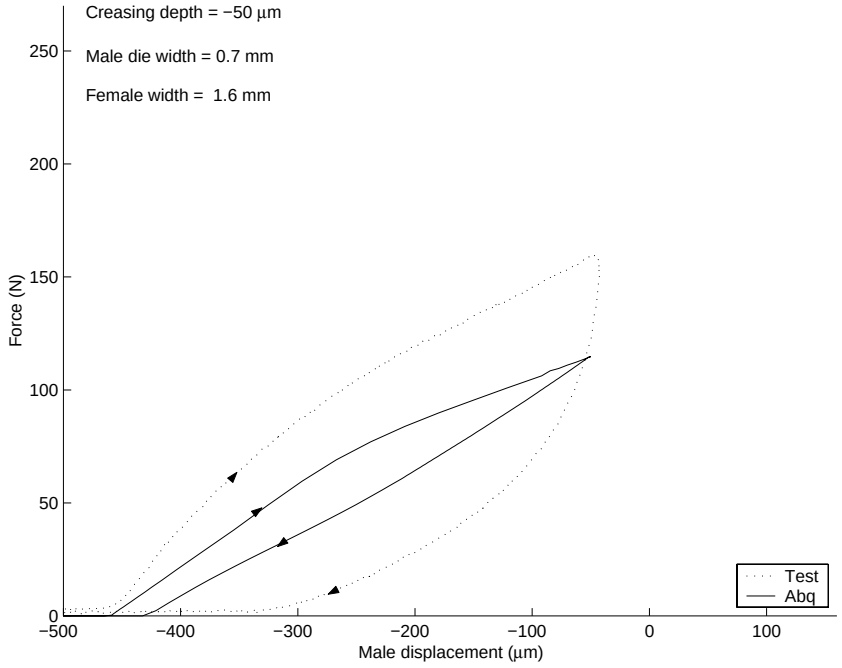

Figure A.9: Creasing, configuration 5

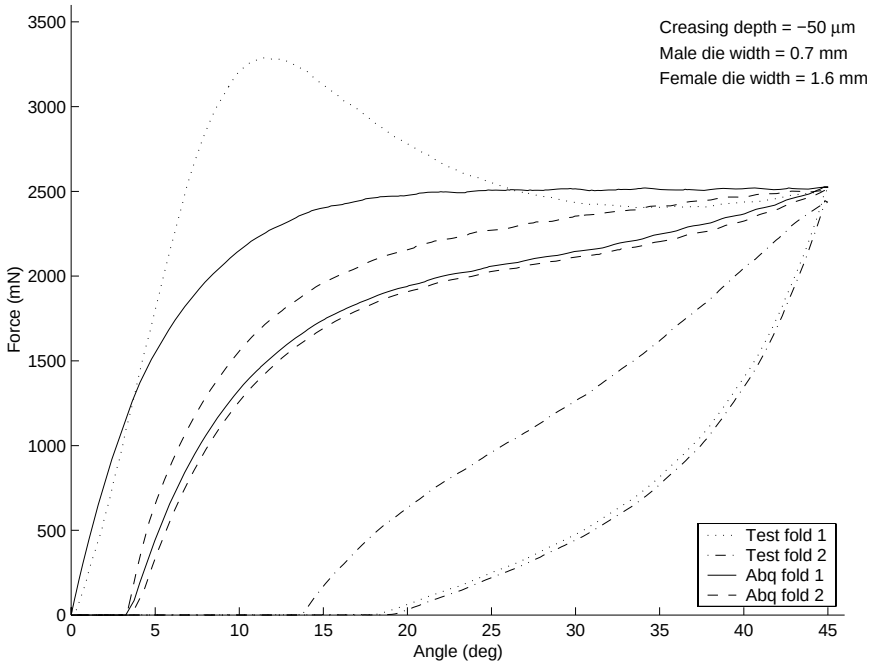

Figure A.10: Folding, configuration 5

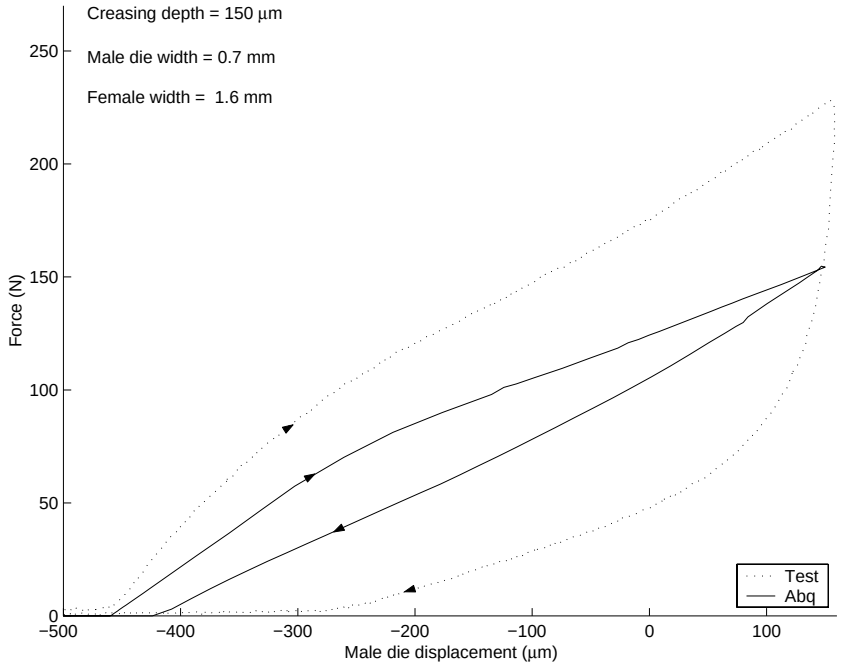

Figure A.11: Creasing, configuration 6

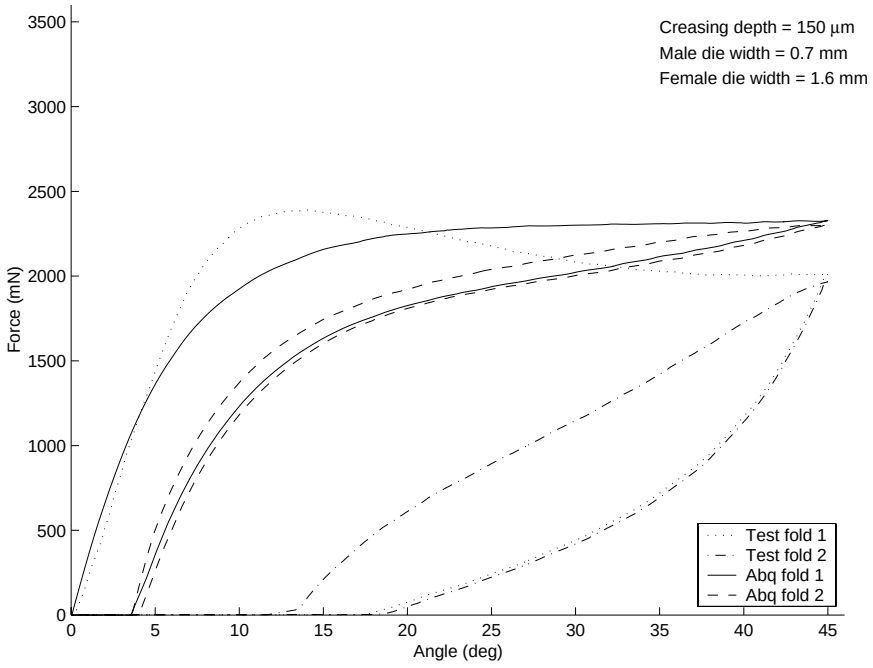

Figure A.12: Folding, configuration 6

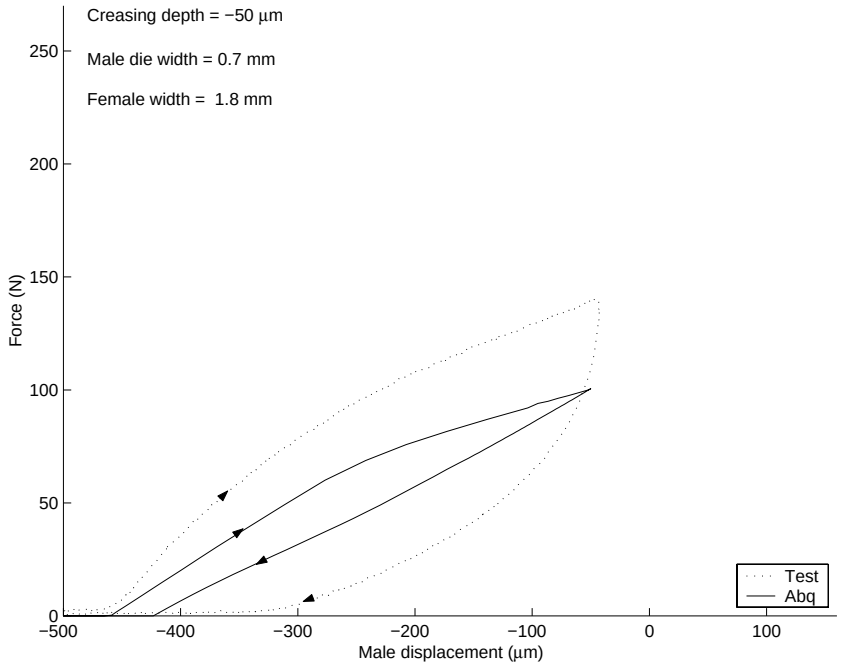

Figure A.13: Creasing, configuration 7

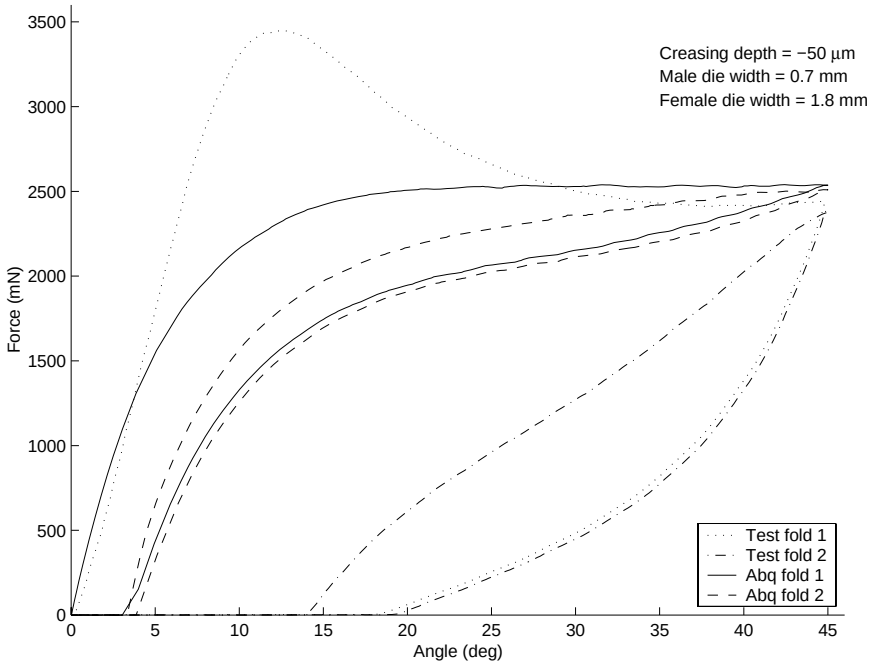

Figure A.14: Folding, configuration 7

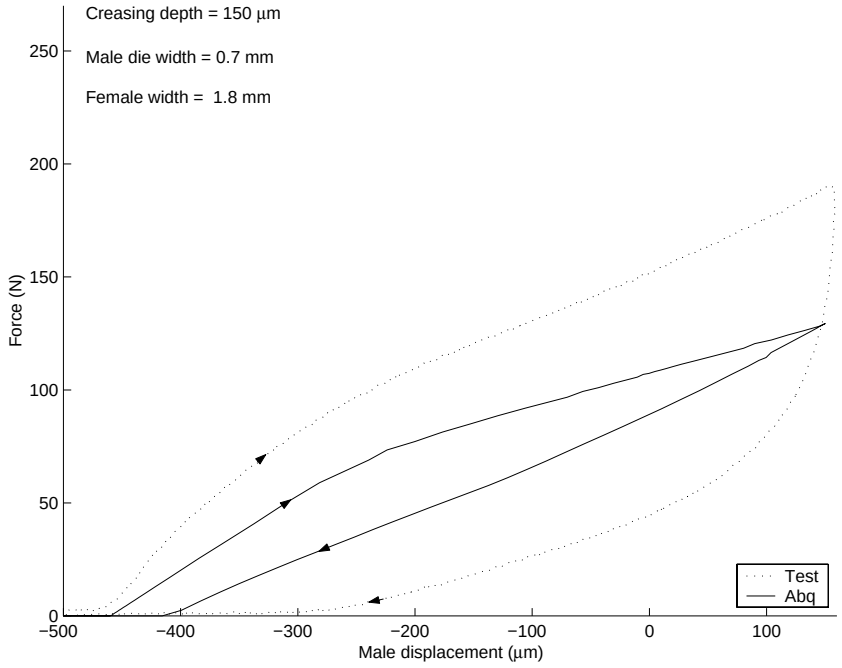

Figure A.15: Creasing, configuration 8

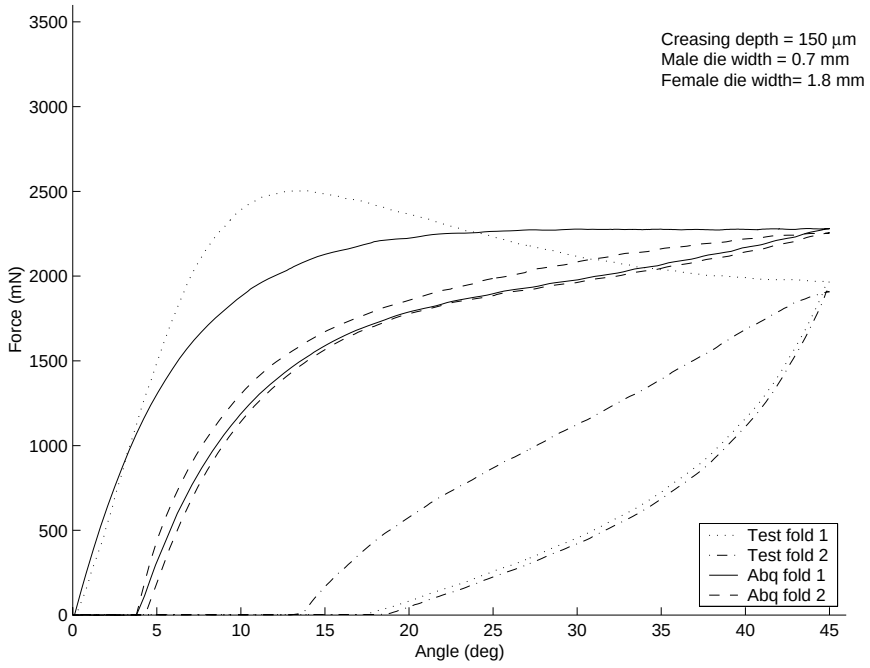

Figure A.16: Folding, configuration 8

Appendix B

Configuration 4 with modified interface parameters

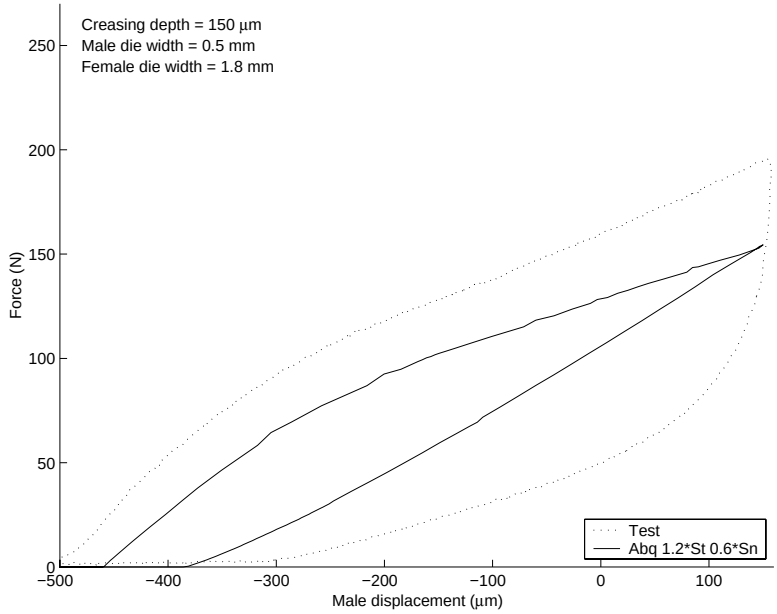

Figure B.1: Creasing $10 * (K^0_{t_1}, K^0_{t_2})$, $1.2 * (S^0_{t_1},\ S^0_{t_2})$ and $0.6 * S^0_n$

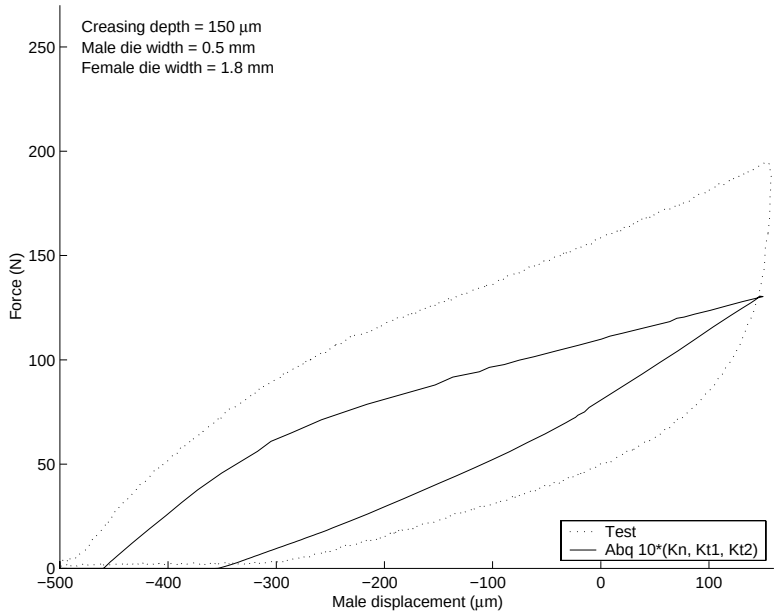

Figure B.2: Creasing $10 * (K_n^0, K_{t_1}^0, K_{t_2}^0)$

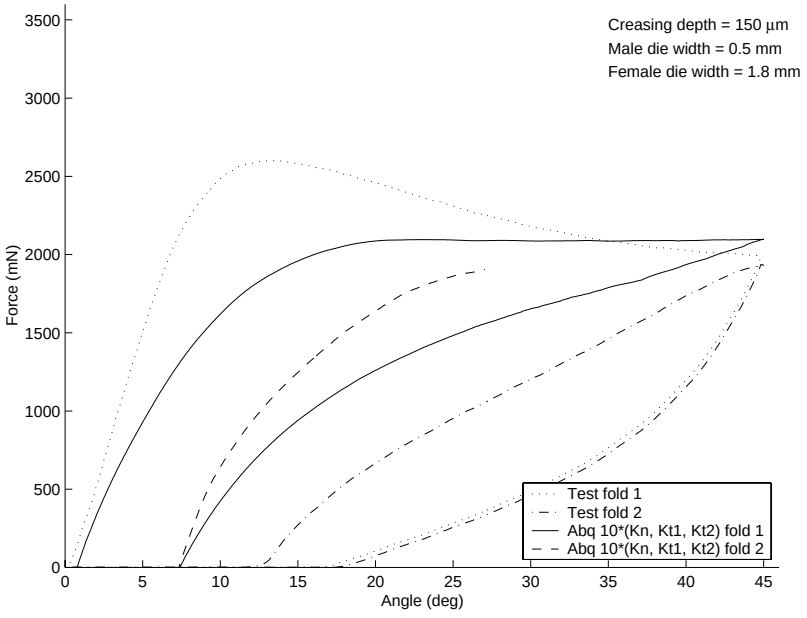

Figure B.3: Folding $10 * (K_n^0, K_{t_1}^0, K_{t_2}^0)$

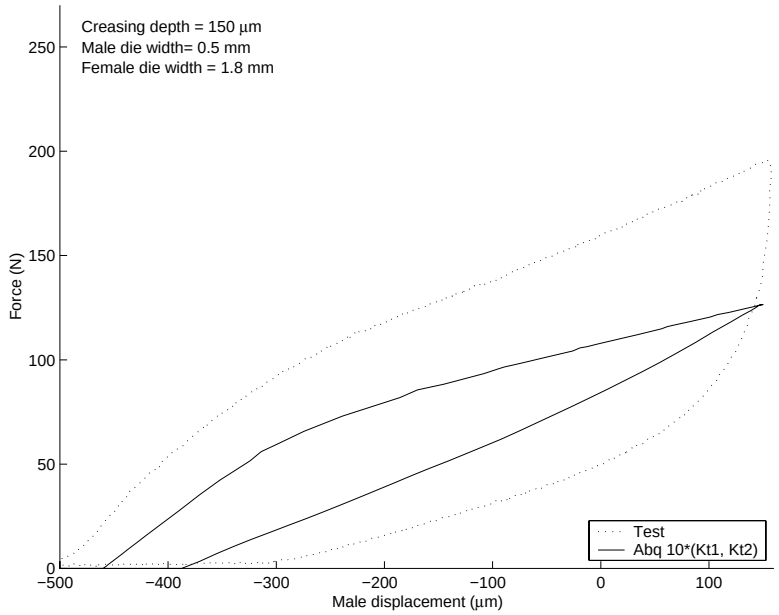

Figure B.4: Creasing $10 * (K^0_{t_1}, K^0_{t_2})$

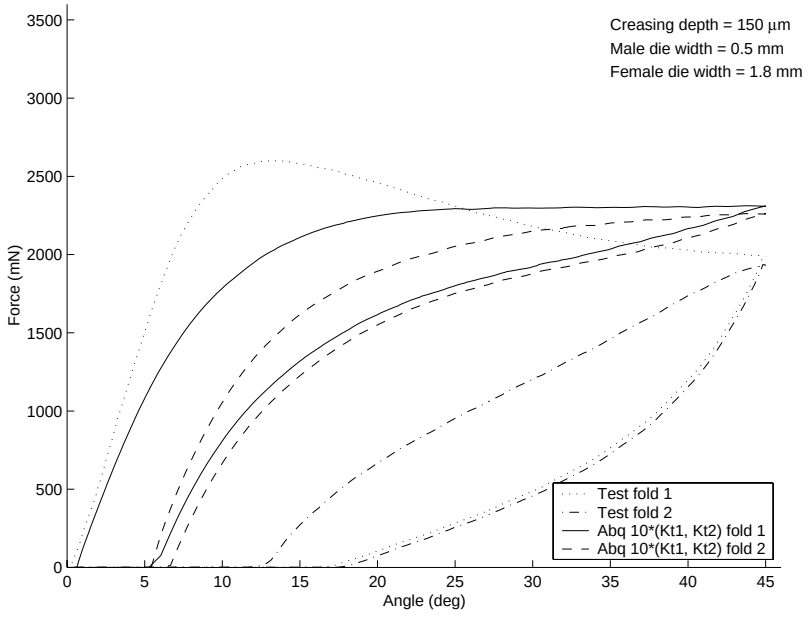

Figure B.5: Folding $10 * (K^0_{t_1}, K^0_{t_2})$

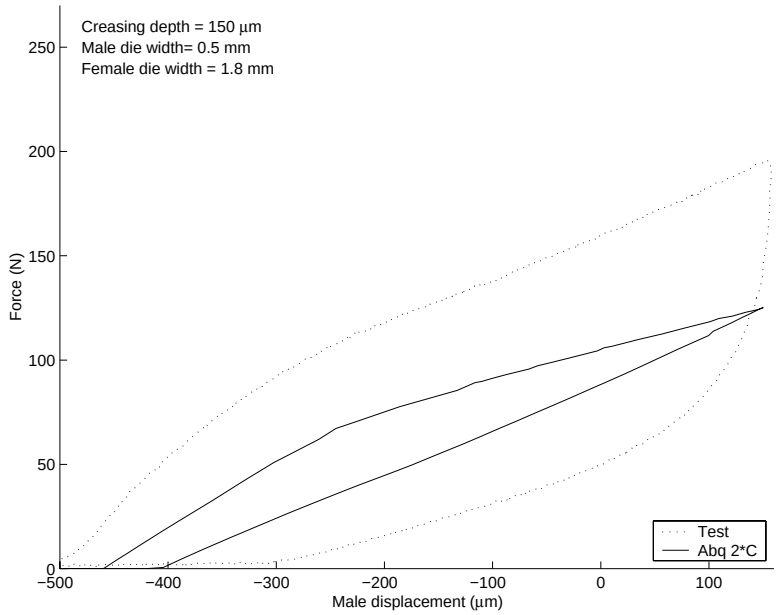

Figure B.6: Creasing $2 * C$

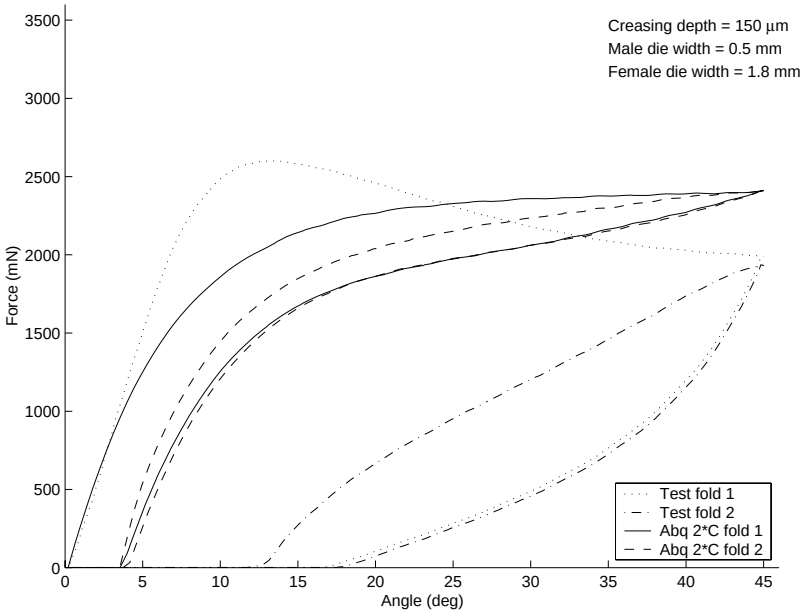

Figure B.7: Folding $2 * C$

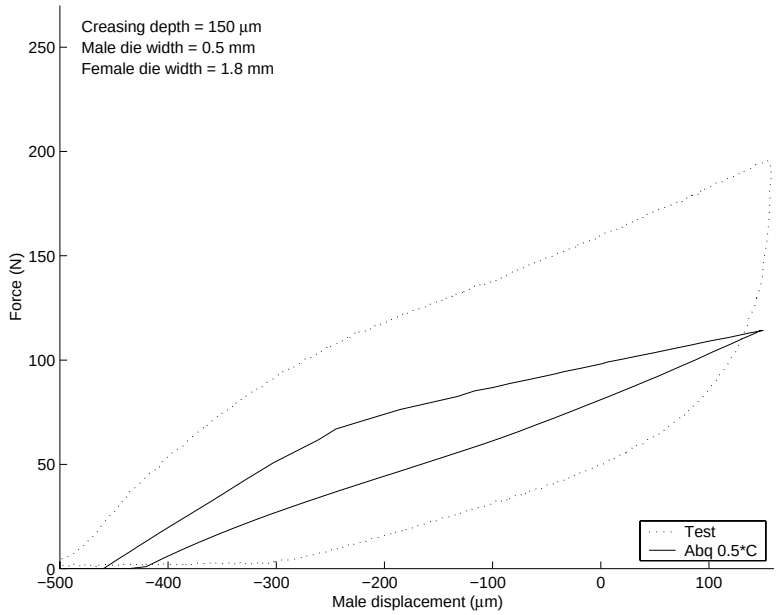

Figure B.8: Creasing $0.5 * C$

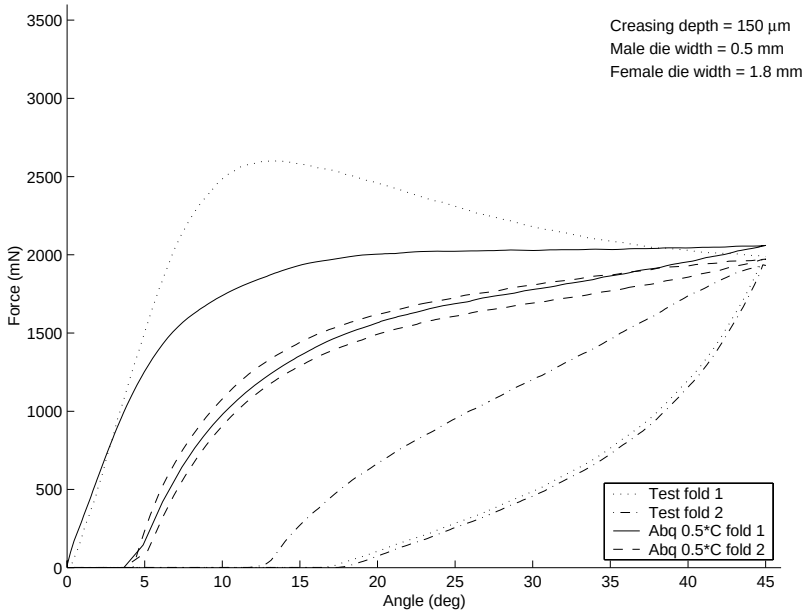

Figure B.9: Folding $0.5 * C$

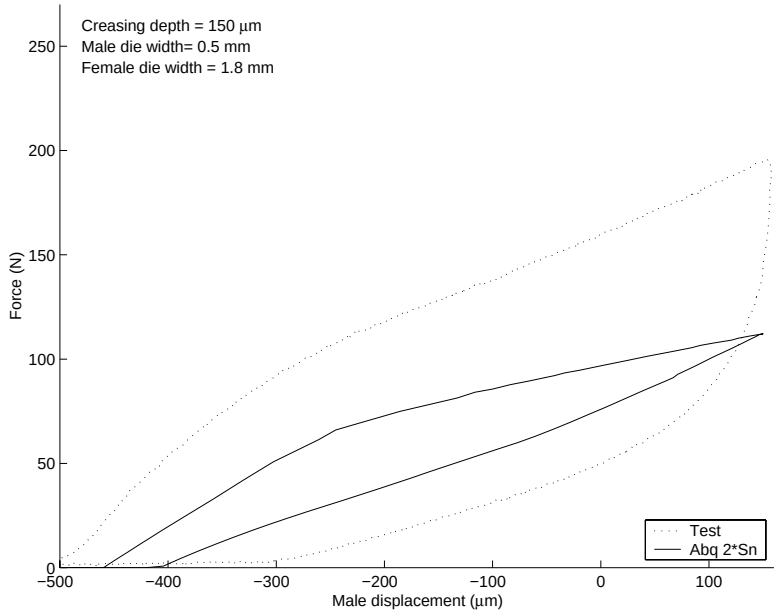

Figure B.10: Creasing $2 * S_n^0$

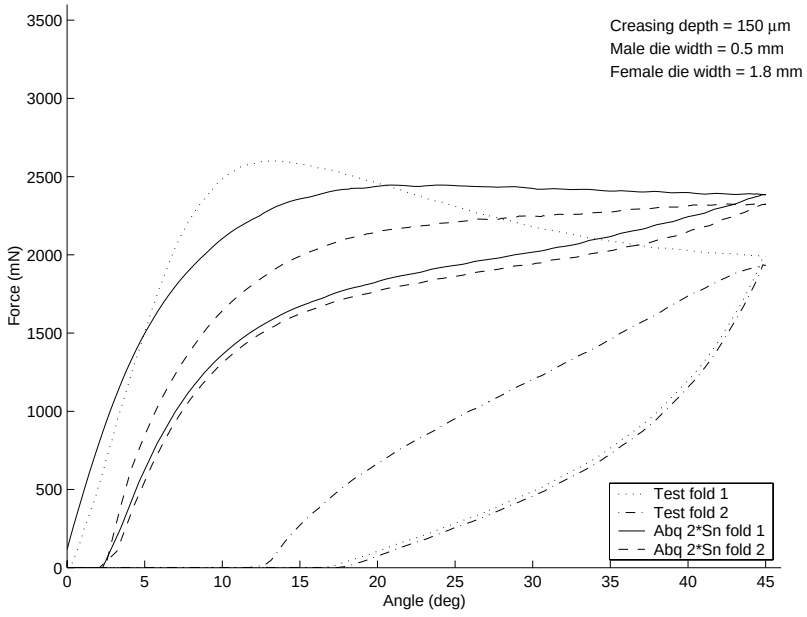

Figure B.11: Folding $2 * S_n^0$

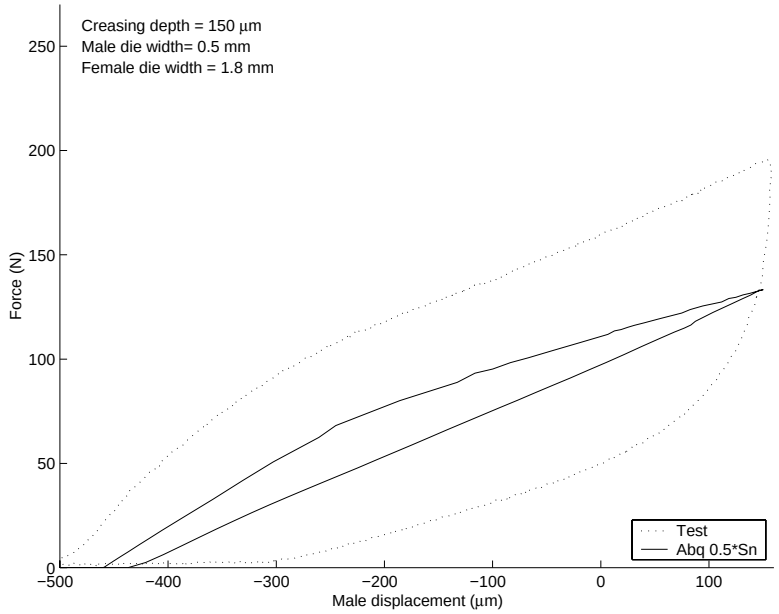

Figure B.12: Creasing $0.5 * S_n^0$

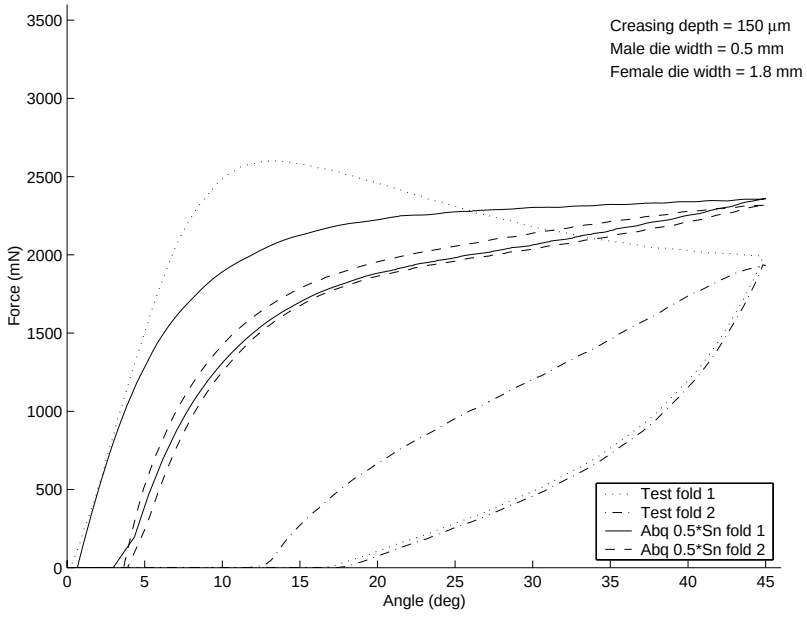

Figure B.13: Folding $0.5 * S_n^0$

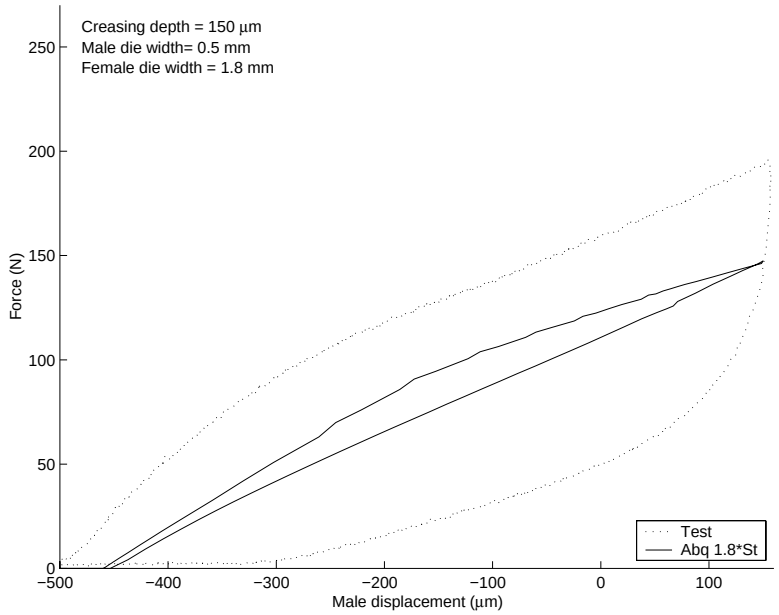

Figure B.14: Creasing $1.8 * (S^0_{t_1}, S^0_{t_2})$

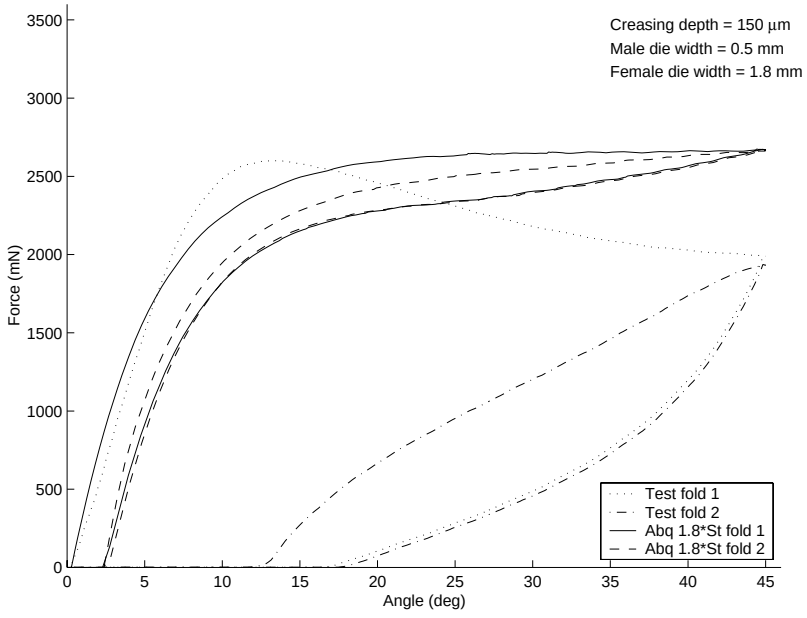

Figure B.15: Folding $1.8 * (S^0_{t_1}, S^0_{t_2})$

Appendix C

Logarithmic strain development during creasing

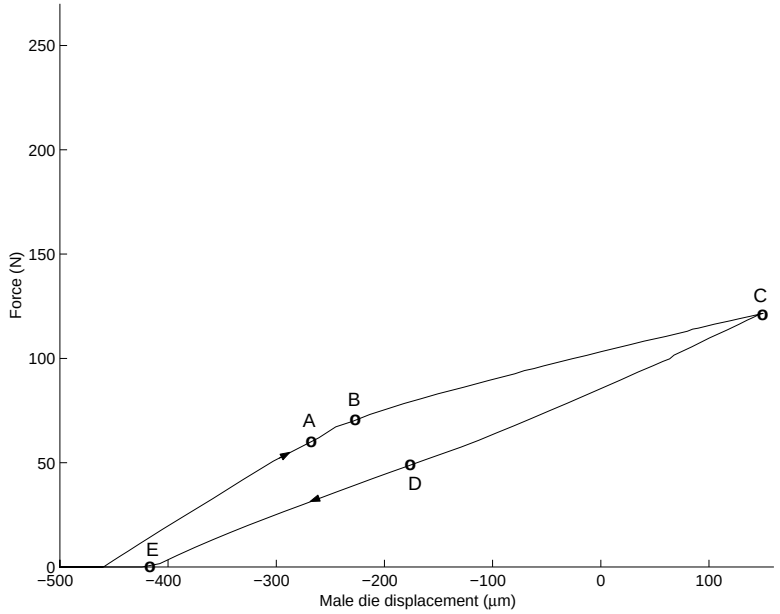

Figure C.1: Study points for creasing

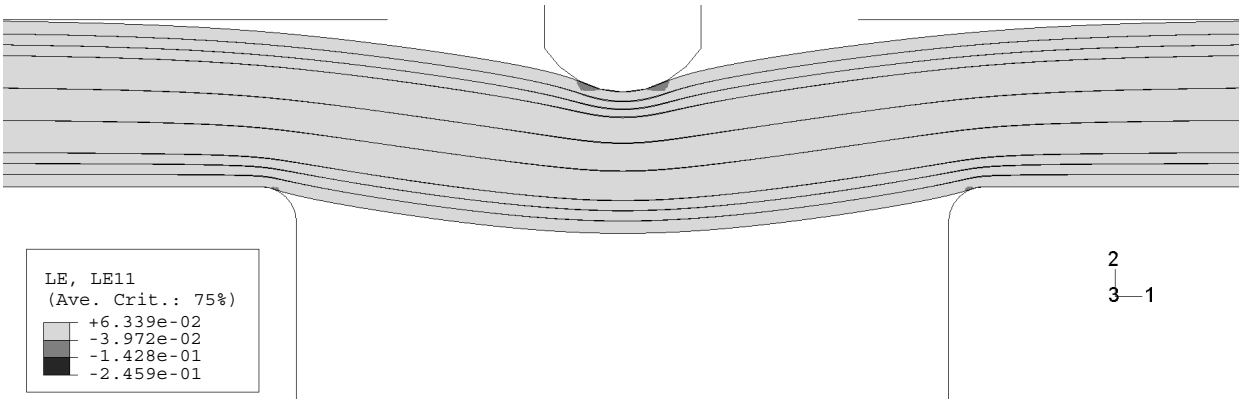

Figure C.2: LE11 point A

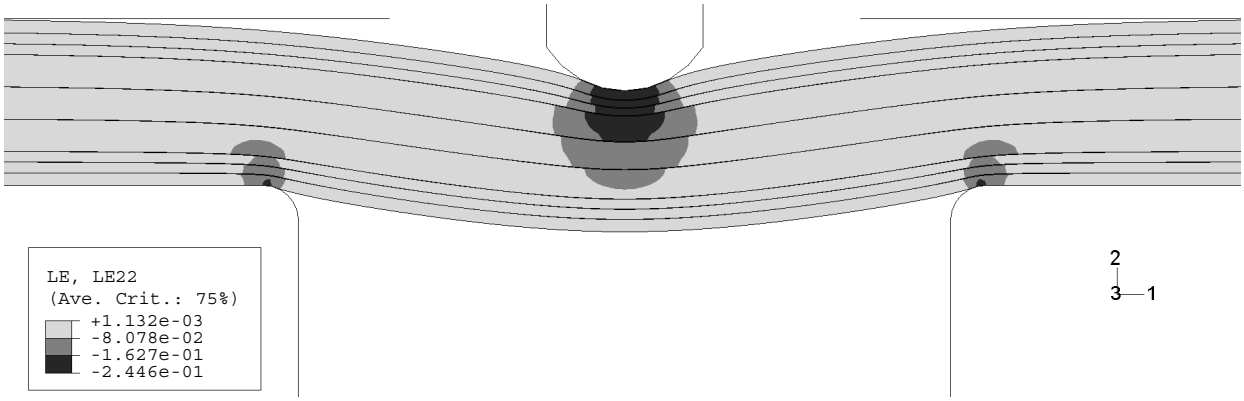

Figure C.3: LE22 point A

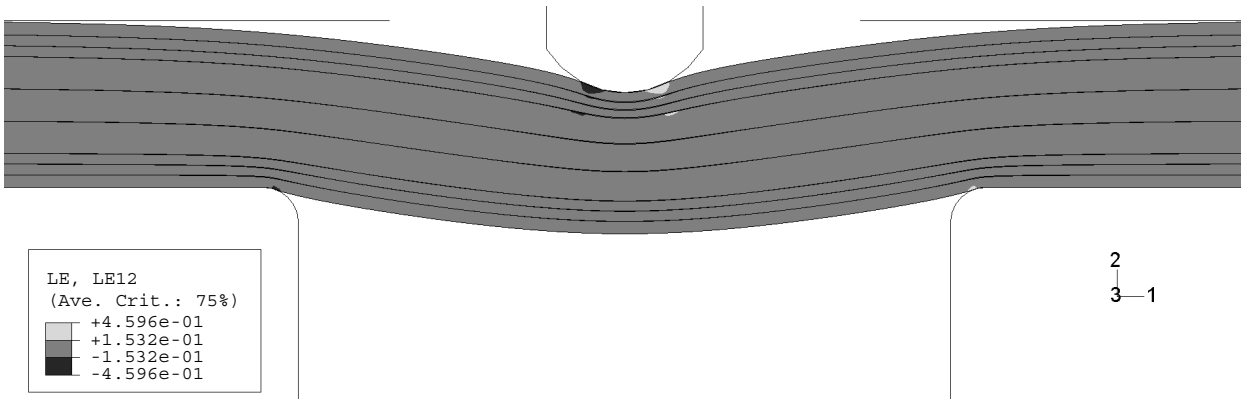

Figure C.4: LE12 point A

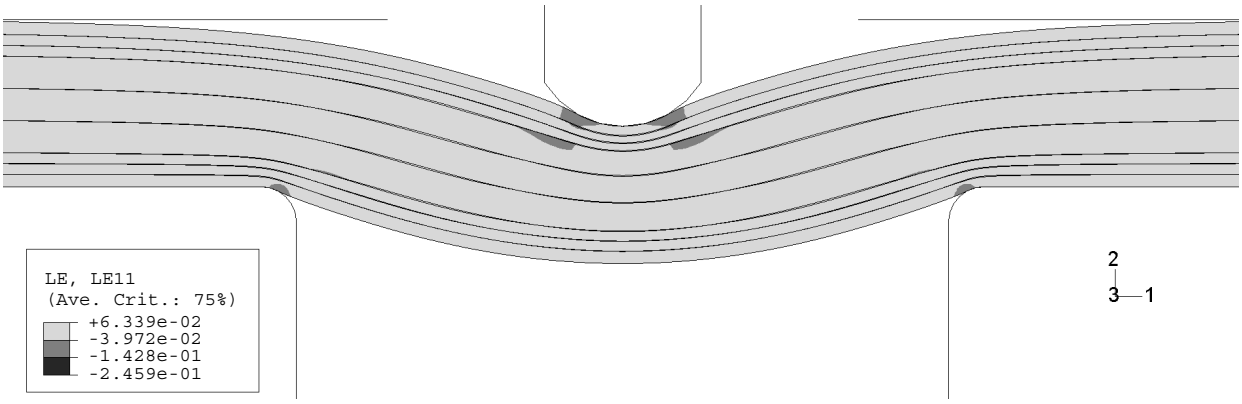

Figure C.5: LE11 point B

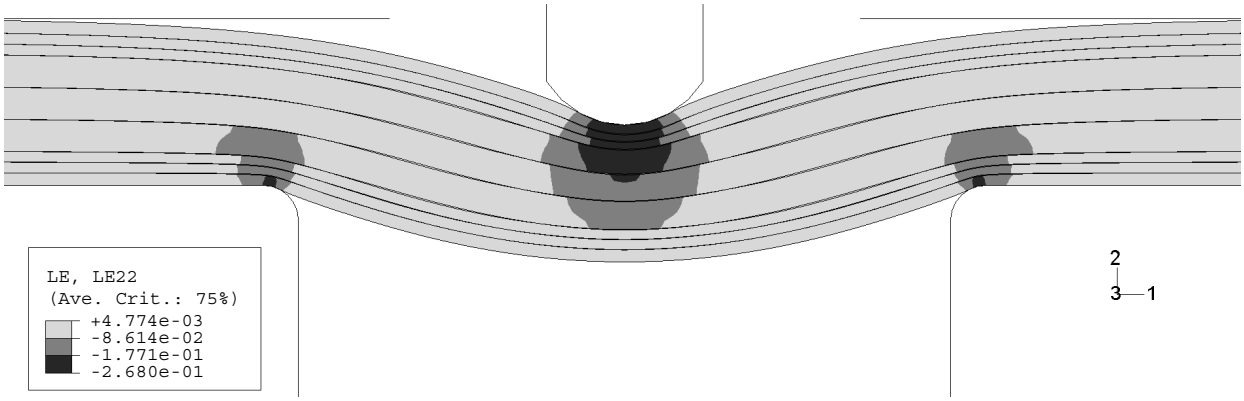

Figure C.6: LE22 point B

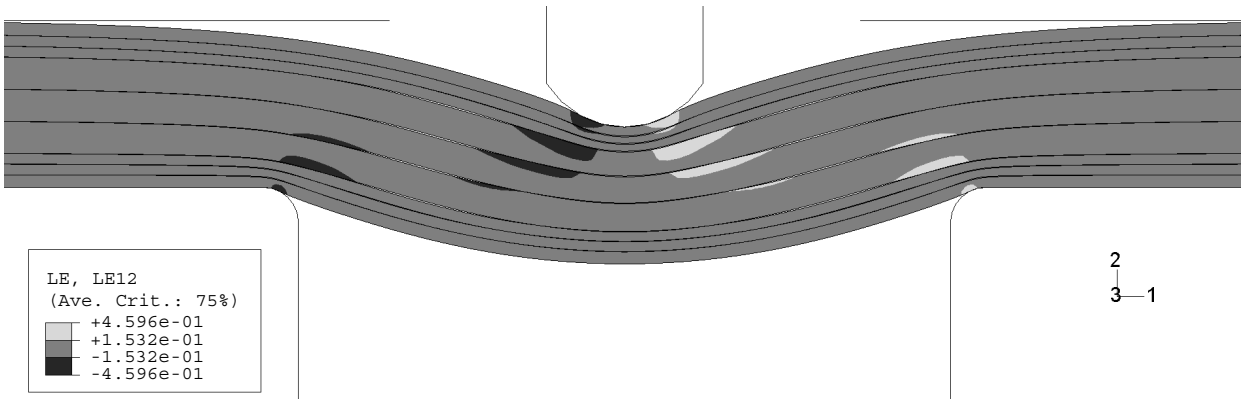

Figure C.7: LE12 point B

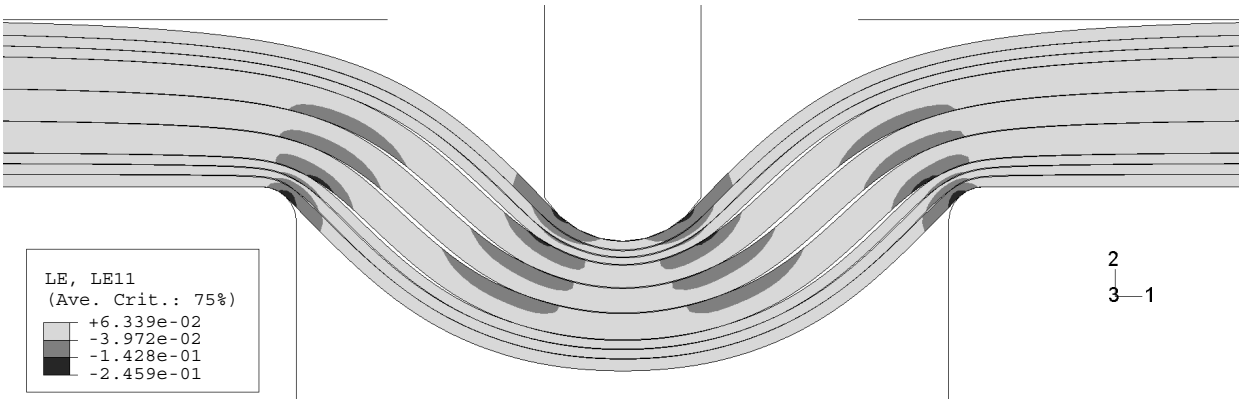

Figure C.8: LE11 point C

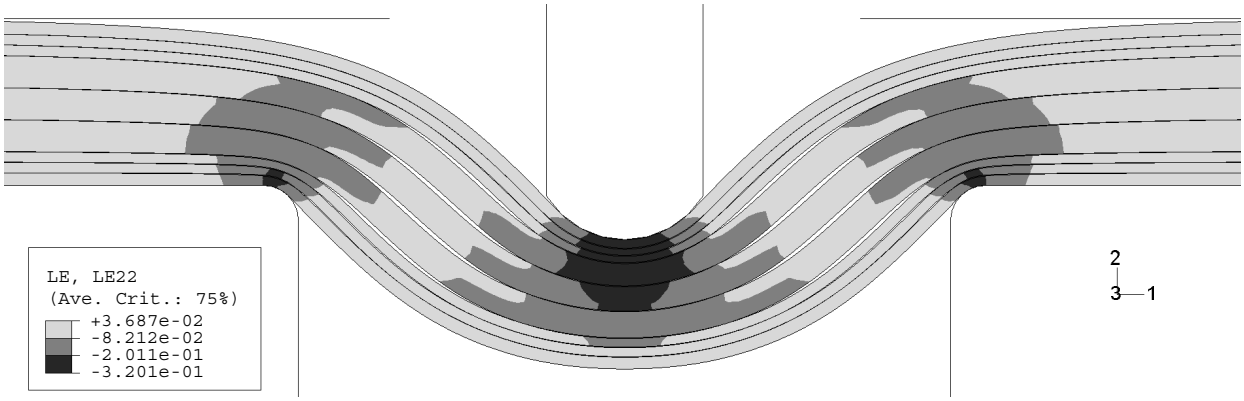

Figure C.9: LE22 point C

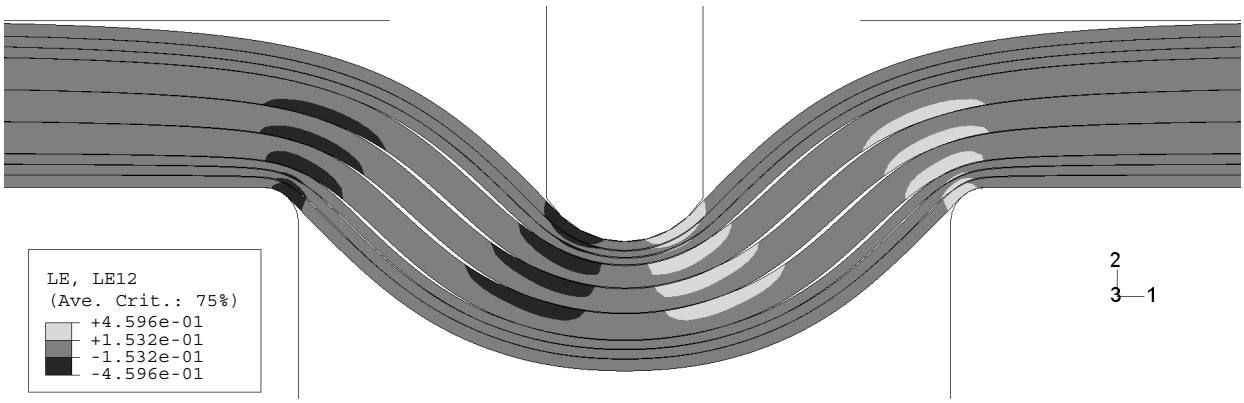

Figure C.10: LE12 point C

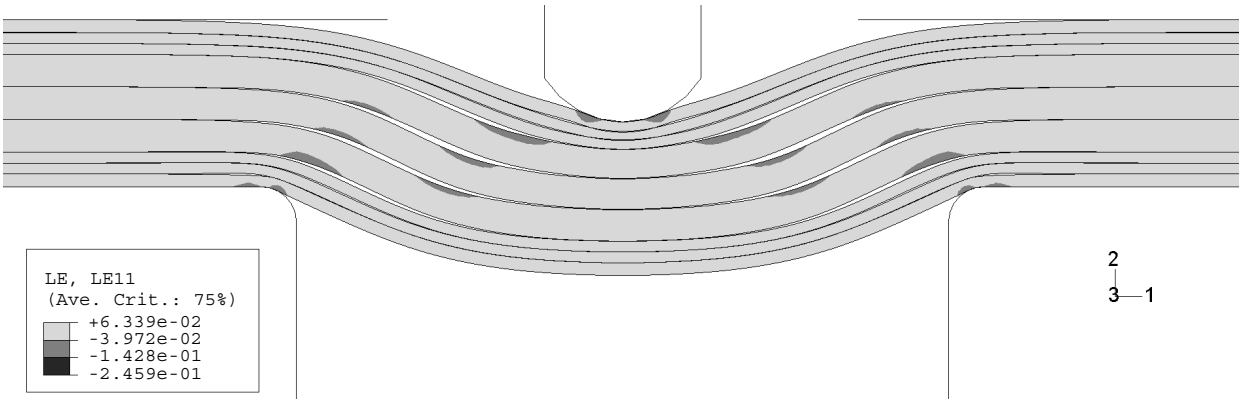

Figure C.11: LE11 point D

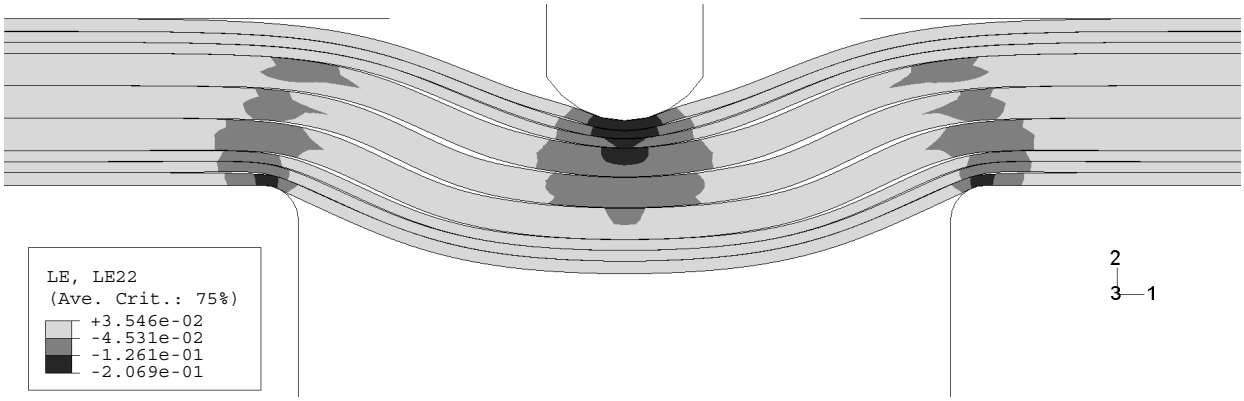

Figure C.12: LE22 point D

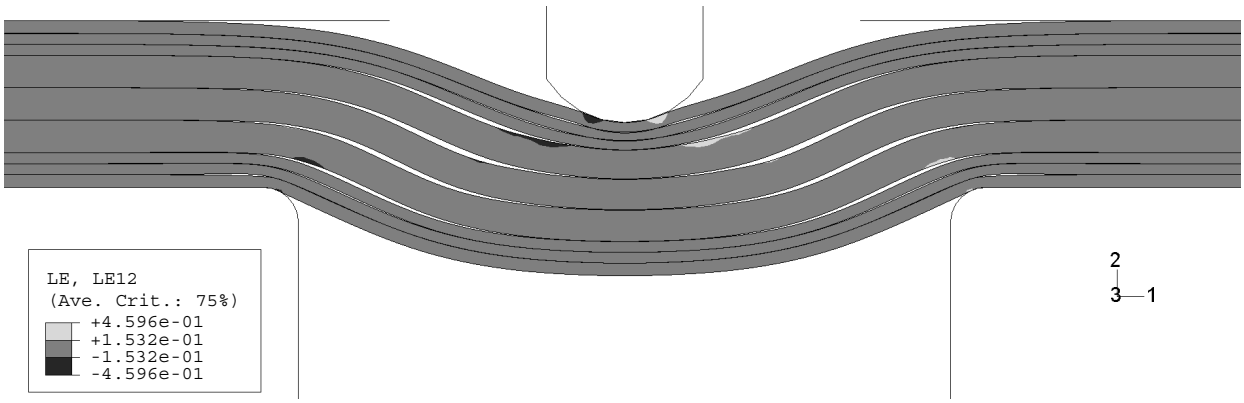

Figure C.13: LE12 point D

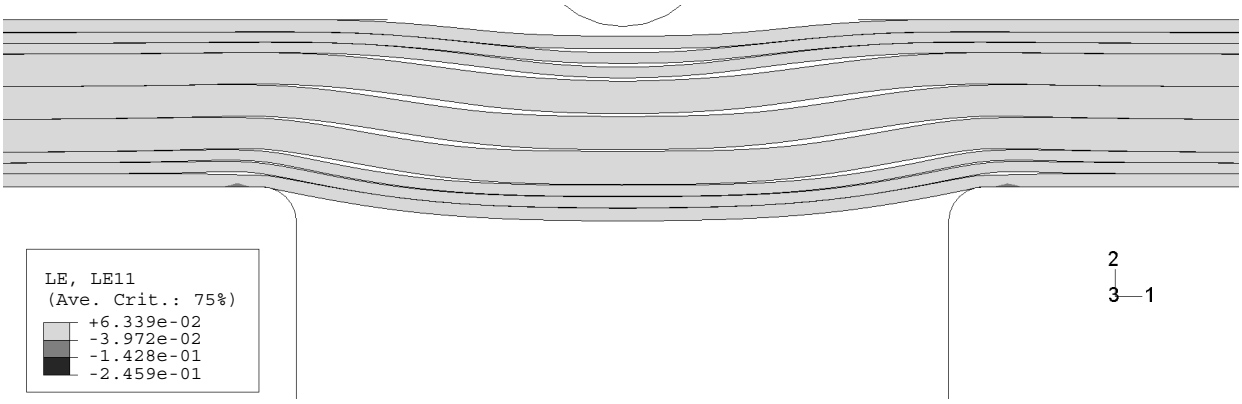

Figure C.14: LE11 point E

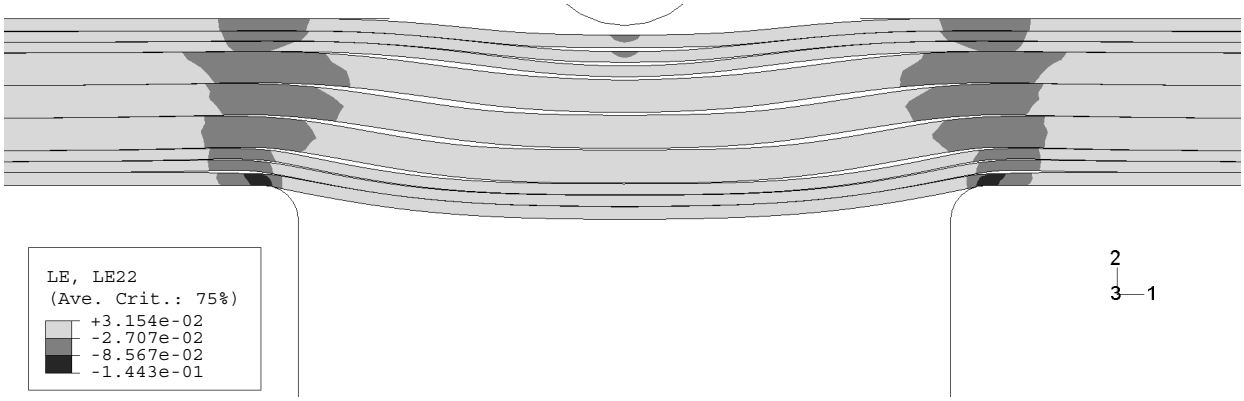

Figure C.15: LE22 point E

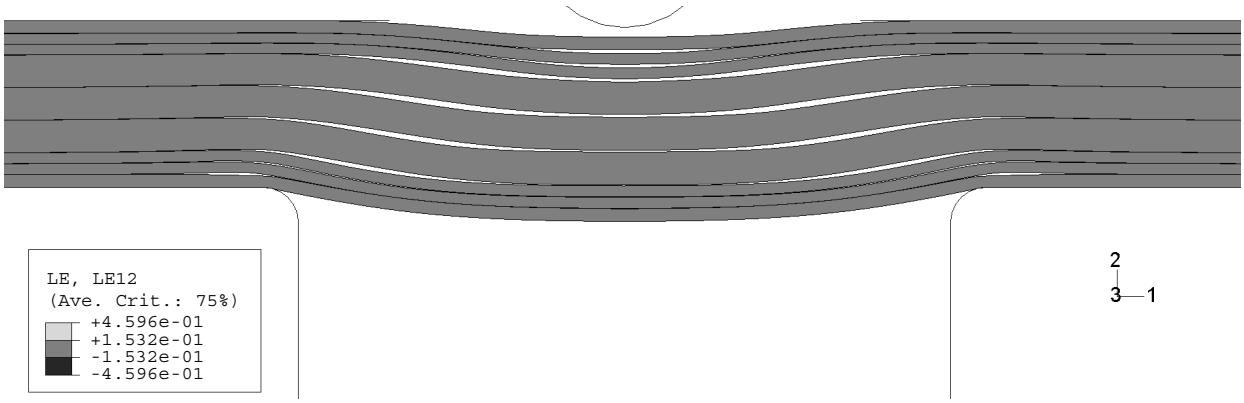

Figure C.16: LE12 point E

Appendix D

Logarithmic strain development during folding

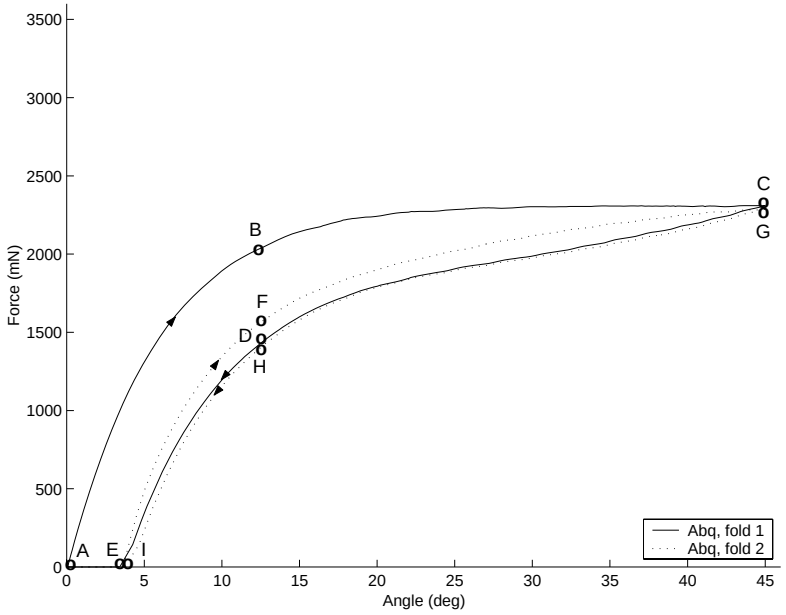

Figure D.1: Study points for folding

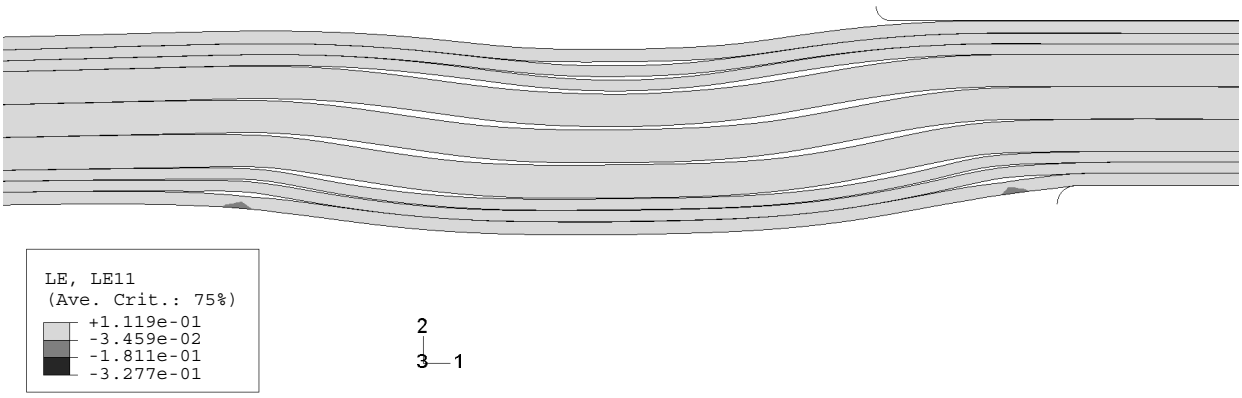

Figure D.2: LE11 point A

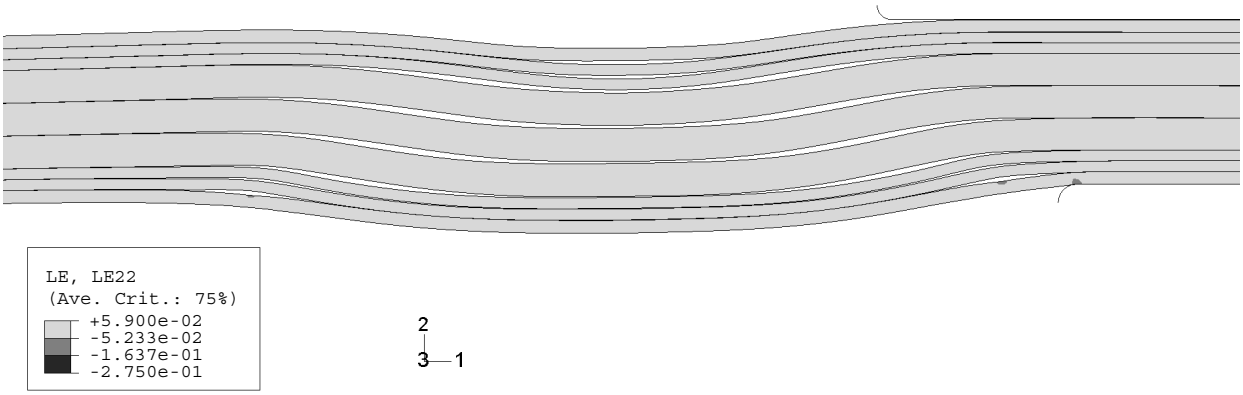

Figure D.3: LE22 point A

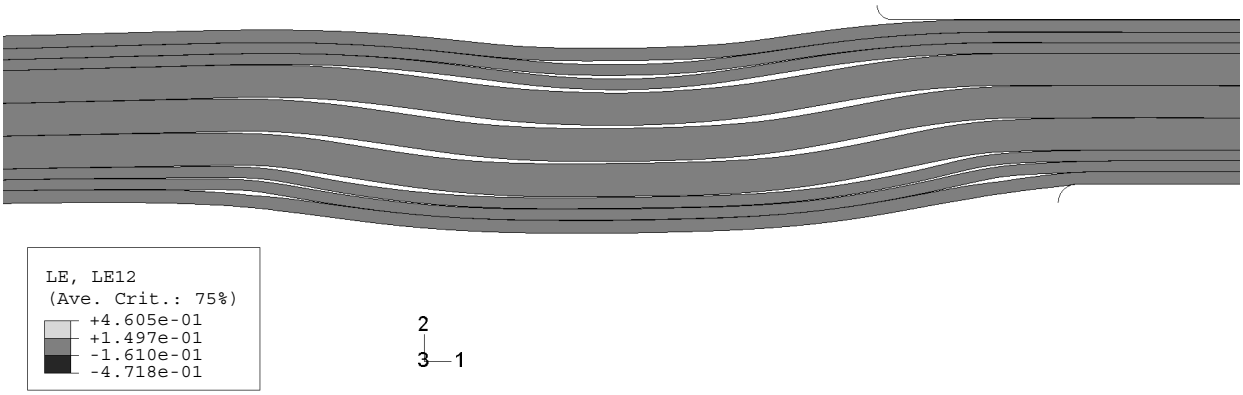

Figure D.4: LE12 point A

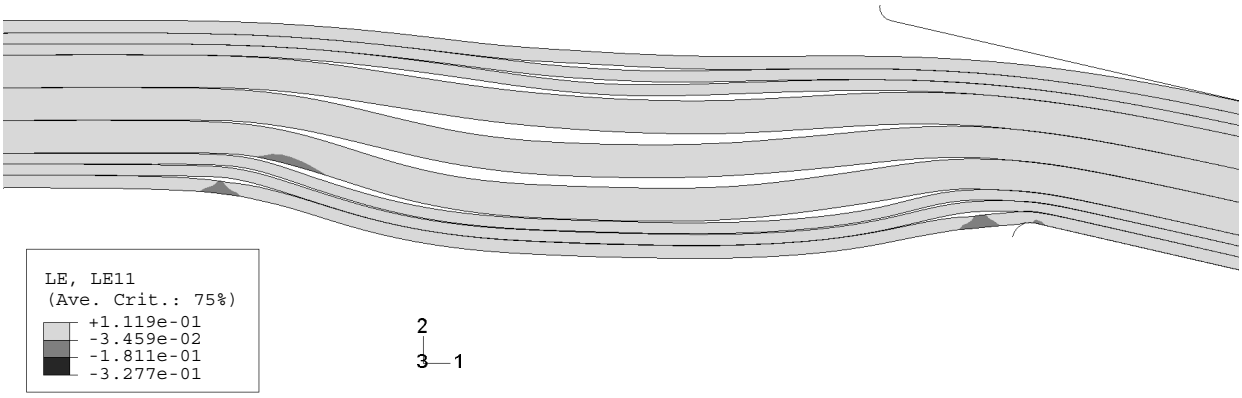

Figure D.5: LE11 point B

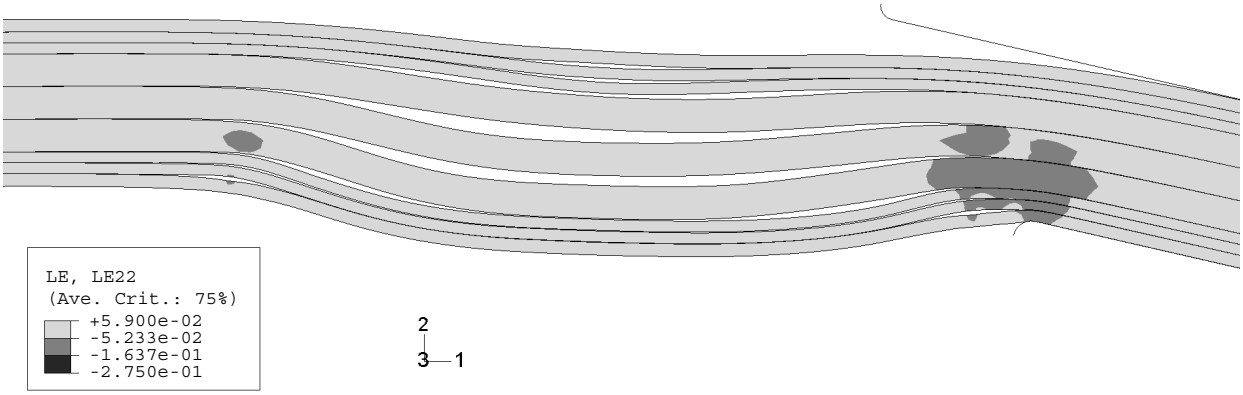

Figure D.6: LE22 point B

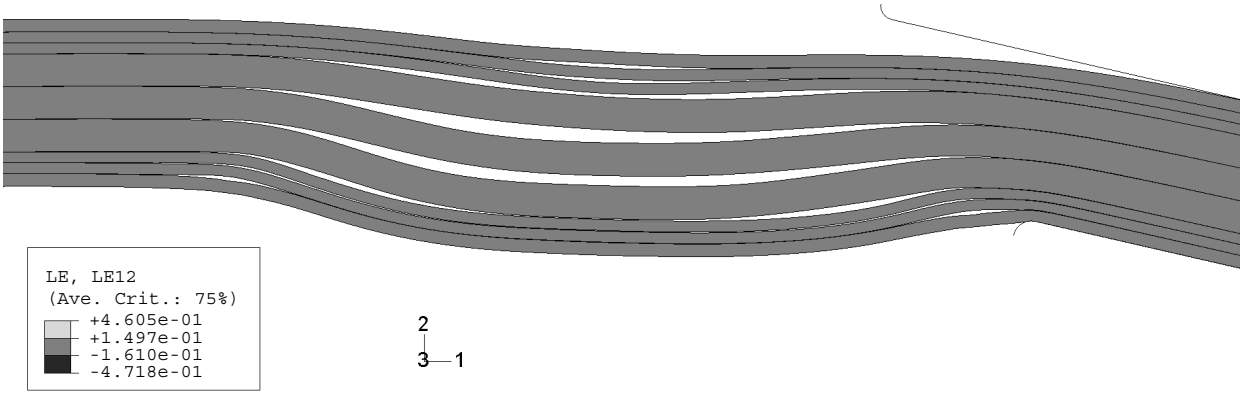

Figure D.7: LE12 point B

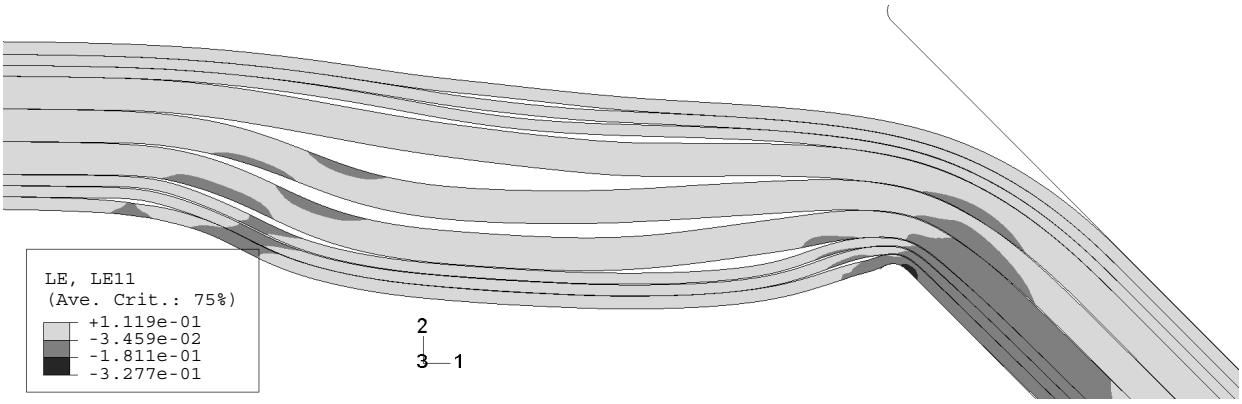

Figure D.8: LE11 point C

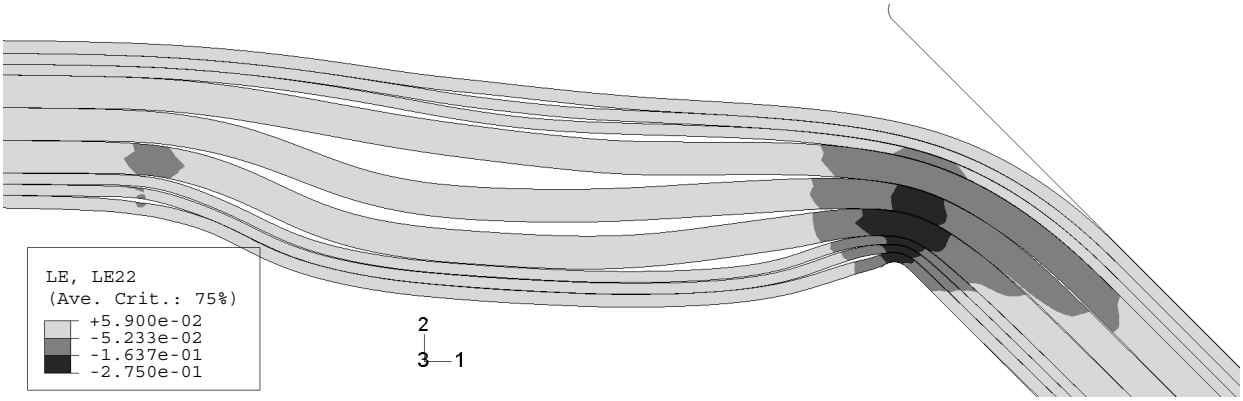

Figure D.9: LE22 point C

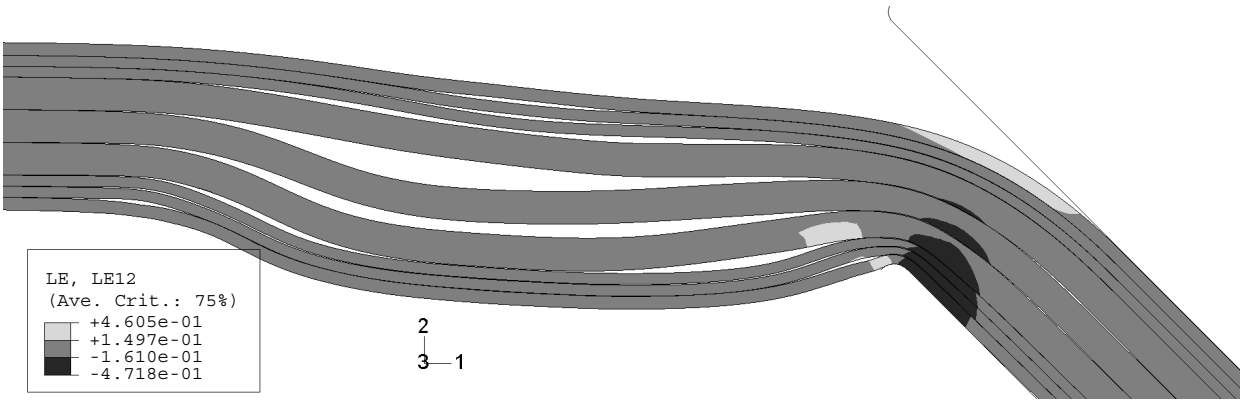

Figure D.10: LE12 point C

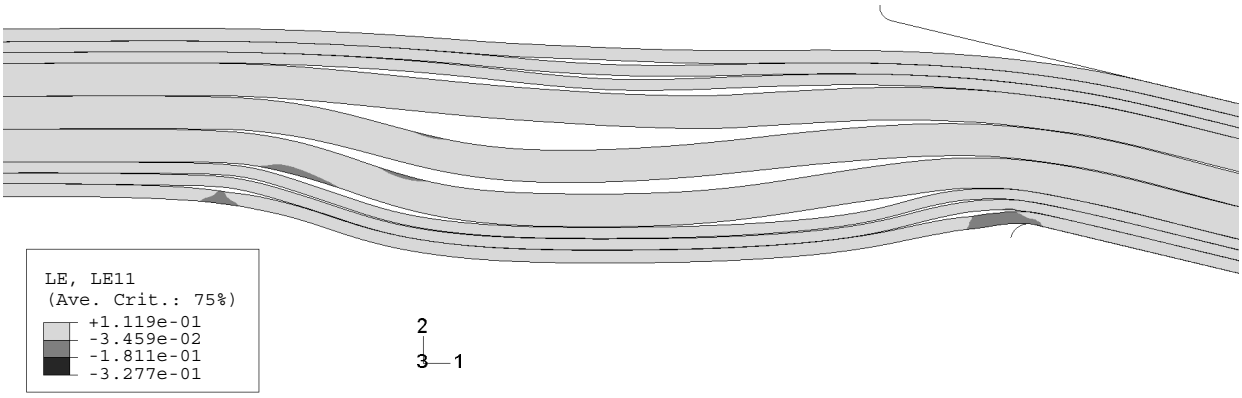

Figure D.11: LE11 point D

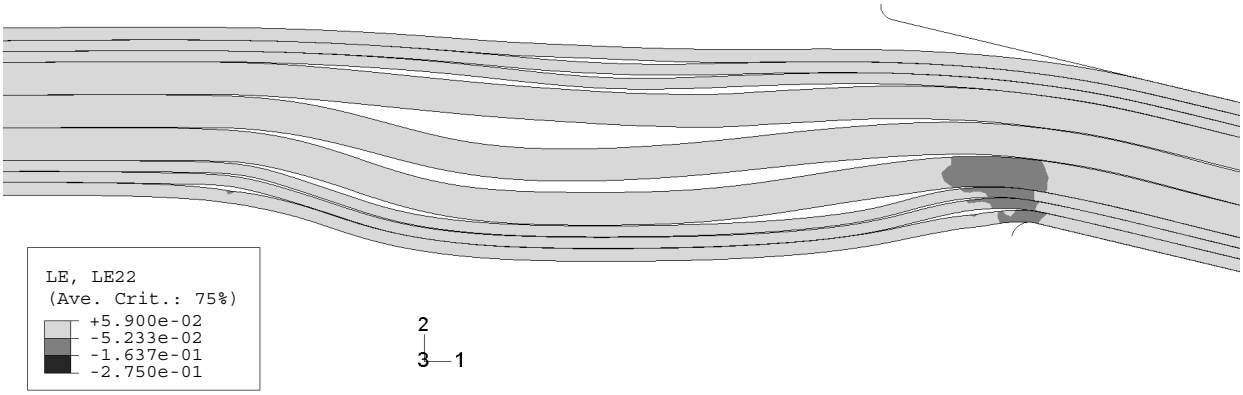

Figure D.12: LE22 point D

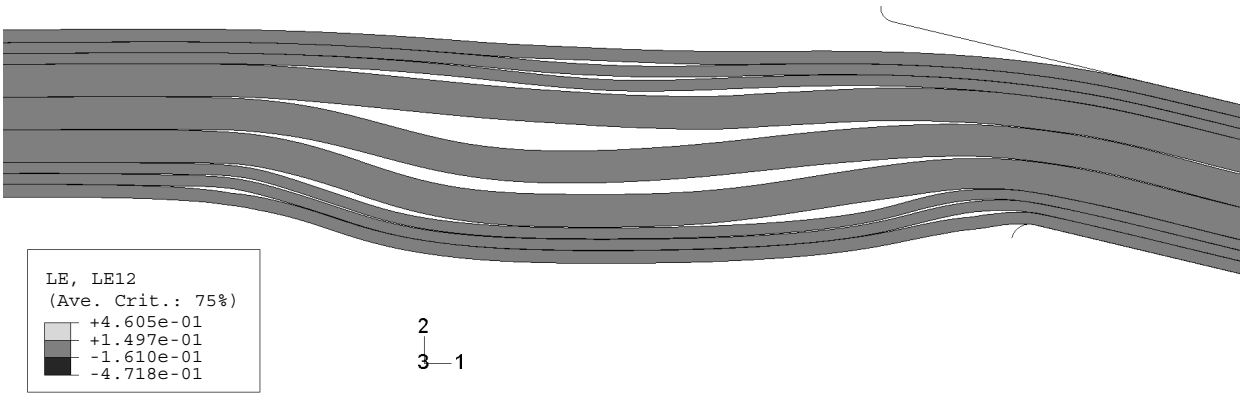

Figure D.13: LE12 point D

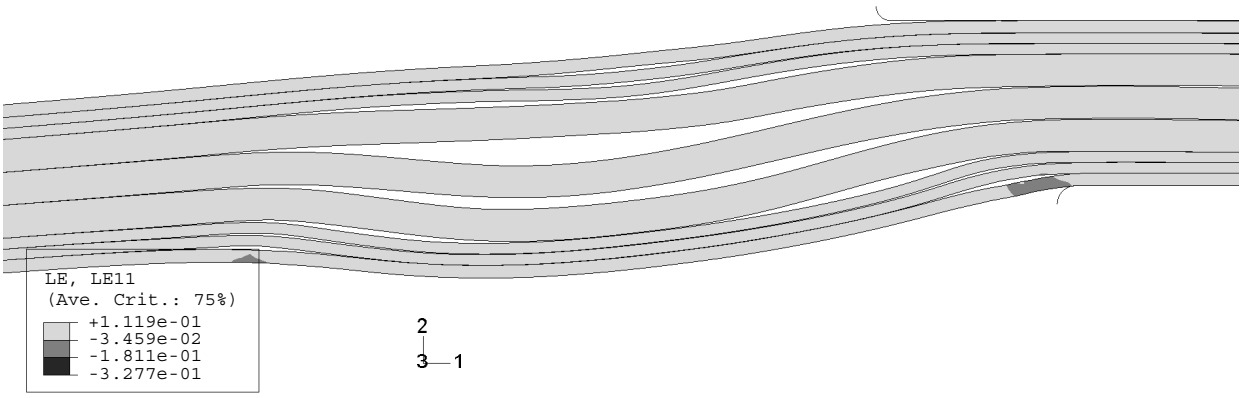

Figure D.14: LE11 point E

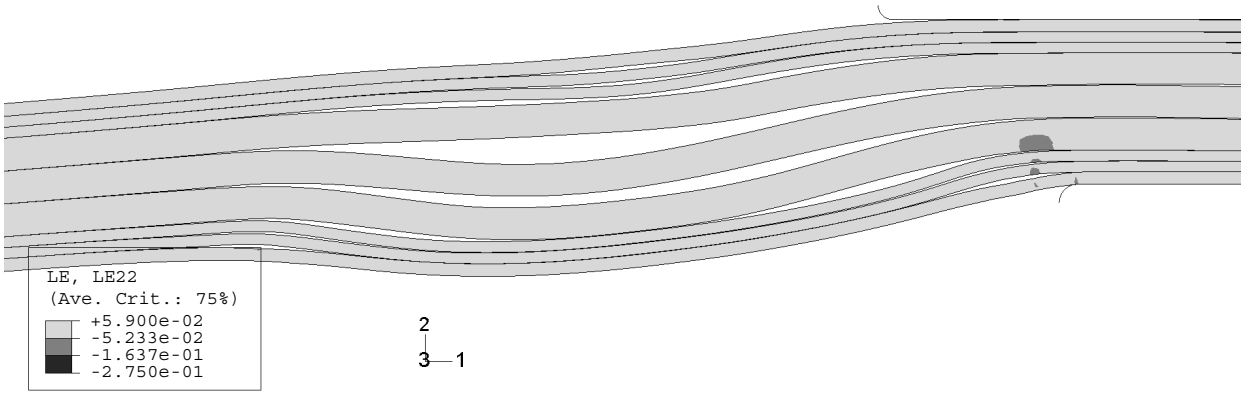

Figure D.15: LE22 point E

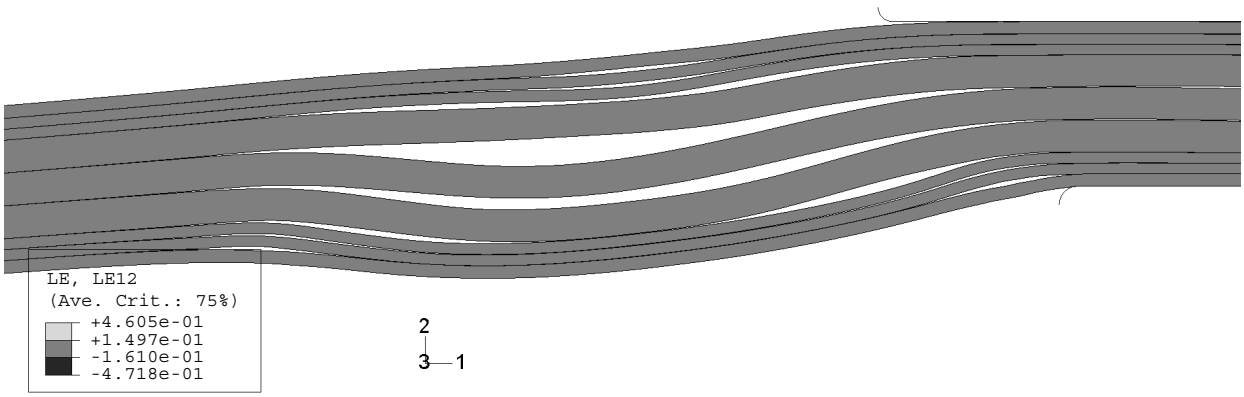

Figure D.16: LE12 point E

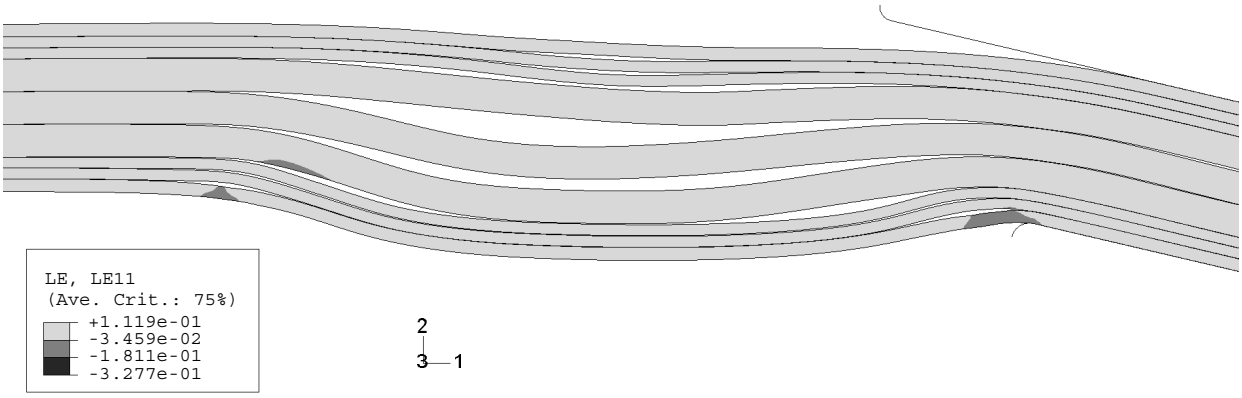

Figure D.17: LE11 point F

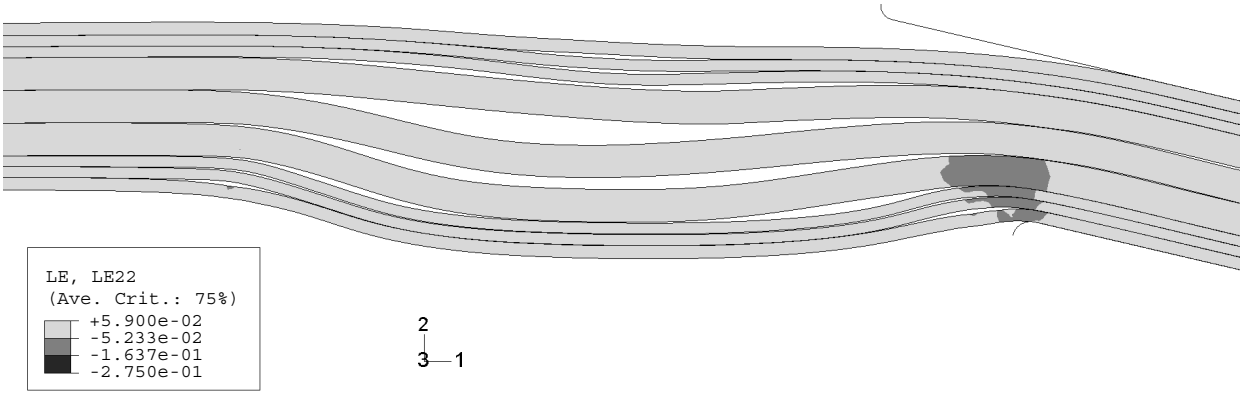

Figure D.18: LE22 point F

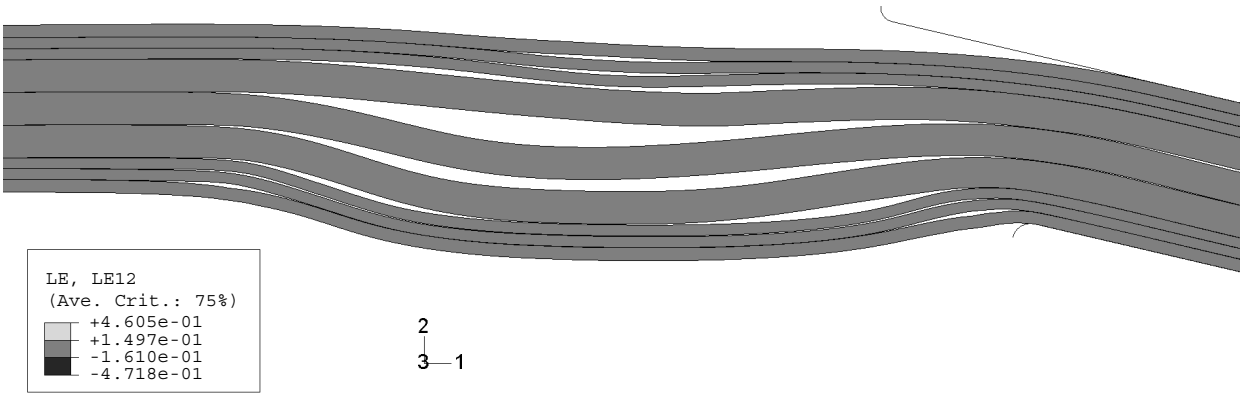

Figure D.19: LE12 point F

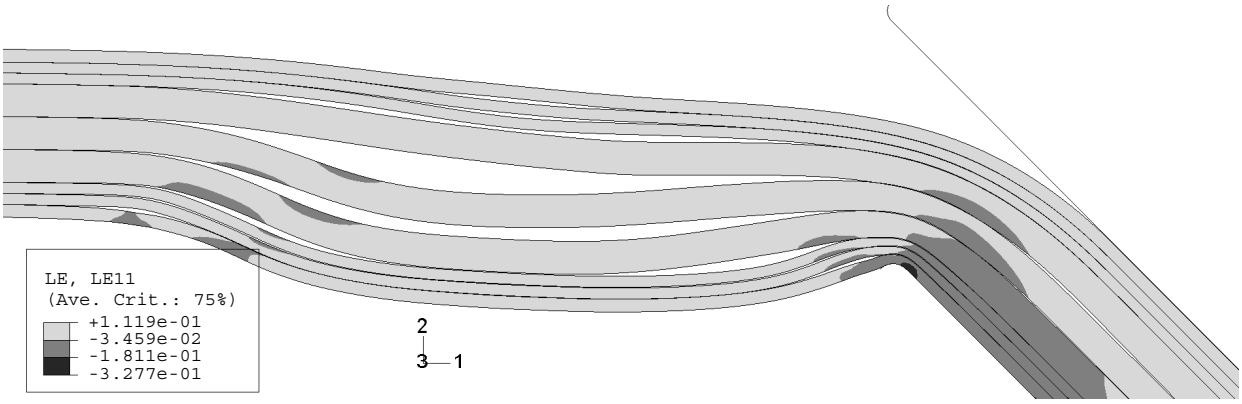

Figure D.20: LE11 point G

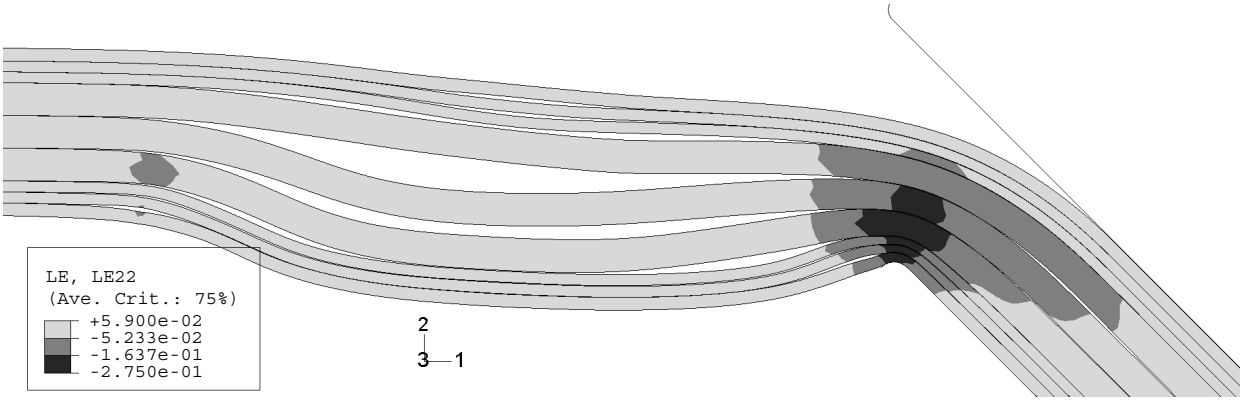

Figure D.21: LE22 point G

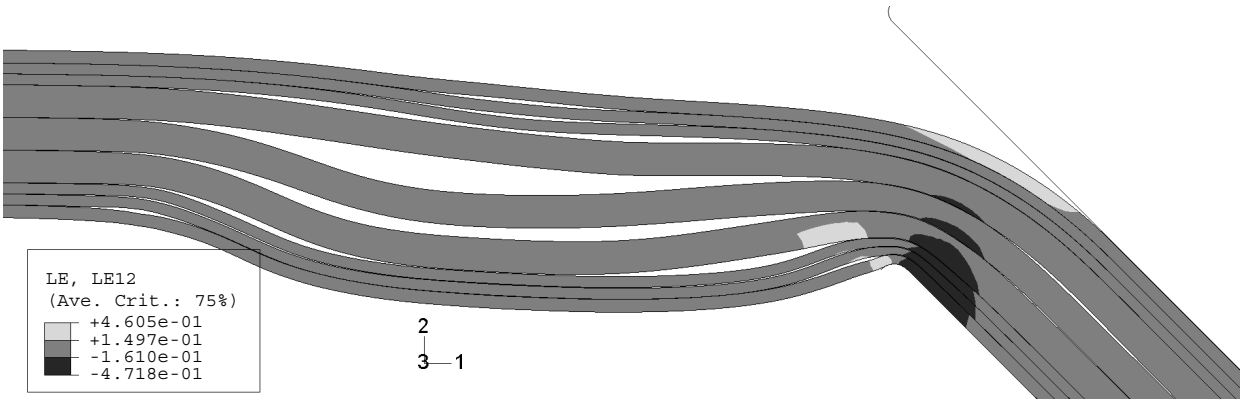

Figure D.22: LE12 point G

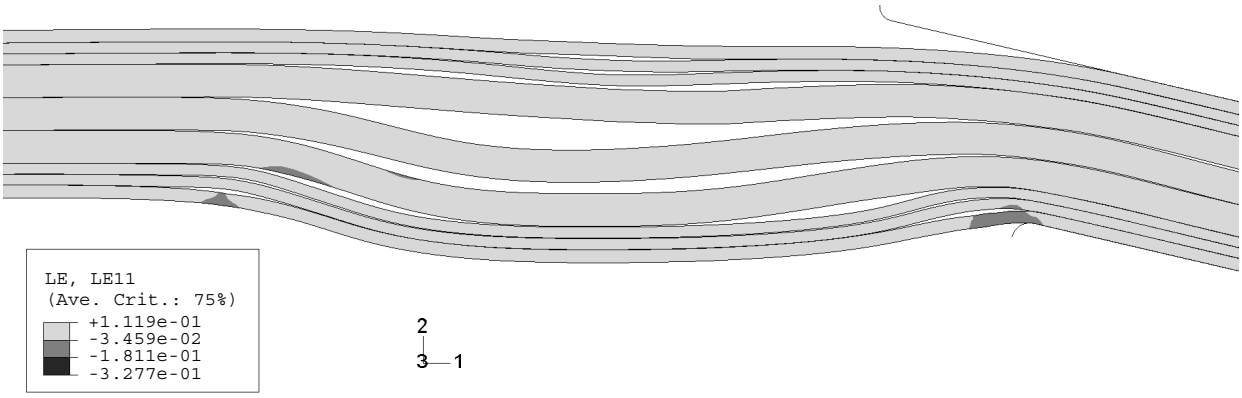

Figure D.23: LE11 point H

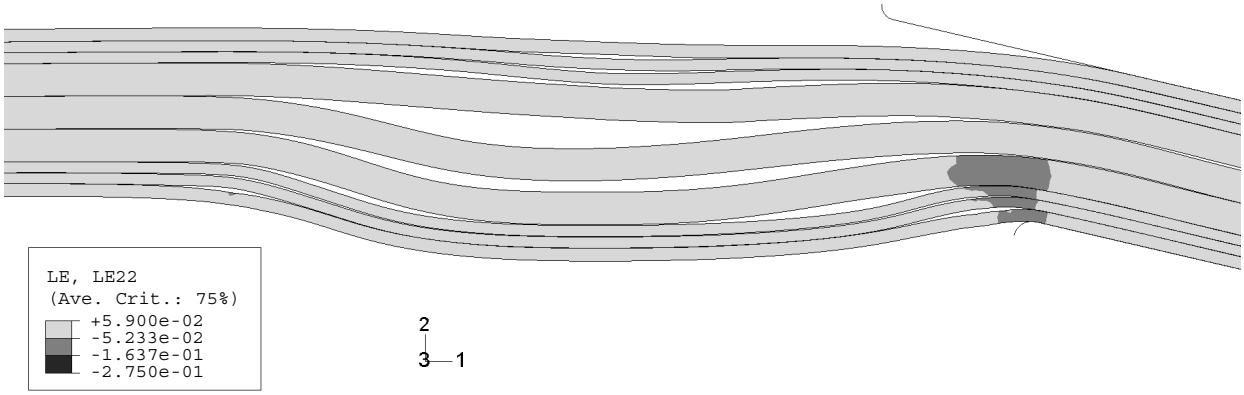

Figure D.24: LE22 point H

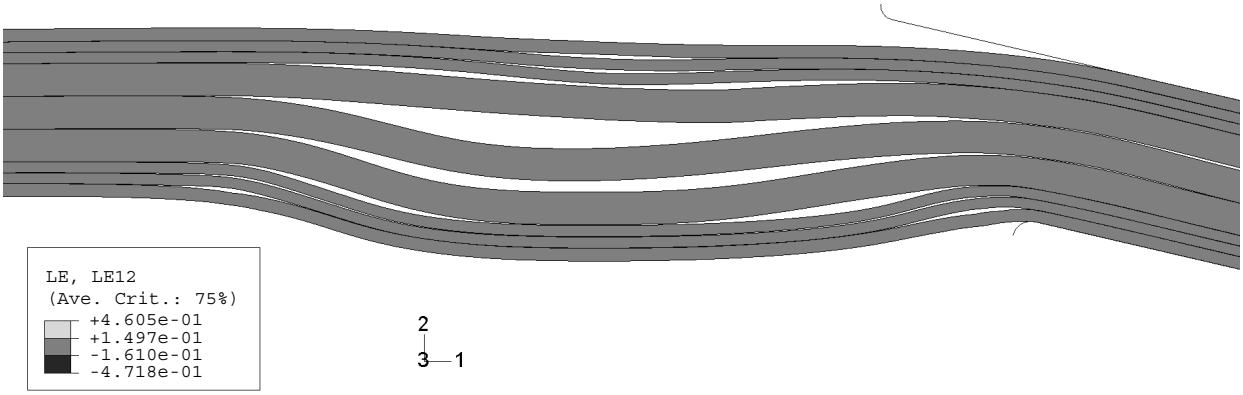

Figure D.25: LE12 point H

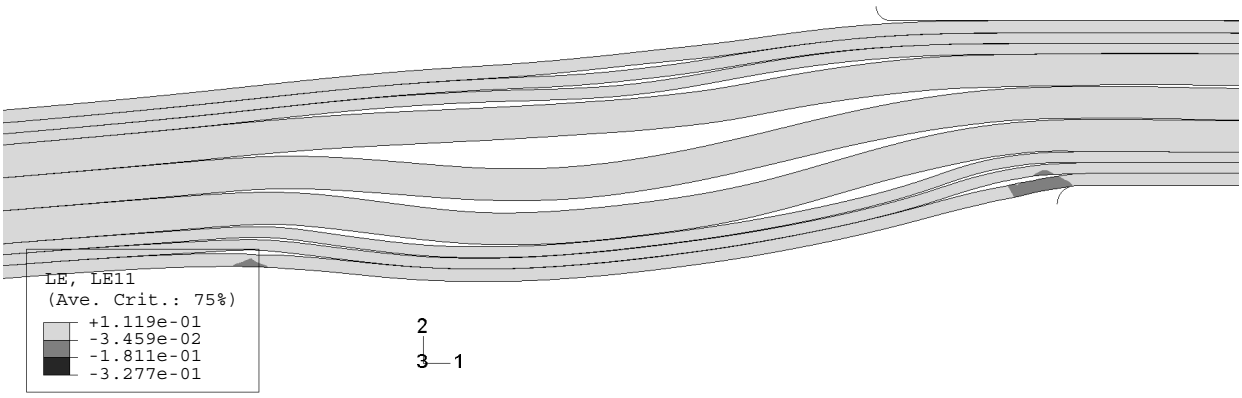

Figure D.26: LE11 point I

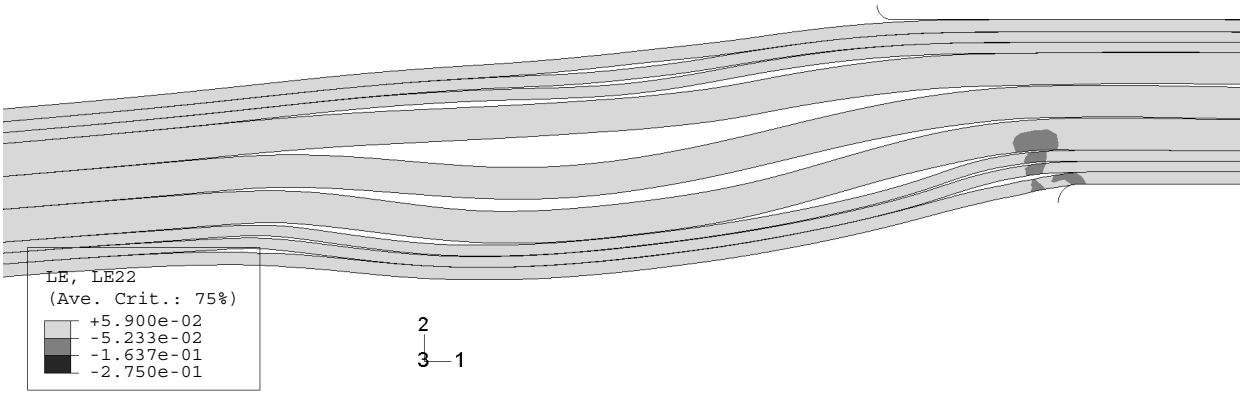

Figure D.27: LE22 point I

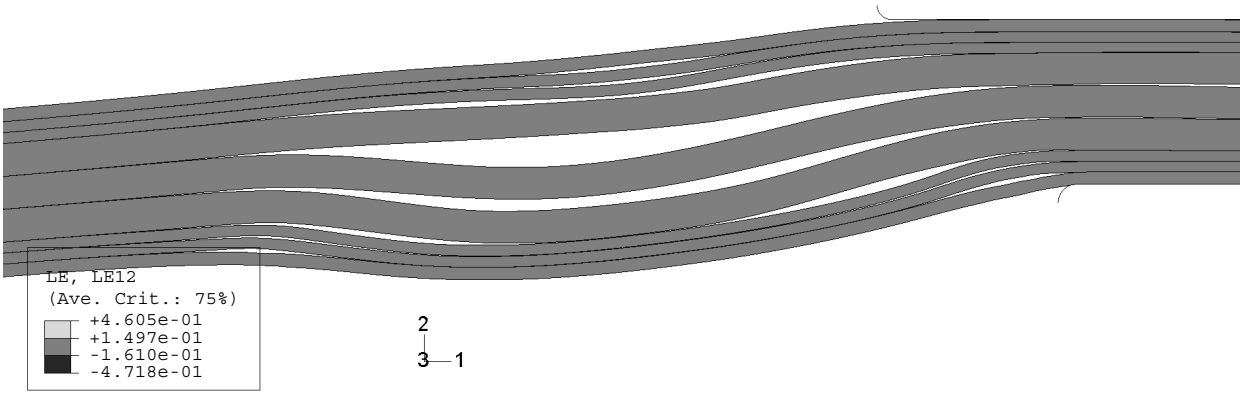

Figure D.28: LE12 point I

Appendix E

Residual deformation after creasing

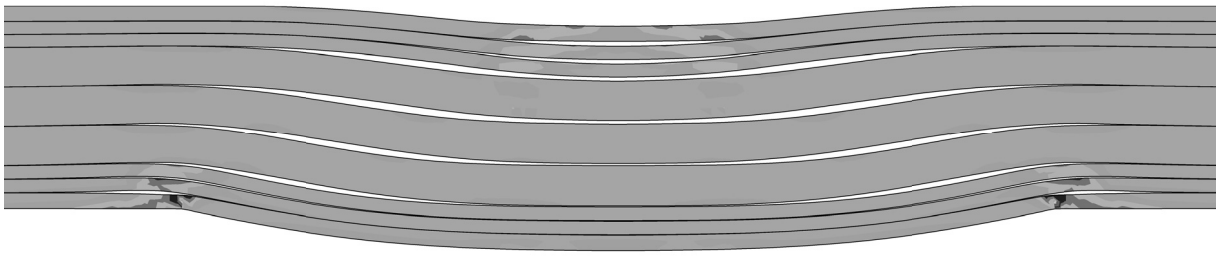

Figure E.1: Configuration 4

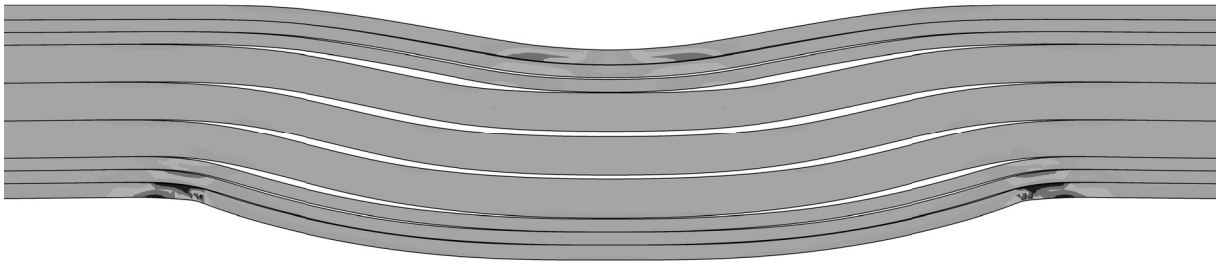

Figure E.2: $10 * (K_n^0, K_{t_1}^0, K_{t_2}^0)$

Figure E.3: $2 * S_n^0$

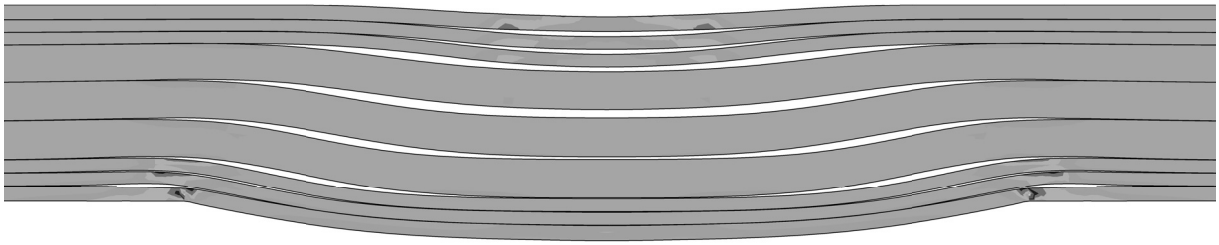

Figure E.4: $0.5 * S_n^0$

Figure E.5: $1.8 * (S_{t_1}^0,\ S_{t_2}^0)$

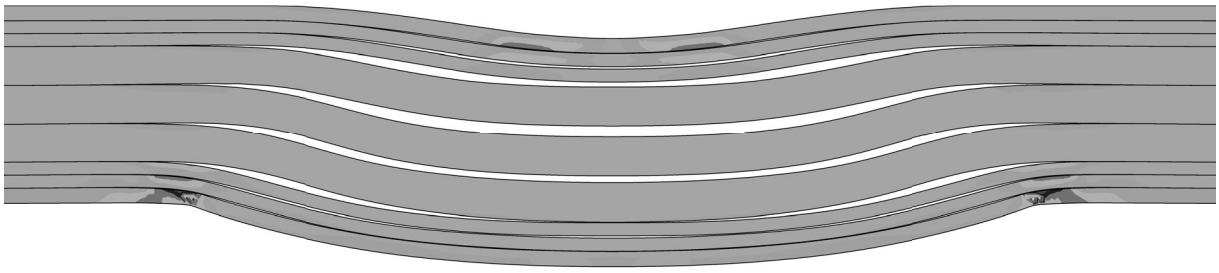

Figure E.6: $10^*(K_{t_1}^0, K_{t_2}^0)$, $1.2^*(S_{t_1}^0,\ S_{t_2}^0)$ and $0.6^* S_n^0$

Appendix F

Experimental test results statistics

The statistics in Table F.1 and Table F.2 are calculated using the maximum force. In Table F.2 the first and second row of statistics in each configuration are from the first and second fold, respectively.

Table F.1: Creasing data statistics (N)

Config.	Median	Mean	StDev	95% conf. interval
1	182.91	184.57	5.79	184.57±5.07
2	265.12	265.29	5.96	265.29±5.22
3	145.01	145.24	3.86	145.24±3.38
4	196.21	197.10	6.72	197.10±5.89
5	160.21	160.37	1.90	160.37±1.67
6	229.51	229.19	2.51	229.19±2.20
7	140.11	140.63	3.91	140.63±3.43
8	189.52	194.51	8.78	194.51±7.69

Table F.2: Statistics from the folding to 45° (mN)

Config.	Median	Mean	StDev	95% conf. interval
1	3059.50	3047.25	72.35	3047.25±50.14
	2361.50	2337.00	61.74	2337.00±42.78
2	2177.00	2180.88	34.94	2180.88±24.21
	1855.00	1850.25	50.28	1850.25±34.84
3	3558.50	3575.88	95.51	3575.88±66.18
	2470.00	2498.00	93.53	2498.00±64.81
4	2608.50	2602.75	51.21	2602.75±35.49
	1936.00	1936.13	40.11	1936.13±27.79
5	3264.00	3290.88	52.47	3290.88±36.36
	2444.00	2445.38	70.48	2445.38±48.84
6	2390.50	2390.25	43.10	2390.25±29.85
	1966.50	1973.38	45.95	1973.38±31.84
7	3460.50	3451.63	97.38	3451.63±67.48
	2394.00	2383.00	72.91	2383.00±50.53
8	2504.50	2504.50	68.07	2504.50±47.17
	1910.50	1911.88	67.65	1911.88±46.88

Appendix G

The *Controls settings

In ABAQUS the convergence tolerance can be modified with the command *Controls. See ABAQUS Inc. (2003) for a detailed description of the modified *Controls settings. The settings for the eight configurations and for the parameter study are shown in the tables below.

Table G.1: The default *Controls settings in ABAQUS/Standard

	Field=displacement	Time incrementation
Default	0.005,0.01, , ,0.02	4,8,9,16,10,4,12,5,6,3

Table G.2: The *Controls settings for configuration 1

Config 1	Field=displacement	Time incrementation
Step 2	0.05, 0.10, , ,0.20	, ,12,20, , , ,10
Step 3	0.5, 0.5, , ,0.80	, ,12,20, , , ,10
Step 9	0.04,0.08, , ,0.2	,15,12,20, , , ,10
Step 10	default	default
Step 11	default	default
Step 12	default	default

Table G.3: The *Controls settings for configuration 2

Config 2	Field=displacement	Time incrementation
Step 2	0.15, 0.15, , ,0.25	,15,12,20, , , ,10
Step 3	default	default
Step 9	0.01,0.04, , ,0.1	,15,12,20, , , ,10
Step 10	default	default
Step 11	0.01,0.04, , ,0.1	,15,12,20, , , ,10
Step 12	default	default

Table G.4: The *Controls settings for configuration 3

Config 3	Field=displacement	Time incrementation
Step 2	0.01,0.04, , ,0.1	,15,12,20, , , ,10
Step 3	0.06,0.06, , ,0.2	,15,10,20, , , ,10
Step 9	0.08,0.12, , ,0.25	,15,12,20, , , ,10
Step 10	0.08,0.12, , ,0.25	,15,12,20, , , ,10
Step 11	0.08,0.12, , ,0.25	,15,12,20, , , ,10
Step 12	default	default

Table G.5: The *Controls settings for configuration 4

Config 4	Field=displacement	Time incrementation
Step 2	0.10, 0.10, , ,0.25	, ,12,20, , , ,10
Step 3	0.10, 0.10, , ,0.25	, ,12,20, , , ,10
Step 9	0.01,0.04, , ,0.1	8, 12, ,20, , , , 10
Step 10	default	default
Step 11	default	default
Step 12	default	default

Table G.6: The *Controls settings for configuration 5

Config 5	Field=displacement	Time incrementation
Step 2	0.01, 0.02, , ,0.04	,15,12,15, , , ,10
Step 3	default	,15,12,15, , , ,10
Step 9	0.1,0.1, , ,0.3	,15,12,15, , , ,10
Step 10	default	default
Step 11	default	default
Step 12	default	default

Table G.7: The *Controls settings for configuration 6

Config 6	Field=displacement	Time incrementation
Step 2	0.05, 0.05, , ,0.25	, ,12,20, , , ,10
Step 3	0.1, 0.1, , ,2	, ,12,20, , , ,10
Step 9	0.01,0.04, , ,0.2	,15,12,20, , , ,10
Step 10	default	default
Step 11	default	default
Step 12	default	default

Table G.8: The *Controls settings for configuration 7

Config 7	Field=displacement	Time incrementation
Step 2	0.01, 0.01, , ,0.04	,15,12,15, , , ,10
Step 3	0.01, 0.01, , ,0.04	,15,12,15, , , ,10
Step 9	0.04,0.06, , ,0.1	8,15,12,15, , , ,10
Step 10	default	default
Step 11	0.04,0.04, , ,0.1	,15,12,15, , , ,10
Step 12	default	default

Table G.9: The *Controls settings for configuration 8

Config 8	Field=displacement	Time incrementation
Step 2	0.10,0.10„ ,0.20	default
Step 3	0.10,0.10„ ,0.20	default
Step 9	0.01,0.04, , ,0.1	,15,12,20, , , ,10
Step 10	default	default
Step 11	0.01,0.04, , ,0.1	,15,12,20, , , ,10
Step 12	default	default

Table G.10: The *Controls settings for Study (a)

Study (a)	Field=displacement	Time incrementation
Step 2	0.5, 0.5, , ,0.8	, ,12,20, , , ,10
Step 3	0.5, 0.5, , ,0.8	, ,12,20, , , ,10
Step 9	0.05,0.4, , ,0.4	, , 8, 20, , , , 12
Step 10	0.05,0.4, , ,0.4	, , 8, 20, , , , 12
Step 11	0.05,0.4, , ,0.4	, , 8, 20, , , , 12
Step 12	0.05,0.4, , ,0.4	, , 8, 20, , , , 12

Table G.11: The *Controls settings for Study (b,c,d,e and f)

Study (b,c,d,e and f)	Field=displacement	Time incrementation
Step 2	0.5, 0.5, , ,0.8	, ,12,20, , , ,10
Step 3	0.5, 0.5, , ,0.8	, ,12,20, , , ,10
Step 9	0.01,0.04, , ,0.1	8, 12, ,20, , , , 10
Step 10	0.01,0.04, , ,0.1	8, 12, ,20, , , , 10
Step 11	0.01,0.04, , ,0.1	8, 12, ,20, , , , 10
Step 12	0.01,0.04, , ,0.1	8, 12, ,20, , , , 10

Table G.12: The *Controls settings for Study (g)

Study (g)	Field=displacement	Time incrementation
Step 2	0.6, 0.8, , ,1.0	, ,12,20, , , ,10
Step 3	0.6, 0.8, , ,1.0	, ,12,20, , , ,10
Step 9	0.01,0.04, , ,0.1	8, 12, ,20, , , , 10
Step 10	0.01,0.04, , ,0.1	8, 12, ,20, , , , 10
Step 11	0.01,0.04, , ,0.1	8, 12, ,20, , , , 10
Step 12	0.01,0.04, , ,0.1	8, 12, ,20, , , , 10

Table G.13: The *Controls settings for Study (h)

Study (h)	Field=displacement	Time incrementation
Step 2	0.5, 0.5, , ,0.8	, ,12,20, , , ,10
Step 3	0.5, 0.5, , ,0.8	, ,12,20, , , ,10
Step 9	0.1,0.4, , ,0.4	, , 8, 20, , , , 12
Step 10	0.1,0.4, , ,0.4	, , 8, 20, , , , 12
Step 11	0.1,0.4, , ,0.4	, , 8, 20, , , , 12
Step 12	0.1,0.4, , ,0.4	, , 8, 20, , , , 12

Appendix H

Triplex 360 mN material data

In this report all results from the ABAQUS simulations are based on the material properties described in Tables H.1, H.2, H.3 and H.4.

Table H.1: Experimental data for Triplex 360 mN provided by Stenberg (2002)

	Tensile yield strength (MPa)	Compressive yield strength (MPa)	Plastic strain ratio $d\epsilon^p_\perp / d\epsilon^p_\parallel$
MD	12.0	7.3	-0.5
CD	6.5	5.0	-0.133
45°	8.0		

Table H.2: The in-plane model elastic material properties. Numerical values for the entire Triplex 360 mN paperboard, the chemical and the mechanical plies are included. Taken from Nygårds (2004)

Notation	Description	Triplex	Chemical	Mechanical
E_1	Elastic modulus in MD	5.6 GPa	8.9 Gpa	3.4 GPa
E_2	Elastic modulus in ZD	18.0 MPa	25 Mpa	16 MPa
E_3	Elastic modulus in CD	2.0 GPa	3.4 Gpa	0.96 GPa
ν_{21}	Out-of-plane Poisson's ratio	0.0	0.0	0.0
ν_{13}	In-plane Poisson's ratio	0.37	0.37	0.37
ν_{23}	Out-of-plane Poisson's ratio	0.0	0.0	0.0
G_{12}	Out-of-plane shear modulus	34.0 Mpa	58.0 MPa	20.0 Mpa
G_{13}	In-plane shear modulus	1.3 GPa	2.4 GPa	0.8 GPa
G_{23}	Out-of-plane shear modulus	26.0 Mpa	38.0 MPa	15.0 MPa
ϕ	Angle between MD and global axis	0.0	0.0	0.0
a	Exponent in penalty func. (22-comp)	5.4	5.4	5.4
b	Exponent in penalty func. (12-comp)	1.5	1.5	1.5
c	Exponent in penalty func. (23-comp)	1.5	1.5	1.5

Table H.3: The in-plane model plastic material properties. Numerical values for the entire Triplex 360 mN paperboard, the chemical and the mechanical plies are included. Taken from Nygårds (2004)

Notation	Description	Triplex	Chemical	Mechanical
2k	Exponent in yield condition	4	4	4
S_1^0	Tensile yield stress in MD	10.7 MPa	22.0 MPa	10.7 MPa
S_2^0	Tensile yield stress in CD	6.5 MPa	16.5 MPa	6.5 MPa
S_3^0	Yield stress in shear	6.0 MPa	8.0 MPa	6.0 MPa
S_4^0	Compression yield stress in MD	6.5 MPa	6.3 MPa	6.3 MPa
S_5^0	Compression yield stress in CD	6.3 MPa	6.3 MPa	6.3 MPa
A_1	Hardening parameter	19.0 MPa	44.0 MPa	19.0 MPa
A_2	Hardening parameter	7.4 MPa	7.4 MPa	7.4 MPa
A_3	Hardening parameter	8.0 MPa	18.0 MPa	7.5 MPa
A_4	Hardening parameter	6.0 MPa	12.0 MPa	6.0 MPa
A_5	Hardening parameter	9.0 MPa	12.5 MPa	9.0 MPa
B_1	Hardening parameter	260.0 MPa	260.0 MPa	260.0 MPa
B_2	Hardening parameter	160.0 MPa	160.0 MPa	160.0 MPa
B_3	Hardening parameter	375.0 MPa	375.0 MPa	375.0 MPa
B_4	Hardening parameter	160.0 MPa	160.0 MPa	160.0 MPa
B_5	Hardening parameter	310.0 MPa	310.0 MPa	310.0 MPa
C_1	Hardening parameter	800.0 MPa	800.0 MPa	800.0 MPa
C_2	Hardening parameter	160.0 MPa	160.0 MPa	160.0 MPa
C_3	Hardening parameter	200.0 MPa	200.0 MPa	200.0 MPa
C_4	Hardening parameter	300.0 MPa	300.0 MPa	300.0 MPa
C_5	Hardening parameter	225.0 MPa	225.0 MPa	225.0 MPa

Table H.4: The interface model material properties for Triplex 360 mN. Taken from Nygårds (2004)

Notation	Description	Outer	Inner
$K^0_{t_1}$	Initial stiffness in MD shear	800 MPa	640 MPa
K^0_n	Initial stiffness in ZD tension	400 MPa	320 MPa
$S^0_{t_1}$	Initial yield stress in MD shear	1.45 MPa	1.18 MPa
S^0_n	Initial yield stress in ZD tension	0..45 MPa	0.35 MPa
$K^0_{t_2}$	Initial stiffness in CD shear	800 MPa	640 MPa
$S^0_{t_2}$	Initial yield stress in CD shear	1.45 MPa	1.18 MPa
A	see Eq. (6.16)	0.28	0.28
B	see Eq. (6.16)	0.8	0.8
C	see Eq. (6.7)	0.085	0.085
R^s_n	Residual strength factor in ZD tension, Eq. (6.10)	0.97 MPa	0.97 MPa
$R^s_{t_1}$	Residual strength factor in MD shear, Eq. (6.10)	0.87 MPa	0.87 MPa
$R^s_{t_2}$	Residual strength factor in CD shear, Eq. (6.10)	0.87 MPa	0.87 MPa
R^k_n	Residual strength factor in ZD tension, Eq. (6.6)	0.97 MPa	0.97 MPa
$R^k_{t_1}$	Residual strength factor in MD shear, Eq. (6.6)	0.87 MPa	0.87 MPa
$R^k_{t_2}$	Residual strength factor in CD shear, Eq. (6.6)	0.87 MPa	0.87 MPa
A_1	see Eq. (6.8)	0.5	0.5
B_1	see Eq. (6.8)	140	140

Appendix I

ABAQUS/Standard input file

```
*Heading
 Written by Oscar Elison and Lars Hansson
 Job name: 3DM Material A
 Model name: Configuration 4
**
**------------------------------------------------------------------
**
**                              PARTS
**
**------------------------------------------------------------------
**
*Part, name=FEMALE_DIE
*End Part
*Part, name=MALE_DIE
*End Part
*Part, name=STOPER_L
*End Part
*Part, name=STOPER_R
*End Part
*Part, name=LOAD_CELL
*End Part
*Part, name=CLAMP_O
*End Part\newline
*Part, name=CLAMP_U
*End Part
*Part, name=P_Mesh_Fine
*Orientation, Name=Plane, System=Rectangular
 1, 0, 0, 0, 1, 0
 1, 0
*End Part
**
**------------------------------------------------------------------
**
**                            ASSEMBLY
**
**------------------------------------------------------------------
**
*Assembly, name=Assembly
**
*Instance, name=FEMALE_DIE-1, part=FEMALE_DIE
*Node
 100000,           0.,           -0.005
*Surface, type=SEGMENTS, name=Surf:Female_Die
START,         -13.,           -0.005
 LINE,          -1.,           -0.005
 CIRCL,         -0.9,         -0.1,          -1.,         -0.1
 LINE,         -0.9,         -0.9
 LINE,          0.9,         -0.9
 LINE,          0.9,         -0.1
 CIRCL,           1.,           -0.005,           1.,         -0.1
 LINE,          13.,           -0.005
*End Instance
**
*Instance, name=MALE_DIE-1, part=MALE_DIE
*Node
 200000,           0.,          0.5
*Surface, type=SEGMENTS, name=Surf:Male_Die
START,       0.2169,           2.
 LINE,        0.2169,        0.6200
 CIRCL,       0.,        0.5,           0.,        0.7560
 CIRCL,       -0.2169,    0.6200,         0.,        0.7560
 LINE,        -0.2169,           2.
*End Instance
**
*Instance, name=STOPER_L-1, part=STOPER_L
```

```
*Node
 300001,        -0.65,         0.455
*Surface, type=SEGMENTS, name=Surf:Stoper_L
START,        -0.65,        0.454
 LINE,         -13.,        0.454
*End Instance
**
*Instance, name=STOPER_R-1, part=STOPER_R
*Node
 300002,         0.65,         0.455
*Surface, type=SEGMENTS, name=Surf:Stoper_R
START,          13.,        0.454
 LINE,         0.65,        0.454
*End Instance
**
*Instance, name=LOAD_CELL-1, part=LOAD_CELL
*Node
 400000,         -9.30,         4.235,           0.
*Surface, type=SEGMENTS, name=Surf:Load_Cell
START,         -9.10,           6.
 LINE,         -9.10,         4.435
 CIRCL,        -9.30,         4.235,         -9.3,         4.435
 CIRCL,        -9.50,         4.435,         -9.3,         4.435
 LINE,         -9.50,           6.
*End Instance
**
*Instance, name=CLAMP_O-1, part=CLAMP_O
*Node
 500001,           0.74,        4.448
*Surface, type=SEGMENTS, name=Surf:Clamp_O
START,        12.25,        4.452
 LINE,          0.74,        4.452
 CIRCL,         0.70,        4.492,          0.74,        4.492
*End Instance
**
*Instance, name=CLAMP_U-1, part=CLAMP_U
*Node
 500002,           0.74,        -3.552
*Surface, type=SEGMENTS, name=Surf:Clamp_U
START,         1.20,       -4.052
 CIRCL,         1.25,     -4.002,         1.25,       -4.052
 LINE,        12.25,       -4.002
*End Instance
**
*Instance, name=P_Mesh_Fine-1, part=P_Mesh_Fine
*Node
      1,       -12.25,         0.455
      2,       -12.25,         0.42
      3,    -12.19012,         0.455
.
   .
   .
  12277,     12.19012,        -0.005
  12278,        12.25,     0.02999997
  12279,        12.25,        -0.005
**
*Element, type=CPE4
   1,     1,     2,     4,     3
   2,     3,     4,     6,     5
   3,     5,     6,     8,     7
 .
 .
 .
7909, 12272, 12273, 12275, 12274
7910, 12274, 12275, 12277, 12276
```

```
7911, 12276, 12277, 12279, 12278
**
**------------------------------------------------------------------
**
**                               MPC
**
**------------------------------------------------------------------
**
*MPC
 Linear, 335, 337, 336
 Linear, 1572, 1574, 1573
 Linear, 2809, 2811, 2810
 .
 .
 .
**
**------------------------------------------------------------------
**
**      ELEMENT SETS IN INSTANCE DEFINED FOR SOLID SECTION
**
**------------------------------------------------------------------
**
*Elset, elset=El_TopPly, instance=P_Mesh_Fine-1
    1,    2,    3,    4,    5,    6,    7,    8,    9,   10,   11,   12,   13,   14,   15,   16
   17,   18,   19,   20,   21,   22,   23,   24,   25,   26,   27,   28,   29,   30,   31,   32
   33,   34,   35,   36,   37,   38,   39,   40,   41,   42,   43,   44,   45,   46,   47,   48
   .
   .
   .
*Elset, elset=El_BotPly, instance=P_Mesh_Fine-1
*Elset, elset=El_MidPly, instance=P_Mesh_Fine-1
**
**------------------------------------------------------------------
**
**                  MATERIAL MODEL FOR INSTANCE
**
**------------------------------------------------------------------
**
*SOLID SECTION, ELSET=El_TopPly ,MATERIAL=PULPMAT_OUT, ORIENTATION=Plane
  1
*SOLID SECTION, ELSET=El_MidPly ,MATERIAL=PULPMAT_MID, ORIENTATION=Plane
  1
*SOLID SECTION, ELSET=El_BotPly ,MATERIAL=PULPMAT_OUT, ORIENTATION=Plane
 1
**
*End Instance
**
**------------------------------------------------------------------
**
**                    ELEMENT SETS IN ASSEMBLY
**
**------------------------------------------------------------------
**
*Elset, elset=El_Bot, instance=P_Mesh_Fine-1
*Elset, elset=El_BotPly_int1U, instance=P_Mesh_Fine-1
*Elset, elset=El_TopPly_int1O_LM, instance=P_MESH_FINE-1
*Elset, elset=El_TopPly_int1O_R, instance=P_MESH_FINE-1, generate
*Elset, elset=El_TopPly_int2U_LM, instance=P_MESH_FINE-1
*Elset, elset=El_BotPly_int1O, instance=P_Mesh_Fine-1
*Elset, elset=El_BotPly_int2U, instance=P_Mesh_Fine-1
*Elset, elset=EL_TopPly_Int2U_R, instance=P_MESH_FINE-1, generate
*Elset, elset=El_BotPly_int2O, instance=P_Mesh_Fine-1
*Elset, elset=El_Cnt_O, instance=P_Mesh_Fine-1
*Elset, elset=El_Cnt_U, instance=P_Mesh_Fine-1
*Elset, elset=El_End_R1, instance=P_MESH_FINE-1
```

```
*Elset, elset=El_End_R2, instance=P_MESH_FINE-1
*Elset, elset=El_End_L, instance=P_Mesh_Fine-1
*Elset, elset=El_Top, instance=P_Mesh_Fine-1
*Elset, elset=El_TopPly_int1U, instance=P_Mesh_Fine-1
*Elset, elset=El_TopPly_int2O, instance=P_Mesh_Fine-1
*Elset, elset=El_Top_CR, instance=P_Mesh_Fine-1, generate
*Elset, elset=El_Top_L, instance=P_Mesh_Fine-1
*Elset, elset=El_Top_R, instance=P_Mesh_Fine-1
*Elset, elset=El_int1O, instance=P_Mesh_Fine-1
*Elset, elset=El_int1U, instance=P_Mesh_Fine-1
*Elset, elset=El_int2O, instance=P_Mesh_Fine-1
*Elset, elset=El_int2U, instance=P_Mesh_Fine-1
*Elset, elset=El_int3O, instance=P_Mesh_Fine-1
*Elset, elset=El_int3U, instance=P_Mesh_Fine-1
*Elset, elset=El_int4O, instance=P_Mesh_Fine-1
*Elset, elset=El_int4U, instance=P_Mesh_Fine-1
**
**------------------------------------------------------------------
**
**                      NODE SETS IN ASSEMBLY
**
**------------------------------------------------------------------
**
*Nset, nset=FEMALENODE, instance=FEMALE_DIE-1
 100000,
**
*Nset, nset=MALENODE, instance=MALE_DIE-1
 200000,
**
*Nset, nset=STOPERNODE_L, instance=STOPER_L-1
 300001,
**
*Nset, nset=STOPERNODE_R, instance=STOPER_R-1
 300002,
**
*Nset, nset=LOADCELLNODE, instance=LOAD_CELL-1
 400000,
**
*Nset, nset=ROTNODE_O, instance=CLAMP_O-1
 500001,
**
*Nset, nset=ROTNODE_U, instance=CLAMP_U-1
 500002,
**
*Nset, nset=MESHNODES, instance=P_Mesh_Fine-1
 785, 786, 787, 2022, 2023, 2024, 3259, 3260, 3261, 4357, 4358, 4359, 4360, 4361, 5382, 5383
 5384, 5385, 5386, 6407, 6408, 6409, 6410, 6411, 7571, 7572, 7573, 8808, 8809, 8810, 10045, 10046,
 10047
**
**------------------------------------------------------------------
**
**                        SURFACES IN ASSEMBLY
**
**------------------------------------------------------------------
**
*Surface, type=ELEMENT, name=PSurf:Cnt_O
 El_Cnt_O, S4
*Surface, type=ELEMENT, name=PSurf:Cnt_U
 El_Cnt_U, S2
*Surface, type=ELEMENT, name=PSurf:El_End_L
 El_End_L, S1
*Surface, type=ELEMENT, name=PSurf:El_End_R
 El_End_R1, S3
 El_End_R2, S1
*Surface, type=ELEMENT, name=PSurf:Top
```

```
 El_Top, S4
*Surface, type=ELEMENT, name=PSurf:Top_CR
 El_Top_CR, S4
*Surface, type=ELEMENT, name=PSurf:Top_L
 El_Top_L, S4
*Surface, type=ELEMENT, name=PSurf:Top_R
 El_Top_R, S4
*Surface, type=ELEMENT, name=PSurf:TopPly_int1O
 El_TopPly_int1O_LM, S2
 El_TopPly_int1O_R, S4
*Surface, type=ELEMENT, name=PSurf:TopPly_int1U
 El_TopPly_int1U, S4
*Surface, type=ELEMENT, name=PSurf:TopPly_int2O
 El_TopPly_int2O, S2
*Surface, type=ELEMENT, name=PSurf:TopPly_int2U
 El_TopPly_int2U_LM, S4
 El_TopPly_int2U_R, S2
*Surface, type=ELEMENT, name=PSurf:Int1O
 El_Int1O, S2
*Surface, type=ELEMENT, name=PSurf:Int1U
 El_Int1U, S4
*Surface, type=ELEMENT, name=PSurf:Int2O
 El_Int2O, S2
*Surface, type=ELEMENT, name=PSurf:Int2U
 El_Int2U, S4
*Surface, type=ELEMENT, name=PSurf:Int3O
 El_Int3O, S2
*Surface, type=ELEMENT, name=PSurf:Int3U
 El_Int3U, S4
*Surface, type=ELEMENT, name=PSurf:Int4O
 El_Int4O, S2
*Surface, type=ELEMENT, name=PSurf:Int4U
 El_Int4U, S4
*Surface, type=ELEMENT, name=PSurf:Bot
 El_Bot, S2
*Surface, type=ELEMENT, name=PSurf:BotPly_int1O
 El_BotPly_int1O, S2
*Surface, type=ELEMENT, name=PSurf:BotPly_int1U
 El_BotPly_int1U, S4
*Surface, type=ELEMENT, name=PSurf:BotPly_int2O
 El_BotPly_int2O, S2
*Surface, type=ELEMENT, name=PSurf:BotPly_int2U
 El_BotPly_int2U, S4
**
**------------------------------------------------------------------
**
**                       CONSTRAINTS IN ASSEMBLY
**
**------------------------------------------------------------------
**
*Rigid Body, ref node=FEMALENODE, analytical surface=Female_Die-1.Surf:Female_Die
**
*Rigid Body, ref node=MALENODE, analytical surface=Male_Die-1.Surf:Male_Die
**
*Rigid Body, ref node=STOPERNODE_L, analytical surface=Stoper_L-1.Surf:Stoper_L
**
*Rigid Body, ref node=STOPERNODE_R, analytical surface=Stoper_R-1.Surf:Stoper_R
**
*Rigid Body, ref node=LOADCELLNODE, analytical surface=Load_Cell-1.Surf:Load_Cell
**
*Rigid Body, ref node=ROTNODE_O, analytical surface=Clamp_O-1.Surf:Clamp_O
**
*Rigid Body, ref node=ROTNODE_U, analytical surface=Clamp_U-1.Surf:Clamp_U
**
*End Assembly
```

```
**
**------------------------------------------------------------------
**
**                              MATERIALS
**
**------------------------------------------------------------------
**
*Material, name=PULPMAT_MID
*Depvar
     45,
*User Material, constants=44, unsymm
 3400.,     16.,    960.,      0.,    0.37,      0.,     20.,    800.
     15.,      0.,     5.4,     1.5,     1.5,      4.,    10.7,     6.5
      6.,     6.3,     6.3,     19.,     7.4,     7.5,      6.,      9.
    260.,    160.,    375.,    160.,    310.,    800.,    160.,    200.
    300.,    225.,  0.8944, -0.4472, -0.1322,  0.9912,  0.7071, -0.8944
  0.4472,  0.1322, -0.9912, -0.7071
**
*Material, name=PULPMAT_OUT
*Depvar
     45,
*User Material, constants=44, unsymm
 8900.,     25.,   3400.,      0.,    0.37,      0.,     58.,   2400.
     38.,      0.,     5.4,     1.5,     1.5,      4.,     22.,    16.5
      8.,     6.3,     6.3,     44.,     7.4,     18.,     12.,    12.5
    260.,    160.,    375.,    160.,    310.,    800.,    160.,    200.
    300.,    225.,  0.8944, -0.4472, -0.1322,  0.9912,  0.7071, -0.8944
  0.4472,  0.1322, -0.9912, -0.7071
**
**------------------------------------------------------------------
**
**                              AMPLITUDES
**
**------------------------------------------------------------------
**
*Amplitude, name=Amp:Fold
 0., 0., 1., 1.
**
*Amplitude, name=Amp:Pred_1
 0., 0., 1., 1.
**
*Amplitude, name=Amp:Pred_2
 0., 1., 1., 0
**
*Amplitude, name=Amp:Web, time=TOTAL TIME
 0., 0., 1., 1., 2., 1., 3., 1.,
 4., 1., 5., 0.
**
**------------------------------------------------------------------
**
**                    INTERACTION PROPERTIES
**
**------------------------------------------------------------------
**
*Surface Interaction, name=FEMALE_TOOL
 1.,
*Surface Interaction, name=MALE_TOOL
 1.,
*Surface Behavior, pressure-overclosure=EXPONENTIAL
 0.0005, 5.
*Surface Interaction, name=STOPER
 1.,
*Surface Interaction, name=LOAD_CELL
 1.,
*Surface Interaction, name=CLAMP
```

```
*Friction
 0.3
*Surface Behavior, pressure-overclosure=EXPONENTIAL
 0.0005, 5.
**
*Surface Interaction, name=Inter_Mid_Mid, USER, DEPVAR=20, PROPERTIES=15, UNSYMM
 1.0
 640.0, 320.0, 1.18, 0.35, 640.0, 1.18, 0.28, 0.8,
 0.085,  0.97, 0.87, 0.87,  0.97, 0.87, 0.87
**
*Surface Interaction, name=Inter_Mid_Out, USER, DEPVAR=20, PROPERTIES=15, UNSYMM
 1.0
 800.0, 400.0, 1.45, 0.45, 800.0, 1.45, 0.28, 0.8,
 0.085,  0.97, 0.87, 0.87,  0.97, 0.87, 0.87
**
*Surface Interaction, name=Inter_Out_Out, USER, DEPVAR=20, PROPERTIES=15, UNSYMM
 1.0
 800.0, 400.0, 1.45, 0.45, 800.0, 1.45, 0.28, 0.8,
 0.085,  0.97, 0.87, 0.87,  0.97, 0.87, 0.87
**
**----------------------------------------------------------------
**
**                            INTERACTIONS
**
**----------------------------------------------------------------
**
*Contact Pair, interaction=FEMALE_TOOL
 PSurf:Bot, Female_Die-1.Surf:Female_Die
**
*Contact Pair, interaction=MALE_TOOL
 PSurf:Top_CR, Male_Die-1.Surf:Male_Die
**
*Contact Pair, interaction=STOPER
 PSurf:Top_L, Stoper_L-1.Surf:Stoper_L
**
*Contact Pair, interaction=STOPER
 PSurf:Top_R, Stoper_R-1.Surf:Stoper_R
**
*Contact Pair, interaction=LOAD_CELL
 PSurf:Top_L, Load_Cell-1.Surf:Load_Cell
**
*Contact Pair, interaction=CLAMP
 PSurf:Cnt_O, Clamp_O-1.Surf:Clamp_O
 PSurf:Cnt_U, Clamp_U-1.Surf:Clamp_U
**
*Contact Pair, interaction=Inter_Out_Out
 PSurf:BotPly_int1U, PSurf:BotPly_int1O
**
*Contact Pair, interaction=Inter_Out_Out
 PSurf:BotPly_int2U, PSurf:BotPly_int2O
**
*Contact Pair, interaction=Inter_Mid_Out
 PSurf:Int1U, PSurf:Int1O
**
*Contact Pair, interaction=Inter_Mid_Mid
 PSurf:Int2O, PSurf:Int2U
**
*Contact Pair, interaction=Inter_Mid_Mid
 PSurf:Int3U, PSurf:Int3O
**
*Contact Pair, interaction=Inter_Mid_Out
 PSurf:Int4O, PSurf:Int4U
**
*Contact Pair, interaction=Inter_Out_Out
 PSurf:TopPly_int1U, PSurf:TopPly_int1O
```

```
**
*Contact Pair, interaction=Inter_Out_Out
 PSurf:TopPly_int2U, PSurf:TopPly_int2O
**
**------------------------------------------------------------------
**
**                      BOUNDARY CONDITIONS
**
**------------------------------------------------------------------
**
** Name: BC:Femalenode Type: Displacement/Rotation
*Boundary
 FEMALENODE, 1, 1
*Boundary
 FEMALENODE, 2, 2
*Boundary
 FEMALENODE, 6, 6
**
** Name: BC:Malenode Type: Displacement/Rotation
*Boundary
 MALENODE, 1, 1
*Boundary
 MALENODE, 2, 2
*Boundary
 MALENODE, 6, 6
**
** Name: BC:Stopernode_L Type: Displacement/Rotation
*Boundary
 STOPERNODE_L, 1, 1
*Boundary
 STOPERNODE_L, 2, 2
*Boundary
 STOPERNODE_L, 6, 6
**
** Name: BC:Stopernode_R Type: Displacement/Rotation
*Boundary
 STOPERNODE_R, 1, 1
*Boundary
 STOPERNODE_R, 2, 2
*Boundary
 STOPERNODE_R, 6, 6
**
** Name: BC:Loadcellnode Type: Displacement/Rotation
*Boundary
 LOADCELLNODE, 1, 1
*Boundary
 LOADCELLNODE, 2, 2
*Boundary
 LOADCELLNODE, 6, 6
**
** Name: BC:Clamp_O Type: Displacement/Rotation
*Boundary
 ROTNODE_O, 1, 1
*Boundary
 ROTNODE_O, 2, 2
*Boundary
 ROTNODE_O, 6, 6
**
** Name: BC:Clamp_U Type: Displacement/Rotation
*Boundary
 ROTNODE_U, 1, 1
*Boundary
 ROTNODE_U, 2, 2
*Boundary
 ROTNODE_U, 6, 6
```

```
**
** Name: BC:MESHNODES Type: Displacement/Rotation
*Boundary
 MESHNODES, 1, 1
**
**------------------------------------------------------------------
**
**                              STEP 1
**
**------------------------------------------------------------------
**
*Step, name="Step-1:Apply webtension", nlgeom=YES, inc=50000, unsymm=YES
*Static
 0.1, 1., 1e-05, 1.
**
** CONTROLS
*Controls, reset
**
** LOADS
*Dsload, amplitude=Amp:Web
 PSurf:El_End_L, P, -2.2222
*Dsload, amplitude=Amp:Web
 PSurf:El_End_R, P, -2.2222
**
** OUTPUT REQUESTS
*Restart, write, overlay, frequency=1
*Print, contact=YES
**
** FIELD OUTPUT
*Output, field, frequency=3
*Contact Output
 CDISP, CSTRESS
*Node Output
 CF, RF, U
*Element Output
 E, LE, S, SDV
**
*End Step
**
**------------------------------------------------------------------
**
**                              STEP 2
**
**------------------------------------------------------------------
**
*Step, name="Step-2:Male_Die punch", nlgeom=YES, inc=250, unsymm=YES
*Static
 0.025, 1., 1e-08, 0.1
**
** CONTROLS
*CONTROLS, PARAMETERS=TIME INCREMENTATION
  , ,12,20, , , ,10,
*Controls, parameter=field
 0.10, 0.10, , ,0.25
**
** BOUNDARY CONDITIONS
*Boundary, amplitude=Amp:Pred_1
 MALENODE, 2, 2, -0.655
**
** OUTPUT REQUESTS
*Print, contact=YES
**
** FIELD OUTPUT
*Output, field
*Contact Output
```

```
 CDISP, CSTRESS
*Node Output
 CF, RF, U
*Element Output
 E, LE, S, SDV
**
** HISTORY OUTPUT
*Output, History, FREQ=1
*Node Output, Nset=MALENODE
 RF, U
**
*End Step
**
**------------------------------------------------------------------
**
**                              STEP 3
**
**------------------------------------------------------------------
**
*Step, name="Step-3:Male_Die remove", nlgeom=YES, inc=50000, unsymm=YES
*Static
 0.005, 1., 1e-12, 0.025
**
** BOUNDARY CONDITIONS
*Boundary, amplitude=Amp:Pred_2
 MALENODE, 2, 2, -0.655
**
** OUTPUT REQUESTS
*Print, contact=YES
**
** FIELD OUTPUT
*Output, field
*Contact Output
 CDISP, CSTRESS
*Node Output
 CF, RF, U
*Element Output
 E, LE, S, SDV
**
** HISTORY OUTPUT
*Output, History, FREQ=1
*Node Output, Nset=MALENODE
 RF, U
**
*End Step
**
**------------------------------------------------------------------
**
**                              STEP 4
**
**------------------------------------------------------------------
**
*Step, name="Step-4:Add Clamps", nlgeom=YES, inc=50000, unsymm=YES
*Static
 0.01, 1., 1.e-8, 1.0
**
** CONTROLS
*Controls, reset
**
** BOUNDARY CONDITIONS
*Boundary
 ROTNODE_O,  2, 2, -4.000
 ROTNODE_U,  2, 2, 4.000
**
** OUTPUT REQUESTS
```

```
*Print, contact=YES
**
** FIELD OUTPUT
*Output, field, FREQ=1
*Contact Output, Var=PRE
*Node Output, Var=PRE
*Element Output
 E, LE, S, SDV
**
** HISTORY OUTPUT
*Output, History, FREQ=0
**
*End Step
**
**------------------------------------------------------------------
**
**                              STEP 5
**
**------------------------------------------------------------------
**
*Step, name="Step-5:Remove Female_Die, Male_Die and Stoppers and Remove Web Tension", nlgeom=YES, inc=50000, unsymm=YES
*Static
 0.01, 1., 1.e-8, 1.0
**
** BOUNDARY CONDITIONS
*Boundary
 FEMALENODE,2, 2, -6
 MALENODE,2, 2, 4
 STOPERNODE_L,2, 2, 4
 STOPERNODE_R,2, 2, 4
**
** OUTPUT REQUESTS
*Print, contact=YES
**
** FIELD OUTPUT
*Output, field, FREQ=3
*Contact Output, Var=PRE
*Node Output, Var=PRE
*Element Output
 E, LE, S, SDV
**
** HISTORY OUTPUT
*Output, History, FREQ=0
**
*End Step
**
**------------------------------------------------------------------
**
**                              STEP 6
**
**------------------------------------------------------------------
**
*Step, name="Step-6:Contact Change", nlgeom=YES, inc=50000, unsymm=YES
*Static
 0.01, 1., 1.e-8, 1.0
**
** CONTACT PAIRS
*Model Change, Type=Contact Pair, Remove
 PSurf:Bot,  Female_Die-1.Surf:Female_Die
 PSurf:Top_CR,Male_Die-1.Surf:Male_Die
 PSurf:Top_L,  Stoper_L-1.Surf:Stoper_L
 PSurf:Top_R,  Stoper_R-1.Surf:Stoper_R
**
** OUTPUT REQUESTS
*Print, contact=YES
```

```
**
** FIELD OUTPUT
*Output, field, FREQ=1
*Contact Output, Var=PRE
*Node Output, Var=PRE
*Element Output
 E, LE, S, SDV
**
** HISTORY OUTPUT
*Output, History, FREQ=0
**
*End Step
**
**------------------------------------------------------------------
**
**                              STEP 7
**
**------------------------------------------------------------------
**
*Step, name="Step-7:Remove BC MESHNODES", nlgeom=YES, inc=50000, unsymm=YES
*Static
 0.01, 1., 1.e-8, 1.0
**
** BOUNDARY CONDITIONS
**
*Boundary, OP=new, FIXED
 LOADCELLNODE,1,2
 LOADCELLNODE,6,6
 ROTNODE_O,1,2
 ROTNODE_O,6,6
 ROTNODE_U,1,2
 ROTNODE_U,6,6
**
** OUTPUT REQUESTS
*Print, contact=YES
**
** FIELD OUTPUT
*Output, field, FREQ=1
*Contact Output, Var=PRE
*Node Output, Var=PRE
*Element Output
 E, LE, S, SDV
**
** HISTORY OUTPUT
*Output, History, FREQ=0
**
*End Step
**
**------------------------------------------------------------------
**
**                              STEP 8
**
**------------------------------------------------------------------
**
*Step, name="Step-8:Add Loadcell", nlgeom=YES, inc=50000, unsymm=YES
*Static
 0.01, 1., 1.e-8, 1.0
**
** BOUNDARY CONDITIONS
*Boundary
 LOADCELLNODE, 2, 2, -3.985
**
** OUTPUT REQUESTS
*Print, contact=YES
**
```

```
** FIELD OUTPUT
*Output, field, FREQ=1
*Contact Output, Var=PRE
*Node Output, Var=PRE
*Element Output
 E, LE, S, SDV
**
** HISTORY OUTPUT
*Output, History, FREQ=0
**
*End Step
**
**------------------------------------------------------------------
**
**                              STEP 9
**
**------------------------------------------------------------------
**
*Step, name="Step-9:Folding", nlgeom=YES, inc=50000, unsymm=YES
*Static
 0.005, 1., 1e-12, 0.5
**
** CONTROLS
*CONTROLS, PARAMETERS=TIME INCREMENTATION
 8, 12, ,20, , , , 10,
*Controls,PARAMETERS=Field,FIELD=Displacement
 0.01,0.04,  ,  ,0.1
**
** BOUNDARY CONDITIONS
*Boundary
 ROTNODE_O, 6, 6, -0.7854
 ROTNODE_U, 6, 6, -0.7854
*Boundary, FIXED
 LOADCELLNODE, 2, 2
 LOADCELLNODE,6, 6
**
** OUTPUT REQUESTS
*Print, contact=YES
**
** FIELD OUTPUT
*Output, field, FREQ=1
*Contact Output, Var=PRE
*Node Output, Var=PRE
*Element Output
 E, LE, S, SDV
**
** HISTORY OUTPUT
*Output, History, FREQ=1
*Node Output, Nset=LOADCELLNODE
 RF
*Node Output, Nset=ROTNODE_U
 UR3
*MONITOR, NODE=ROTNODE_U, DOF=6
**
*End Step
**
**------------------------------------------------------------------
**
**                              STEP 10
**
**------------------------------------------------------------------
**
*Step, name="Step-10:Relax", nlgeom=YES, inc=50000, unsymm=YES
*Static
 0.005, 1., 1.e-8, 1.0
```

```
**
** CONTROLS
*Controls, reset
**
** BOUNDARY CONDITIONS
*Boundary
 ROTNODE_O, 6, 6, 0
 ROTNODE_U, 6, 6, 0
*Boundary, FIXED
 LOADCELLNODE, 2, 2
 LOADCELLNODE,6, 6
**
** OUTPUT REQUESTS
*Print, contact=YES
**
** FIELD OUTPUT
*Output, field, FREQ=1
*Contact Output, Var=PRE
*Node Output, Var=PRE
*Element Output
 E, LE, S, SDV
**
** HISTORY OUTPUT
*Output, History, FREQ=1
*Node Output, Nset=LOADCELLNODE
 RF
*Node Output, Nset=ROTNODE_U
 UR3
*MONITOR, NODE=ROTNODE_U, DOF=6
**
*End Step
**
**------------------------------------------------------------------
**
**                              STEP 11
**
**------------------------------------------------------------------
**
*Step, name="Step-11:Re-Folding", nlgeom=YES, inc=50000, unsymm=YES
*Static
 0.005, 1., 1.e-8, 1.0
**
** BOUNDARY CONDITIONS
*Boundary
 ROTNODE_O, 6, 6, -0.7854
 ROTNODE_U, 6, 6, -0.7854
*Boundary, FIXED
 LOADCELLNODE, 2, 2
 LOADCELLNODE,6, 6
**
** OUTPUT REQUESTS
*Print, contact=YES
**
** FIELD OUTPUT
*Output, field, FREQ=1
*Contact Output, Var=PRE
*Node Output, Var=PRE
*Element Output
 E, LE, S, SDV
**
** HISTORY OUTPUT
*Output, History, FREQ=1
*Node Output, Nset=LOADCELLNODE
 RF
*Node Output, Nset=ROTNODE_U
```

```
 UR3
*MONITOR, NODE=ROTNODE_U, DOF=6
**
*End Step
**
**------------------------------------------------------------------
**
**                              STEP 12
**
**------------------------------------------------------------------
**
*Step, name="Step-12:Relax2", nlgeom=YES, inc=50000, unsymm=YES
*Static
 0.005, 1., 1.e-8, 1.0
**
** CONTROLS
*Controls, reset
**
** BOUNDARY CONDITIONS
*Boundary
 ROTNODE_O, 6, 6, 0
 ROTNODE_U, 6, 6, 0
*Boundary, FIXED
 LOADCELLNODE, 2, 2
 LOADCELLNODE,6, 6
**
** OUTPUT REQUESTS
*Print, contact=YES
**
** FIELD OUTPUT
*Output, field, FREQ=1
*Contact Output, Var=PRE
*Node Output, Var=PRE
*Element Output
 E, LE, S, SDV
**
** HISTORY OUTPUT
*Output, History, FREQ=1
*Node Output, Nset=LOADCELLNODE
 RF
*Node Output, Nset=ROTNODE_U
 UR3
*MONITOR, NODE=ROTNODE_U, DOF=6
**
*End Step
```